MASTER OF SCIENCE IN ELECTRICAL AND ELECTRONIC ENGINEERING

DEVELOPMENT OF AN EXTREMELY LOW LOSS PHOTONIC CRYSTAL FIBER FOR THz REGIME

By

Farhana Akter Mou

Department of Electrical and Electronic Engineering

Islamic University of Technology (IUT)

Organization of Islamic Cooperation (OIC)

Board Bazar, Gazipur-1704, Bangladesh

September – 2019

DECLARATION OF CANDIDATE

I hereby declare that the work reported in the M.Sc. thesis entitled "**DEVELOPMENT OF AN EXTREMELY LOW LOSS PHOTONIC CRYSTAL FIBER FOR THz REGIME**" submitted at **Islamic University of Technology (IUT),** OIC, Board Bazar, Gazipur, Bangladesh, is an authentic record of my work carried out under the supervision of **Prof. Dr. Mohammad Rakibul Islam**. I have not submitted this work elsewhere for any other degree or diploma. I am fully responsible for the contents of my M.Sc. thesis.

Farhana Akter Mou
Student Number: 161021006
Academic Year: 2016-2017

CERTIFICATE OF APPROVAL

The thesis titled "**DEVELOPMENT OF AN EXTREMELY LOW LOSS PHOTONIC CRYSTAL FIBER FOR THz REGIME**" submitted by **Farhana Akter Mou** bearing Student No. 161021006 of Academic Year 2016-2017 has been found as satisfactory and accepted as partial fulfilment of the requirement for the degree of Master of Science in Electrical and Electronic Engineering on 30 August 2019.

BOARD OF EXAMINERS

1. **Dr. Mohammad Rakibul Islam** — Chairman (Supervisor)
   Professor
   Department of Electrical & Electronic Engineering
   IUT, Gazipur-1704, Bangladesh.

2. **Dr. Md. Ruhul Amin** — Member (Ex-Officio)
   Professor and Head
   Department of Electrical & Electronic Engineering
   IUT, Gazipur-1704, Bangladesh.

3. **Dr. Md. Ashraful Hoque** — Member
   Professor
   Department of Electrical & Electronic Engineering
   IUT, Gazipur-1704, Bangladesh.

4. **Dr. Ashik Ahmed** — Member
   Associated Professor
   Department of Electrical & Electronic Engineering
   IUT, Gazipur-1704, Bangladesh.

5. **Dr. Mohammed Imamul Hassan Bhuiyan** — Member (External)
   Professor
   Department of Electrical & Electronic Engineering
   BUET, Dhaka-1000, Bangladesh.

TO MY FAMILY & TEACHERS

TABLE OF CONTENTS

	Page No
DECLARATION OF CANDIDATE	i
CERTIFICATE OF APPROVAL	ii
LIST OF ACRONYMS AND ABBREVIATIONS	vii
LIST OF SYMBOLS	viii
LIST OF FIGURES	x
LIST OF TABLES	xiii
ACKNOWLEDGEMENT	xiv
ABSTRACT	xv
Chapter 1 Introduction	**1**
1.1 Background and present state of PCF design	1
1.2 Motivation	5
1.3 Objectives with specific aims	5
1.4 Outcomes	6
1.5 Organization of this Thesis	6
Chapter 2 Theoretical Framework of Photonic Crystal Fiber for THz Waveguide and Sensing Application	**7**
2.1 Photonic Crystal Fiber	7
2.1.1 Index-guided Microstructure Fiber	9
2.1.2 Photonic Bandgap Fibers	10
2.2 THz Waveguide	11
2.2.1. Metallic Waveguides	12

2.2.2. Dielectric Waveguides 14

2.2.2.1. Hollow-Core Waveguides/Fibers 16

2.2.2.2. Solid-Core Waveguides/Fibers 18

2.2.2.3. Porous Core Waveguides 19

2.3 Applications of PCF 20

2.4 Characterization of THz wave guiding and sensing properties 21

2.5 Conclusion 26

Chapter 3 **27**

Proposed Terahertz Waveguide

3.1 Design Methodology of Proposed PCF 27

3.2 Numerical Analysis 28

3.3 Fabrication Possibilities 38

3.4 Conclusion 39

Chapter 4 **40**

Proposed Polarization Maintaining THz Waveguide

4.1 Design Methodology of Proposed PCF 40

4.2 Numerical Analysis 41

4.3 Conclusion 49

Chapter 5 **50**

Proposed Terahertz Analytes Sensor

5.1 Design Methodology of Proposed PCF 50

5.2 Numerical Analysis 52

5.3 Comparison among proposed designs for sensing applications 64

5.4 Fabrication Possibilities 65

5.5 Conclusion 65

Chapter 6 **66**
Conclusion and Future Work

6.1 Contributions 66

6.2 Future Directions 67

References **68**

LIST OF ACRONYMS AND ABBREVIATIONS

Abbreviation	Definition
dB	Decibel
ERI	Effective Refractive Index
EML	Effective Material Loss
FEM	Finite Element Methode
FET	Field Effect Transistor
HC	Hollow Core
MMF	Multi-Mode Fiber
MOFs	Microstructured Optical Fibers
NA	Numerical Aperture
PML	Perfectly Matched Layer
PCF	Photonic Crystal Fiber
PBG	Photonic Band Gap
PC	Porous Core
PTFE	polytetrafluoroethylene
PMMA	Poly Methyl Methacrylate
SMF	Single Mode Fiber
THz	Terahertz
TDS	Time Domain Spectroscopy

LIST OF SYMBOLS

Abbreviation	Definition
α_{eff}	Effective material loss
ϵ_0	Relative permeability
n_{mat}	Refractive index
α_{mat}	Bulk absorption loss
S_z	Z-component of the Poynting vector
E	Electric field component
H	Magnetic field component
L_c	Confinement loss
f	Operating frequency
c	Speed of light
$Im(n_{eff})$	Imaginary part of the complex effective refractive index
A_{eff}	Effective area
x	Area of the region of interest
n_{eff}	Effective refractive index
n_1	Effective refractive index core region
n_2	Effective refractive index cladding region
I(f)	Intensities of light with the presence of the analyte needed to be detected
I_0	Intensities of light without the presence of the analyte needed to be detected
r	Relative sensitivity
α_m	Absorption coefficient
l_c	Channel length
n_r	Refractive index of the sample
k	Light interaction
B	Birefringence
n_x	Effective refractive index of the x polarization mode
n_y	Effective refractive index of the y polarization mode

$\mathbf{R}$	Radius of the lattice
w_{eff}	Spot size
γ	Nonlinearities
θ_{radian}	Beam Divergence
η	Core Power Fraction
$\boldsymbol{\alpha_{BL}}$	Bending loss
$\mathbf{R_b}$	Bending Radius

LIST OF FIGURES

Figure Number	Caption	Page Number
2.1	Photonic Crystal Fiber	8
2.2	Index-guided microstructure fiber and Photonic bandgap fibers	11
2.3	a) Hollow-core single clad waveguide, indicating the diameter, d, and the dielectric/metal thickness, t. Hollow-core hybrid-clad waveguides (b) Metal waveguides with dielectric inner coating, (c) Metal waveguides with a thin layer of metamaterial	17
2.4	Kagome Structure hollow core fiber	18
2.5	Solid core and microstructured cladding waveguide	19
2.6	Porous Core waveguide	20
3.1	Geometry of the proposed PC-PCF design.	28
3.2	Distribution of light at different frequencies.	29
3.3	EML and Confinement loss as a function of frequency for different core size (Ls).	30
3.4	EML and Confinement loss as a function of frequency for different porosity.	30
3.5	EML and Confinement loss as a function of porosity for different core size (Ls).	31
3.6	EML and Confinement loss as a function of core side length for different porosity.	31
3.7	Bending loss with respect to frequency for different bending radius.	32
3.8	Effective area and Core Power Fraction as a function of frequency for different core size (Ls).	34
3.9	Effective area and Core Power Fraction as a function of frequency for different core porosity.	35
3.10	Effective area and Core Power Fraction as a function of porosity for different core size (Ls).	35
3.11	Effective area and Core Power Fraction as a function of core side length for different porosity.	36
3.12	Dispersion with respect to Frequency for different Porosities.	36

3.13	V-parameter with respect to Frequency for different Porosities	37
4.1	End face view of proposed PCF with enlargement of core.	41
4.2	Electromagnetic field distribution of proposed PCF, x-mode (left), y-mode (right).	42
4.3	Response of EMI with respect to frequency.	42
4.4	Birefringence with respect to frequency.	42
4.5	Birefringence with respect to core diameter at different porosity.	43
4.6	EML and confinement loss with respect to frequency at different core diameter (a) x-polarization, (b) y-polarization	44
4.7	EML and confinement loss with respect to frequency at different porosity (a) x-polarization, (b) y-polarization	45
4.8	Effective area and core power fraction with respect to frequency at different core diameter (a) x-polarization, (b) y-polarization	47
4.9	Waveguide dispersion with respect to frequency at different core diameter (a) x-polarization, (b) y-polarization.	48
5.1	Geometry of Proposed PCF.	51
5.2	Electric field distribution of proposed PCF based sensor for different analytes in both polarizations at 3 THz (a) Water (b)Ethanol (c) Methanol and (d) Benzene	52
5.3	Sensitivity versus frequency x-polarization	53
5.4	Sensitivity Vs D_{core} with x-polarization	53
5.5	EML Vs frequency with X polarization	54
5.6	EML Vs frequency with Y polarization	54
5.7	EML Vs D_{core} with X polarization	55
5.8	EML Vs D_{core} with Y polarization	56
5.9	Effective Area Vs frequency with x-polarization	57
5.10	Effective Area Vs D_{core} with x-polarization	57
5.11	Confinement Loss Vs Frequency.	58
5.12	Waveguide dispersion Vs frequency.	58
5.13	Numerical Aperture Vs Frequency.	59
5.14	Effective refractive index Vs Frequency.	60
5.15	Nonlinear coefficient Vs wavelength	61

5.16 V-parameter Vs wavelength 61

5.17 Spot size Vs wavelength 62

5.18 Beam divergence Vs wavelength 62

5.19 Sensitivity Vs Frequency for different proposed PCFs (a) hexagonal hollow core (b) hexagonal porous core (c) square porous core 64

LIST OF TABLES

Table Number	Title	Page Number
3.1	Comparison among different previously remarkable porous core PCFs and proposed PC-PCF	38
5.1	Comparison among previously remarkable porous core PCFs for analytes sensing and proposed THz sensor.	63
5.2	Comparison among our proposed PCFs for different chemical sensing	65

ACKNOWLEDGEMENTS

First of all, I would like to express my deep and sincere gratitude to my supervisor **Dr. Mohammad Rakibul Islam**, Professor, Department of Electrical and Electronic Engineering (EEE), Islamic University of Technology (IUT), OIC, Dhaka, Bangladesh, for his kind guidance, support and encouragement. His regular helps and supervision on this thesis really made me to complete this work within very short time. His valuable advice and constructive criticism guided me to learn and enjoy the art of research. His ability to quickly understand the depth of the problem and suggesting a clear solution has always inspired me. In every sense, this thesis could never have come into existence without his help. Learning from him has been a very fruitful and enjoyable experience. I shall always remain grateful to him.

I would like to express my deepest cordial thanks to my parents for their supporting and tolerance of being far away from them.

My heartfelt acknowledgement also goes to Head of the EEE department, Prof. Dr. Md. Ruhul Amin, Prof. Md. Ashraful Hoque, Dr. Ashik Ahmed and Prof. Dr. Mohammed Imamul Hassan Bhuiyan for being members on my committee.

Last but not the least I am thankful to Allah, who gave me enough patience, strength and courage to complete this work. I am highly grateful to the Almighty.

ABSTRACT

In this research, the main focus is to develop Photonic Crystal Fiber (PCF) structures which exhibit ultra-low loss in THz wave propagation. Several researchers recently proposed different types of PCF geometry to minimize the losses. These proposed PCF structure depicted a moderate effective material loss from 0.029 cm^{-1} to 0.086 cm^{-1}. There are several ways to minimize the losses such as core cladding geometry selection, air holes size optimization, air holes position, core radius, material selections etc. In this context a sectored cladding and square core structured PCF is designed for THz wave propagation and a hexagonal asymmetrical slotted porous core PCF geometry is proposed for polarization maintaining fiber in the THz regime.

The proposed circular sectored cladding and square core PCF design exhibits extremely low effective material loss (EML) of 0.009 cm^{-1} at optimum design parameters. However, it shows very large effective area and a high core power fraction in the THz frequency range. Hence this PCF structure can't meet the requirements of polarization maintaining fiber characteristics. Thus, an asymmetrical hexagonal slotted porous core PCF geometry is developed for polarization maintaining fiber characteristics which exhibits significant differences of refractive index in *x* and *y* polarization mode with a low EML of 0.015 $cm^{-1}$and confinement loss of 0.0001 cm^{-1}.

Presently PCF in the THz regime has gained popularity for chemical sensing applications. In general presented PCF exhibits maximums 90% sensitivity but still have lots of possibilities to improve the sensitivity. In this context hollow core fiber geometry is proposed for chemical sensing application. Hollow core fiber has greater analyte volume inside the core area, thus facilitating tight confinement that increases the sensitivity. This proposed PCF based sensor shows relative sensitivity very close to 100%, along with also shows very low EML of 4×10^{-3} cm^{-1} and negligible confinement loss. Interestingly the asymmetrical hexagonal slotted porous core PCF also exhibits sensitivity in the range of 68% to 94% which is comparable to that of existing structures for chemical sensing applications.

The performances of the proposed designs are also compared with those of state-of-the-art works. In general all the three designs exhibit a superior EML and sensitivity while facilitating ease of fabrication.

Chapter 1

Introduction

Among various optical waveguide platforms, optical fibers are most attractive for day-to-day applications, which include high power lasers, long distance transmission, medical endoscopy, sensing etc. especially in Terahertz frequency range. Additionally, all these excellent qualities of THz radiation make it suitable for imaging of hidden objects, like explosives, metallic weapons etc. It is also useful to monitor the buried defects in IC packages, layer of paints, tiles, or space crafts etc. In conventional optical fiber, the light propagates through a high refractive index medium and the geometry of core and cladding is fixed. Because of these limitations microstructure fibers such as Photonic Crystal Fiber (PCF) come into light which provides excellent design flexibility and the light propagates through a guided air medium. The geometries' parameters such as pitch size, air hole radius, strut size and core radius can be readily selected. Excellent THz guiding properties of PCF and diverse application of THz in different fields, photonic crystal fiber is gained enormous attention not only for communication, but also in sensing application.

1.1 Background and present state of PCF design

Terahertz (THz) indicates far-Infrared region located between microwaves and infrared regions in the electromagnetic spectrum which occupies the frequency range from 0.1 to 10 THz. Currently lots of researchers have given enormous attention to terahertz wave propagation because of diverse applications in the field of medical imaging [1], sensing, security, spectroscopy, oral healthcare, cancer cell detection, bio-technology, telecommunication, military, environmental applications [2], detection of defects in solar panels, characterization of dielectric materials, pharmaceutical drug testing and astronomy [3]. Due to abundant development of modern technology the terahertz wave generator and detector are available now. There are three types of THz sources: they are natural, artificial and THz frequency spectroscopy. In natural, the THz radiation is emitted as a part of the black body radiation from any object when the temperature is greater than 10 Kelvin.

In THz radiation band the gyrotron, quantum cascade laser and backward wave oscillator (BWO) etc. are the practical examples of artificial sources [4,5]. Several viable THz waveguide detectors are direct detection detector, heterodyne detection detector, pair braking photon detector, thermal detector, extrinsic germanium detector and FET detector etc. [6]. Low loss, flexible, long distance and efficient transmission are big challenges for unguided medium. In addition, unguided THz medium generates transmitter receiver alignment related problems and uncertain absorption loss influenced by surroundings atmospheric condition. In this context, last few years back several researcher's proposed different guided medium for THz propagation such as metallic wires, metal coated dielectric tubes , metallic slot waveguides, bare metal wires to minimize these problems but due to high material absorption loss, higher bending loss and lower coupling efficiency the proposed guided mediums are disregarded [7].

Recently they have given attention in polymer fibers such as polymer Bragg fiber, polystyrene foam, plastic fiber, hollow core fiber, solid core fiber and porous core photonic crystal fiber (PCF) [8,9] to reduce the material absorption loss. Due to lots of advantages such as novel light guidance properties, diverse applications including fiber optic communication, fiber laser, nonlinear devices, high-power transmission and highly sensitive devices have emerged with lower material absorption loss, lower confinement loss, high core power fraction, lower dispersion the photonic crystal fiber came to light. Besides the PCF's geometries such as pitch size, air hole radius, and core radius can be readily selected. Moreover, the solid core photonic crystal fiber exhibits high effective material loss (EML). Hence, minimizing the EML it is necessary to replace the solid core into air core PCF, which is called porous core PCF (PC-PCF). Proper geometries and optimum value selection are the main challenges to reduce the losses. Especially the issues including high relative sensitivity, high core power fraction, low effective material loss, high birefringence, low dispersion etc. but proper design is the main issue to achieve these characteristics.

The efficient Porous-Core Photonic Crystal Fibers design is still a big issue with low effective material loss (EML) and high core power fraction. Several researchers are presently working on the design of PCF for better performances. Several types of PC-PCF geometries for THz waveguide have been proposed to minimize the losses. In 2017 A. Kawsar et. al reported a porous core octagonal PCF which exhibits effective material loss of 0.049 cm^{-1} and effective area of 3×10^{-7} m^2 at 1 THz operating frequency but they ignored some

important optical properties such as dispersion, confinement loss etc.[10]. Then M. H. Ahasan et. al proposed a slotted core hexagonal porous core PCF and the proposed structure offers effective material loss (EML) of 0.035 cm^{-1} and bending loss of 1.07×10^{-34} cm^{-1} at an operating frequency of 1.0 THz. However one major drawback in this design is that huge number of asymmetrical rectangular air lattices are used in core region which is very difficult in fabrication [11]. Later M. H. Ahasan et. al modified their previously reported design and introduced hexagonal lattice PCF in which equal size rectangular shaped air holes are inserted in the core region which shown effective material loss of 0.086 cm^{-1} but they were able to reduce the birefringence from 0.088 to 0.045 at 0.85 THz frequency[12]. S. Islam et. al proposed a Zeonex based complex asymmetrical elliptical array shaped core and rectangular shaped cladded photonic crystal fiber with effective material loss of 0.06 cm^{-1}, and confinement loss of 5.45×10^{-13} cm^{-1}, but its exhibit near-zero dispersion flattened property of ±0.02 ps/THz/cm [13]. J. Sultana et al. demonstrated Topas based conventional hexagonal cladding and a penta-hole elliptical structure in the core which offers effective material loss of 0.05 cm^{-1} at 1 THz frequency with a dispersion variation of 0.53 ± 0.07 ps/THz/cm [14]. B.K. Paul et. al proposed and investigate a hexagonal core and cladding structured PCF. The investigation results show effective material loss (EML) of 0.03cm^{-1} at 1.0 THz but this design offers a high confinement loss [15]. A complex Kagome lattice PCF with hexagonal shaped air holes is introduced by S. Rana et. al which exhibits low EML of 0.029 cm^{-1} at an operating frequency of 1.3 THz when they considered an optimized core diameter of 300μm but the practical implementation of kagome structured PCF is very difficult compared to a circular sectored cladding PCF by using existing fabrication process [16].

Several researchers recently proposed different types of geometry of PC-PCF for polarization maintaining fiber for THz wave guidance highlighting the EML reduction. K. Ahmed et al.[17] proposed a hexagonal cladding structure with circular manner elliptical air hole based polarization maintaining PCF which shows an EML of 0.0689 cm^{-1}, but for an efficient THz waveguide many others parameters such as confinement loss, dispersion, core power fraction, effective etc. evaluation is very important. Unfortunately they ignored these parameters evaluation. Later, a hexagonal structure in the cladding and hybrid structure in the core with a reduced EML of 0.03 cm^{-1} at 1 THz operating frequency is suggested by J. Sultana et al.[18]. M. Islam et al.[13] designed a zeonex based asymmetry THz polarization maintain

PCF with an EML of 0.06 cm^{-1} at 1.1THz frequency. Again M. Islam et al proposed a zeonex oligoporus core with kagome structure cladding with an EML of 0.05cm^{-1} [19], practical implementation of kagome structure PCF is not an easy task. M. Faisal et al. proposed a sectored cladding and an elliptical shaped suspended structure core PCF with an EML of 0.047 cm^{-1} at 1THz frequency [20].

After lots of research on PCF application, sensing application of PCF is enough matured. Already lots of PCF design proposed for different types of sensing applications of PCF such as gas sensor, chemical sensors, biosensors, temperature sensors, mechanical sensors, pressure sensors, alcohol, Water etc.

S. Asaduzzaman et al. proposed a hybrid photonic crystal fiber for chemicals sensing application which contains 49.29 % sensitivity with 3.13×10^{-10} dB/m confinement loss for benzene, 49.17 % sensitivity with 2.75×10^{-10} dB/m confinement loss for ethanol and 48.85 % sensitivity with 2.75×10^{-9} dB/m confinement loss of water[21]. Arif et al. design a hexagonal structured PCF as a sensor for liquid sensing with low loss and improved sensitivity 59% [22], which is better from S. Asaduzzaman's et al. proposed design. Later to increase the sensitivity J. Sultana et al. modeled a Zeonex based PCF and they applied their model for ethanol sensing which obtained 68.87% sensitivity with 7.79×10^{-12} cm^{-1} confinement loss at 1 THz frequency[23]. B. K. Paul et al. proposed a micro structure folded cladding porous shaped with circular air hole photonic crystal fiber. In that way, they ordered a relative sensitivity of 64.19% and the confinement loss of 2.07×10^{-5} dB/m are attained at 1.48 μm wavelength [24]. H. Ademgil et al. designed a high sensitivity Photonic Crystal Fiber (PCF) sensor with high birefringence and low confinement losses for liquid analyte sensing applications. The proposed PCF structures are designed with supplementary elliptical air holes in the core region vertically-shaped V-PCF and horizontally-shaped H-PCF but they achieved only 26% sensitivity [25]. M. Islam et al. suggested a Zeonex-based hollow core which is surrounded by a number of asymmetric rectangular air holes. They observed the relative sensitivity from their proposed PCF which is more than 90%. Since their PCF cladding is not symmetrical, so fabrication and practical implementation is very difficult for this proposed design [26].

1.2 Motivation

In the last couple of years, strong efforts have been carried out to design and investigate the optical properties of photonic crystal fiber. Lots of PCF geometry have been proposed and theoretically characterized by different researchers for THz waveguide and sensing applications. Effective material loss and confinement loss are the main limiting factors of efficient PCF devices. There are several ways to minimize the losses in PCF devices such as core cladding geometry selection, air holes size and core radius optimization, air holes position and material selections etc. The Literature Review above indicates the scope of further improving the performance of a PCF by minimizing the losses. . In this context a hexagonal porous core PCF design is presented to reduce the losses an ultra-low level. Furthermore, a square porous core PCF is proposed that additionally maintains polarization with increasing birefringence. Moreover, different analytes sensing specially chemical sensing application of PCF in the THz regime has gained popularity in recent times. In this context, a hollow core PCF is developed that gives high sensitivity chemical sensing applications while ensuring low losses.

1.3 Objectives with specific aims

The key concern of this research is to develop porous core PCF structure which is easily implementable with considerable losses for THz wave propagation and design a hollow core highly sensitive PCF with low effective material loss, which is suitable for different chemical sensing and that, can be easily implemented in industries. The proposed PCF designs may offer negligible EML, high core power fraction, low confinement loss, near zero flat dispersion in THz waveguide propagation and highly sensitive in different chemical sensing applications.

The Objectives is summarized as below:

i. To design a simple air core PCF for THz wave guidance, which offers negligible EML and low confinement loss.
ii. To develop a polarization maintaining fiber geometry with acceptable birefringence.
iii. To analyze the different wave guiding properties by changing design parameters, such as porosity, core size, pitch, frequency and so others of suggested PCFs.

iv. To design a highly sensitive hollow core PCF and evaluation of sensing properties.
v. To find an optimum value of design parameters which impart desire outputs.
vi. To assess the performance of the proposed designs using COMSOL multiphysics software and display the results graphically.
vii. To compare the numerical outcomes of proposed PCFs with exiting PCFs.

1.4 Outcomes

i. Developed a unique PCF structure with negligible EML (less than 0.010 per cm), higher core power fraction and flattened dispersion for THz guidance, which is better than the previously proposed design [10]-[16].
ii. Developed a polarization maintaining fiber geometry with lower design complexity.
iii. A PCF design such that its structural shape allows for maximum sensitivity for different chemicals sensing.
iv. Practical implementation PCF geometry using existing fabrication techniques.

1.5 Organization of this Thesis

In **Chapter 1** introduces the present state of research on PCF, motivation of this work, background of this problem, objectives and possible outcomes.
THz Wave guiding and sensing properties of Photonic Crystal fibers and different losses mechanism associated with PCF are explained in **Chapter 2**.
In **Chapter 3** the PCF design procedures and analysis of the proposed PCF structure for THz wave guidance are described.
A polarization maintaining fiber design methodology and different property characterization for THz wave propagation are discussed in **Chapter 4**
Chapter 5 provides a photonic crystal sensor design and evaluation of different sensing properties for chemical sensing applications.
In **Chapter 6** the findings are summarized. The limitations of the present study and the options for future endeavours have also been mentioned.

Chapter 2

Theoretical Framework of Photonic Crystal Fiber for THz Waveguide and Sensing Application

2.1 Photonic Crystal Fiber

Photonic crystals are composed of periodic dielectric or metallic-dielectric structures that are designed to affect the propagation of electromagnetic waves in the same way as the semiconductor affects the propagation of electrons. Consequently, photons in PC can have band structures, localized defect modes, surface modes, etc. This new ability to mold and guide light leads naturally to many novel phenomena associated with light. The absence of allowed propagating EM modes inside the structures, in a range of wavelengths called a photonic band gap (PBG), gives rise to distinct optical phenomena such as inhibition of spontaneous emission and low-loss waveguides of particular interest is a PC whose band structure possesses a complete photonic band gap. A complete photonic band gap defines a range of frequencies for which light is forbidden to propagate in all directions [27]. The optical analogue is the photonic crystal, in which the atoms or molecules are replaced by macroscopic media with differing dielectric constants, and the periodic potential is replaced by a periodic dielectric function (or, equivalently, a periodic index of refraction). If the dielectric constants of the materials in the crystal are sufficiently different and if the absorption of light by the materials is minimal, then the refractions and reflections of light from all of the various interfaces can produce many of the same phenomena for photons (light modes) that the atomic potential produces for electrons. One solution to the problem of optical control and manipulation is thus a photonic crystal, a low-loss periodic dielectric medium. In particular, we can design and construct photonic crystals with photonic band gaps, preventing light from propagating in certain directions with specified frequencies. We will also see that a photonic crystal can allow propagation in anomalous and useful ways [28].

Photonic crystal fibers (PCFs), which are also called micro structured optical fibers or holey fibers, have been extensively investigated and have considerably altered the traditional fiber optics since they appeared in the mid-1990s [Knight et al., 1996; Knight, 2003; Russell, 2003]. PCFs have a periodic array of micro holes that run along the entire fiber length.

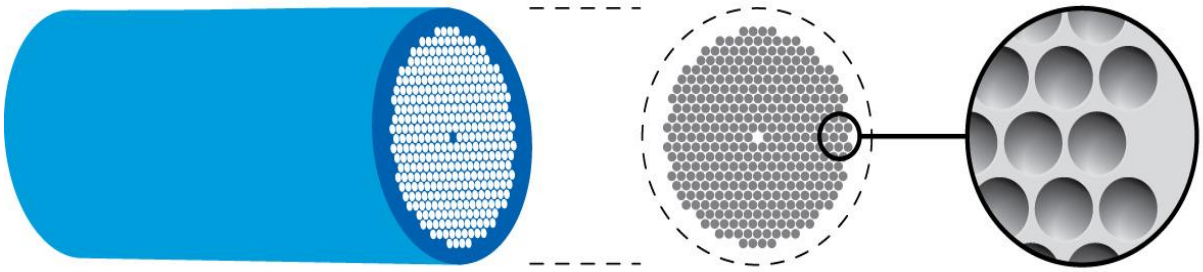

Figure 2.1: Photonic Crystal Fiber [28].

They typically have two kinds of cross sections: an air-silica cladding surrounding a solid silica core or an air–silica cladding surrounding a hollow core. The light-guiding mechanism of the former is provided by means of a modified total internal reflection (index guiding), while the light-guiding mechanism of the latter is based on the photonic band gap effect (PBG guiding). The number, size, shape, and the separation between the air-holes as well as the air-hole arrangement are what confer PCFs unique guiding mechanism and modal properties. This gives PCF many unique properties such as single mode operation over a wide wavelength range, very large mode area, and unusual dispersion. While optical interferometers offer high resolution in metrology applications, the fiber optic technology additionally offers many degrees of freedom and some advantages such as stability, compactness, and absence of moving parts for the construction of interferometers. The two commonly followed approaches to build fiber optic interferometer are: two arm interferometer and modal interferometer. Two- arm interferometer involves splitting and recombining two monochromatic optical beams that propagate in different fibers which requires several meters of optical fiber and one or two couplers. Modal interferometer exploits the relative phase displacement between two modes of the fiber. In modal interferometers compared to their two-arm counterparts the susceptibility to environmental fluctuations is reduced because the modes propagate in the same path or fiber.

There are two guidance mechanisms depending on the PCF geometry.

i. Index guided fiber or holey fiber: Index-guided fiber consists of the solid core where light is guided by the modified total internal reflection.

ii. Photonic bandgap fiber: Photonic bandgap fiber has a hollow core and follows photonic bandgap mechanism.

2.1.1 Index-guided microstructure fiber

Although the principles of guidance and the characteristics of index-guided PCFs are similar to those of conventional fiber, there is greater index contrast since the cladding contains air holes with a refractive index of 1 in comparison with the normal silica cladding index of 1.457 which is close to the germanium-doped core index of 1.462. A fundamental physical difference, however, between index-guided PCFs and conventional fibers arises from the manner in which the guided mode interacts with the cladding region. Whereas in a conventional fiber this interaction is largely first order and independent of wavelength, the large index contrast combined with the small structure dimensions cause the effective cladding index to be a strong function of wavelength. For short wavelengths the effective cladding index is only slightly lower than the core index and hence they remain tightly confined to the core. At longer wavelengths, however, the mode samples more of the cladding and the effective index contrast is larger. This wavelength dependence results in a large number of unusual optical properties which can be tailored. For example, the high index contrast enables the PCF core to be reduced from around 8 μm in conventional fiber to less than 1 μm, which increases the intensity of the light in the core and enhances the nonlinear effects. This property, which cannot be attained in conventional fibers, is particularly significant for broadband applications such as wavelength division multiplexed transmission. As PCFs have a wider range of optical properties in comparison with standard optical fibers, they provide for the possibility of new and technologically important fiber devices. When the holey region covers more than 20% of the fiber cross-section, for instance, index-guided PCFs display an interesting range of dispersive properties which could find application as dispersion-compensating or dispersion-controlling fiber components. In such fibers it is possible to produce very high optical nonlinearity per unit length in which modest light intensities can induce substantial nonlinear effects. In addition, filling the cladding holes with polymers or liquid crystals allows external fields to be used to dynamically vary the fiber properties. The temperature sensitivity of a polymer within the cladding holes may be employed to tune a Bragg grating written into the core. By contrast, index-guided PCFs with small holes and large hole spacings provide very large mode area (and hence low optical

nonlinearities) and have potential applications in high-power delivery (e.g. laser welding and machining) as well as high-power fiber lasers and amplifiers. Furthermore, the large index contrast between silica and air enables production of such PCFs with large multimoded cores which also have very high numerical aperture values (greater than 0.7). Hence these fibers are useful for the collection and transmission of high optical powers in situations where signal distortion is not an issue. Finally, it is apparent that PCFs can be readily spliced to conventional fibers, thus enabling their integration with existing components and subsystems. A Index-guided microstructure fiber and Photonic bandgap fibers are shown in figure 2.2.

2.1.2 Photonic bandgap fibers

Photonic bandgap (PBG) fibers are a class of microstructured fiber in which a periodic arrangement of air holes is required to ensure guidance. This periodic arrangement of cladding air holes provides for the formation of a photonic bandgap in the transverse plane of the fiber. As a PBG fiber exhibits a two-dimensional bandgap, then wavelengths within this bandgap cannot propagate perpendicular to the fiber axis (i.e. in the cladding) and they can therefore be confined to propagate within a region in which the refractive index is lower than the surrounding material. Hence utilizing the photonic bandgap effect light can, for example, be guided within a low-index, air-filled core region creating fiber properties quite different from those obtained without the bandgap. Although, as with index-guided PCFs, PBG fibers can also guide light in regions with higher refractive index, it is the lower index region guidance feature which is of particular interest. In addition, a further distinctive feature is that while index-guiding fibers usually have a guided mode at all wavelengths, PBG fibers only guide in certain wavelength bands, and furthermore it is possible to have wavelengths at which higher order modes are guided while the fundamental mode is not. In this case a large hollow core has been defined by removing the silica around seven air holes in the center of the structure. These fibers, which are termed air-guiding or hollow-core PBG fibers, enable more than 98% of the guided mode field energy to propagate in the air regions. Such air-guiding fibers have attracted attention because they potentially provide an environment in which optical propagation can take place with little attenuation as the localization of light in the air core removes the limitations caused by material absorption losses. The fabrication of hollow-core fiber with low propagation losses, however, has proved to be quite difficult, with

losses of the order of 13 dB km^{-1}. Moreover, the fibers tend to be highly dispersive with narrow transmission windows and while single-mode operation is possible, it is not as straightforward to achieve in comparison with index-guiding PCFs. An Index-guided microstructure fiber and Photonic bandgap fibers are shown in figure 2.2.

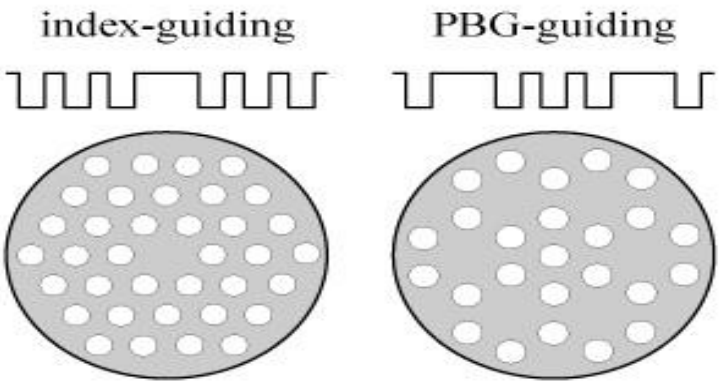

Figure 2.2: Index-guided microstructure fiber and Photonic bandgap fibers [29].

2.2 THz Waveguide

The terahertz (THz) or T-ray part of the electromagnetic spectrum is located between millimetre wave and infrared frequencies. Although there are no clearly defined limits for this region, it is generally defined to be from 0.1 THz to 10 THz. This part of the frequency spectrum was little explored because of the difficulty involved in generation of this radiation and a lack of a perceived need. However, during the last three decades the hardware has evolved to some measure and there have been many research on terahertz spectroscopic applications. Waveguides in the THz regime are no exception; i.e., several waveguide solutions based on technologies from both electronics and photonics have been explored. There are several benefits in having low-loss and low-dispersion waveguides. The primary application of waveguides is to transport electromagnetic waves (and consequently information) from one point to another [30]. Waveguides have also been exploited as sensing and imaging probes [31-32], as the main medium of quantum-cascade lasers [33], to guide waves in subwavelength regimes (beyond the diffraction limit), and to offer tight

confinement of the electromagnetic waves to the structure beyond the Rayleigh range. The potential benefits for the THz region are similar. The foremost advantage is that the bulk optics used for manipulating THz radiation in free space can be replaced by waveguides in THz time-domain spectroscopy (TDS) systems. This will open up new opportunities in further development of compact THz systems and consequently lab-on-chip systems to create advanced biosensors [34]. The diffraction limited spot size can be reduced further, resulting in a resolution improvement over free-space THz imaging systems. Also, tight mode confinement can be achieved by exploiting waveguides with subwavelength features. This is beneficial for THz sensing applications, specifically for noninvasive and label-free molecular detection, and gas and liquid spectroscopy [35-37]. A minute sample (a few micro-liters volume for THz [38]) can be replaced in or at the vicinity of the waveguide where strong interaction with a THz pulse is achieved due to the existence of a large power fraction of the guided mode. Other THz devices such as the near-field scanning optical microscope, THz sources based on quantumcascade lasers, imaging, and communication technologies, which revolve around THz waveguides, will have improved functionalities. Several types of THz waveguides are discussed below.

2.2.1 Metallic Waveguides

Metallic waveguides for THz radiation guidance are mostly scaled down versions (in terms of dimension) of well-known guiding devices from microwave and radio frequencies. The electromagnetic waves at THz frequencies are not as dissipative in metallic components as they are for higher frequencies such as visible light. Thus metallic structures still can be used for guidance in this regime. Hollow metallic circular/rectangular waveguides [39], parallel-plate waveguides [40], coaxial waveguides [41], metal wire waveguides [42], parallel-plate photonic waveguides [43], metal sheet waveguides [44], and metallic slot waveguides [45] are examples of metallic waveguides for guidance of the THz spectrum. In 1999, McGowan et al. [46] demonstrated that circular waveguides have lower loss (α = 0.7 cm^{-1} at 1 THz) relative to coplanar and microstrip transmission lines (α = 14 cm^{-1} and α = 18 cm^{-1}, respectively). This is due to the fact that the propagating THz pulses experience only Ohmic losses due to the metallic body of the circular waveguide, while they suffer from three different loss mechanisms when propagating via transmission lines, i.e., Ohmic losses due to

metal strips, dielectric losses due to substrate, and radiative losses. However, THz pulses propagating through a circular waveguide experience strong dispersion near the cut-off frequency associated with the fact that the transmitted THz pulse through these waveguides is stretched with the higher frequencies arriving earlier in time, i.e., a negative chirp. As an example, a ≈1 ps duration THz pulse after propagating 25 mm through a 280 μm diameter circular brass waveguide stretches to ≈ 40 ps [39]. It was also demonstrated both theoretically and experimentally that rectangular metallic waveguides have similar losses to circular waveguides, for 0.65–3.5 THz bandwidth [39].

Parallel-plate waveguides structure consists of two parallel conducting plates positioned close together (108 μm gap in between the plates for THz [40]). The structure supports single TEM mode propagation, which is the lowest-order TM mode: TM0. The TEM mode has no cut-off frequency. Thus, unlike the circular and rectangular metallic waveguides that suffer from extreme broadening of the THz pulse near the cut-off frequencies, the parallel-plate waveguide has no group-velocity dispersion [47]. Moreover, the electric field of a parallel-plate waveguide is linearly polarized and perpendicular to the plates. This facilitates the coupling of linearly polarized THz pulses into the structure. Attenuation constant less than 0.3 cm^{-1} and with almost no pulse broadening (zero dispersion) is observed for a parallel plate waveguide within the bandwidth from 0.1 to 4 THz [48]. The Ohmic losses due to the finite conductivity of the plates and divergence losses due to beam spreading in the unguided direction are the main loss mechanisms in these waveguides.

The TE1 mode is the second higher-order mode that can be excited in the parallel-plate waveguide [49-50]. The TE1 mode is excited if the input beam is polarized parallel to the plates, while the TEM mode is excited when the input beam is polarized perpendicular to the plates. The selection of which mode to excite in parallel-plate waveguides depends on the application.

Bare metal wires also known as a Sommerfeld wire, is a single cylindrical conductor (wire). Electromagnetic waves propagate as weakly guided radial surface waves along an infinitely long wire of circular cross section, due to the finite conductivity of the metal, and are called surface plasmon waves. Only the principal mode, a radially symmetric transverse magnetic wave (TM01), travels along the wire and has remarkably low loss and low group-velocity

dispersion, whereas all other modes have high attenuation, which makes the wire effectively single mode. The guided surface wave and the single wire are respectively called the Sommerfeld wave and the Sommerfeld wire, because Sommerfeld found the first rigorous solution of Maxwell's equations, for wave propagation on a single wire [42, 51, 52]. In comparison to other metallic waveguides, the metal surface area to propagating THz pulses is reduced, leading to lower Ohmic losses. Despite its superior transmission behavior, the bare metal wire suffers from radiation losses. Any perturbation of the structure, e.g., bending, or even in the vicinity of the wire (within the region of the extended field) leads to high radiation losses due to the loose confinement of the mode to the structure. Coating the wire with a dielectric is an approach to improve the confinement. However, for the THz spectrum, the dielectric coating introduces frequency dependent loss to the propagating mode [51].

Wachter et al. [53] proposed metallic slot waveguides for the guidance of THz radiation to increase the field confinement to the waveguide compared to the metal wire. The structure was made up of two planar slabs (20 mm × 300 μm) located d = 270 μm apart from each other. Compared with the bare metal wire, the electromagnetic fields are more confined to the slot waveguide (more than 50% of guided mode power is within the area not exceeding one wavelentgth around the slot waveguide, while this number is less than 22% for bare metal wire [53]). However, the attentuation loss of slot waveguides is higher than metal wires. The propagating mode in a slot waveguide is in contact with a larger metal area compared to that of a metal wire, leading to higher attenuation losses for the slot waveguide. The attenuation constant of a slot waveguide made from silicon wafer coated with Ti and Au is less than 0.07 cm^{-1} in the frequency range 0.1–1 THz with almost zero dispersion [53].

2.2.2 Dielectric Waveguides

Another major category of non-planar waveguides for the THz spectrum is dielectric waveguides. These waveguides are also known as fibers if they are flexible and have circular cross sections and are mostly used at higher frequencies, such as IR and optical frequencies, where metallic waveguides are dissipative. Dielectric waveguides suffer from material absorption since suitable dielectric materials for fabrication of waveguides are lossy. Although high-resistivity silicon has extremely low loss ($\alpha < 0.05$ cm^{-1} for frequencies below 2.5 THz [54]), it is not amenable for fabrication of many waveguide geometries. The material choice and waveguide structure have a great impact on the waveguide performance, not only

on transmission loss but also on dispersion. As can be observed, polymethyl methacrylate (PMMA) and polycarbonate (PC) have relatively higher losses compared to those of high-density polyethylene (HDPE) and polytetrafluoroethylene (PTFE, best known as Teflon). It should be noted that the material properties listed here are based on published results [55-58], and these values could differ slightly depending on the material supplier [55]. Among the polymers cyclic olefin copolymer (COC), commercially known as TOPAS and Zeonex, has the lowest material absorption losses in the THz range. The refractive index of these polymer materials is in the range of 1.4–1.7. These polymer materials have been widely used as host materials for THz waveguides, as filling materials (materials that are combined with the sample under investigation to exclude saturation of the strong absorption modes) to increase the dynamic range of the measurement, and as a sample cell window material for liquids and gases in the THz range. There are no dielectric materials with negligible absorption in the THz spectrum except for air. Thus, where possible, air is usually the material of choice as the core material for THz bandgap waveguides.

The dielectric waveguides for THz guidance can be divided into three classes: hollow-core, solid-core, and porous-core waveguides. The guiding mechanism for each class of structure is different. The guiding mechanisms in all-dielectric hollow-core waveguides come from formation of either photonic bandgaps or anti resonances with the immediate cladding structure. If the waveguides have an inner metallic coating, then the mode is guided via reflection from the metal coating, which presents a highly reflective mirror. On the other hand, the guiding mechanisms in solid-core and porous-core waveguides are based on total internal reflection if the average refractive index of the core is greater than that of the cladding (e.g., air-clad). When the average refractive index of the core is smaller than that of the cladding, the guiding mechanism is via formation of the photonic bandgap [59]. The fabrication process of dielectric waveguides has benefited from the advance fabrication process of optical waveguides, especially microstructured optical fibers (MOFs) and IR waveguides. The fabrication techniques for MOFs usually have two stages. The first stage is the fabrication of a fiber preform, which is the scaled-up version of the fiber. In the second stage, the fiber preforms are drawn to fibers often via a caning stage to provide a central core region with smaller scale structure. There are a range of techniques available for fabrication of MOF preforms: stacking of capillary tubes, drilling holes in the bulk material, casting into

a microstructured mold, and extrusion [60]. On some occasions, due to the larger dimension of THz waveguides compared to that in the optics, the fabrication of waveguides encountered fewer steps. THz hollow-core and solid-core microstructured waveguides, the waveguide preform by itself is suitable for THz guidance, resulting in the elimination of the second stage in the fabrication process, i.e., the drawing process [61-64]. In the area of fabrication of THz waveguides, there are also some techniques borrowed from fabrication of hollow-core IR waveguides [65], e.g., using a sputtering ring chamber or wet-chemistry technique to deposit metallic/dielectric layers on/inside a tube.

2.2.2.1 Hollow-Core Waveguides/Fibers

Guiding mode through the hollow core is the common feature of waveguides. In general, the guiding mechanisms in all-dielectric hollow-core waveguides are either via formation of photonic bandgaps or due to anti resonances with the immediate cladding structure [66-67]. The cladding features the inner ring and struts resonantly reflect the mode back into the core, and the cladding thickness dictates the width of the transmission bands. In the former guiding mechanism, the cladding does not support modes for certain ranges of frequency, so the guided modes stay in the core. Waveguides such as microstructured bandgap fibers [68-69] and Bragg fibers [70-71] are two well-known examples of this class in optics. In the latter guiding mechanism, there is a low overlap between the core guided modes and cladding modes by virtue of the low density of states in the cladding, which leads to confinement of the mode in the core. Kagomé [72-73] and square [74-75] lattice hollow-core microstructured fibers, in which the guiding mechanism is due to the antiresonance effect of the lattice, are the well-known examples in this class. There is a strong relationship between the bandgap and antiresonance description in 1-D structures [76-77]. For the THz frequency range, the material absorption of hollow-core waveguides is low since the THz radiation is predominately concentrated in the air core, which is transparent to THz radiation. This class of THz waveguides is divided into three types: single/ hybrid-clad waveguides, microstructured bandgap waveguides, and Kagome microstructured waveguides.

In 2003 Hidaka et al. [78] proposed a hollow-core THz waveguide made of ferroelectric poly vinylidene fluoride (PVDF), a flexible polymer, to increase the transmission coefficient. Such waveguides are considered as single clad waveguides.

Hybrid-clad waveguides refer to structures with a minimum of two different clad layers. Each clad layer can be a simple material layer [e.g., dielectric coating] or a composite material layer [e.g. metamaterial] [79]. Generally, each layer has special properties (functionality) and contributes to the propagation of the mode. However, there are cases in which the cladding layer acts only as the supporting base for the next layer [80-82]. A common layer employed in hybrid-clad THz waveguides is a metal layer by virtue of its superior reflecting surface for TE modes [80-81]. This approach was adapted from IR metal-coated hollow glass waveguides [65]. When the thickness of the metal film is greater than the skin depth of the metal at THz, the hollow-core waveguides with an inner metal coating perform like metal waveguides with a circular cross section (metal pipe). In contrast to metal waveguides, these hollow-core waveguides are flexible and have a smoother and homogeneous inner surface.

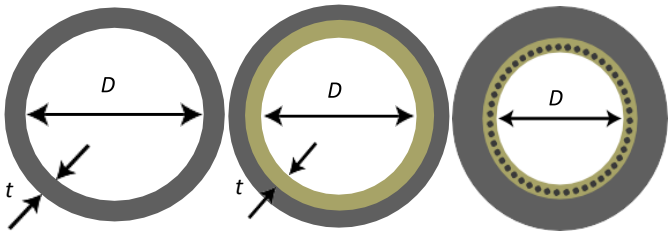

Figure 2.3: (a) Hollow-core single clad waveguide, indicating the diameter, *d*, and the dielectric/metal thickness, *t*. Hollow-core hybrid-clad waveguides (b) Metal waveguides with dielectric inner coating, (c) Metal waveguides with a thin layer of metamaterial [83].

Hollow-core microstructured bandgap waveguides consist of a hollow core surrounded by micrometerscale air holes in the cladding, which run along the length of the waveguide. The mode confines and propagates in the core when the cladding does not support the mode; i.e., the cladding forms a two-dimensional photonic crystal and the excited mode lies in the bandgap of the cladding. The concept of hollow-core microstructured bandgap fibers has been expanded to THz frequencies [84-85]. The advantages of using these fibers for guiding THz are the following: first, like all other hollow-core fibers, most of the electromagnetic field propagates predominantly in the air core (which is a transparent medium for THz); and

second, at THz frequencies (longer wavelength compared to invisible and optics), scattering losses are low and Due to the large core diameter (larger than operating wavelength), these hollow pipe waveguides suffer from multimode propagation, and they are not flexible. Moreover, higher-order modes are easily excited, especially at bends or small discontinuities.

The guiding mechanism in Kagome hollow-core microstructured waveguides is via the formation Von- Neumann Wigner quasi-bound states within a continuum [65]. The cladding of these waveguides does not support photonic bandgaps. The core guided modes cohabitate with those of the cladding modes without notable interation. In other words, the guided modes confined in the hollow core are prevented from efficiently coupling to the cladding due to the antiresonance effect of the Kagome lattice.

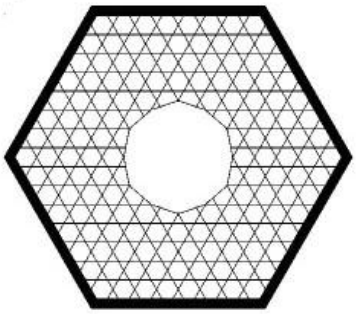

Figure 2.4: Kagome Structure hollow core fiber[86].

2.2.2.2 Solid-Core Waveguides/Fibers

The electromagnetic waves are guided based on well-known total internal reflection in solid-core waveguides/fibers, where the effective refractive index of the core is higher than that of the cladding. Solid-core waveguides have three categories: waveguides with air-cladding (microwires), waveguides with microstructured cladding, and waveguides with single air-hole discontinuity in the core.

The guiding mechanism of solid-core microstructured waveguides, also known as solid-core photonic crystal fiber (PCF), is achieved by total internal reflection, while in PFCs with low-index cores, e.g., air cores, it is achieved by the photonic bandgap effect. Han et al. [87] were the first to realize, fabricate, and experimentally demonstrate the loss and dispersion of solid-core microstructured waveguides in the THz spectrum. The attenuation of a guided mode of

the solid-core microstructured waveguides depends on the field confinement in the core and the core material absorption. It has been shown that the main contribution of the transmission loss is the material absorption loss. The loss of solid-core microstructured waveguides was further improved by using COC, commercially known as TOPAS and Zeonex, as the host material. Compared to air-core microstructured waveguides, the solid-core microstructured waveguides have a broader transition bandwidth since the guiding mechanism in them is based on total internal reflection and not on antiresonance or bandgap effects. Thus these waveguides are better suited for broadband THz guidance. Although the TOPAS solid-core microstructured waveguides can be bent (90° bend) by heating the waveguide, generally they are rigid due to their large dimension (a few millimeters).

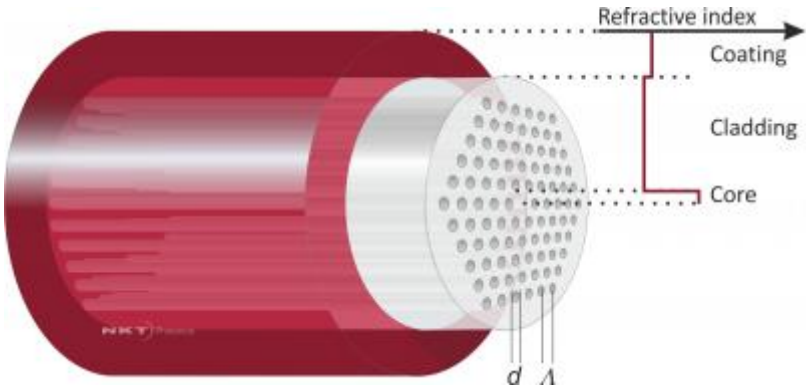

Figure 2.5: Solid core and microstructured cladding waveguide. [87]

2.2.2.3 Porous Core Waveguides

Porous-core waveguides, porous fibers, are created by including a distribution of subwavelength air holes within the core of an air-clad fiber. The guiding mechanism in these waveguides is based on total internal reflection. A typical example of porous fiber is shown in Figure 2.6. The distribution, shape, and size of the holes determine the porosity of the structure, which is defined as the fraction of the air holes to the core area. In the early days of THz porous fibers, only circular air holes were considered [88-90]. However, other geometries can also be introduced into the core of these fibers [91-93]. These porous fibers offer lower material losses compared to a similar diameter of subwavelength air-clad waveguides (microwires) by virtue of less material residing in the core. This concept has

been used in the optical regime; i.e., elongated void regions have previously been used in photonic crystals to improve the transmission efficiency simply by reducing the material [94]. This is not the only benefit of having subwavelength air holes within the core. It has been shown that for similar diameter, porous fiber offers better confinement and consequently lower bending losses [90]. Moreover, it has been shown that for similar loss values, porous fibers enable reduced distortion (frequency dependent loss and dispersion) of a broadband THz pulse compared to microwires. It has also been demonstrated that introducing asymmetrical subwavelength air holes in the core of porous fibers leads to modal birefringence [91]. Modal birefringence arises from effective refractive index differences between x- and y-polarization modes.

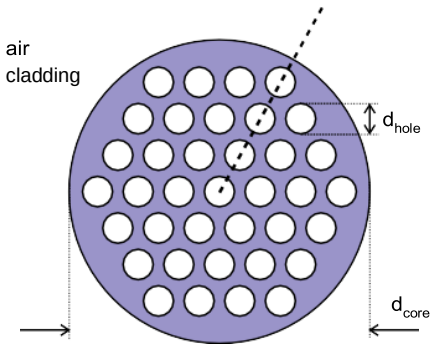

Figure 2.6: Porous Core waveguide [83].

2.3 Applications of PCF

Due to large variety of adjustable parameters, like numerical aperture, dispersion, attenuation, birefringence, non-linear index, the number of modes, etc., which are determined solely by the geometry of PCF, many interesting fiber structures can be fabricated with similar fabrication effort. However, PCF applications are still on the scale of laboratory devices, mainly for the purpose of research and development and mass commercialization have yet to come. We will point out some application aspects regarding high power fiber lasers, as one of the most prominent area for application of PCF technology, and some aspects regarding the use of PCF in telecommunications, being the largest optical fiber industry by far. Besides this, PCFs are very promising in non-linear optics for generation of white light of high spatial coherence (i.e. super continuum), parametric amplification and oscillation, correlated photon-pair formation and many other purposes. PCFs can also be used in sensory systems and laser tweezers applications.

2.4 Characterization of THz wave guiding and sensing properties

In this Section, different properties characterization of THz waveguide and sensor are implied the mathematical relations of the losses, sensitivity, effective area, power fraction, mode test, dispersion. To evaluate the sensing properties additionally numerical aperture, beam divergence, spot size and nonlinearities are mathematically expressed here.

When a light is guided by a PC-PCF with specific mode field profile, it faces a loss mechanism which is called effective material loss (EML). To improve the performance of a PCF THz waveguide, it is necessary to minimize the material absorption loss as much as possible. The EML can be calculated as [13].

$$\alpha_{eff} = \sqrt{\frac{\varepsilon_0}{\mu_0}}\left(\frac{\int_{mat} n_{mat} |E|^2 \alpha_{mat} dA}{\left|\int_{all} S_z dA\right|}\right) \quad (1)$$

where, α_{eff} is the effective material loss, ϵ_0 indicates the relative permittivity and μ_0 indicates relative permeability into the free space, '*mat*' is the material area and '*all*' indicates the whole fiber area and n_{mat} and α_{mat} are represent the refractive index and bulk absorption loss of Topas respectively. S_z denotes the z-component of the Poynting vector. Where, *E* is the electric field component and *H* magnetic field component.

Confinement losses are the losses which are originated from the leaky nature of the modes and the non-perfect structure of the PCF fiber. Then, depending on the wavelength, number of hole rings, and hole size, modes will be guided with a structure dependent loss. Confinement loss exists in every porous core PCF which is attained from the imaginary part of the complex refractive index (n_{eff}), which can be assessed as [95].

$$L_c = \left(\frac{4\pi f}{c}\right) Im(n_{eff})[cm^{-1}] \quad (2)$$

where L_c denotes the confinement loss, f is called operating frequency, c indicates the speed of light in vacuum, and $Im(n_{eff})$ the imaginary part of the complex effective refractive index of the guided mode.

In practical implementation the THz waveguide faces another loss which is called bending

loss. When the bending radius exceeds some critical value of highly porous PCF it creates a large impact on total transmission loss. The refractive index difference of core and cladding of proposed highly porous PCF structure is very small. So small bending radius of PCF forces the light to propagate through the cladding section, which increase the bending loss. The bending loss can be calculated as [20].

$$\alpha_{BL} = \frac{1}{8}\sqrt{\frac{2\pi}{3}}\frac{1}{\beta A_{eff}} F[\frac{2}{3} R_b \frac{(\beta^2 - \beta_{cl}^2)^{2/3}}{\beta^2}] \tag{3}$$

where, α_{BL} is the bending loss and A_{eff} represents effective area. R_b called bending radius and propagation constant $\beta = 2\pi n_{co} / \lambda$, and $\beta_{cl} = 2\pi n_{cl} / \lambda$, here, n_{co} & n_{cl} are the refractive index of core and cladding respectively and function $F(x) = x^{-1/2} e^{-x}$, where $x = \frac{2}{3} R_b \frac{(\beta^2 - \beta_{cl}^2)^{2/3}}{\beta^2}$.

The area covered by the interaction of light intensities with matters is called effective area. Higher value of effective area is desirable for laser and communication devices. It can be characterized as [96]

$$A_{eff} = \frac{\left[\int_{all} I(r) r dr\right]^2}{\left[\int_{all} I^2(r) dr\right]^2} \tag{4}$$

where, A_{eff} denotes the area covered by the guided modes, $I(r) = [E_t]^2$ is the transverse electric intensity distribution of total cross section of the fiber and '*all*' indicates the whole fiber area.

Another important parameter of PC-PCF for THz waveguide is core power fraction which is defined as the ratio of total power propagation through the PCF and the power tightly propagated inside the core region [97]. The core power fraction of the PCF can be calculated as,

$$\eta = \frac{\int_X S_z dA}{\int_{All} S_z dA} \tag{5}$$

where, *X* indicates that the area of the region of interest through which the power is to be calculated and '*All*' denoted the total PCF area.

Low and flat dispersions are essential for efficient transmission because high dispersion limits the data transmission rate. The dispersion is directly affected by the effective refractive index (ERI) of PCF. Hence, the ERI of topas is constant at wide THz frequency range, which exhibits near-to-zero material dispersion and as a result, total dispersion of PCF is termed as waveguide dispersion. The waveguide dispersion β_2 is given by [98]

$$\beta_2 = \frac{2}{c}\frac{dn_{eff}}{dw} + \frac{w}{c}\frac{d^2 n_{eff}}{dw^2}, ps/THz/cm \tag{6}$$

where, $\omega = 2\pi f$ is the angular frequency in radian, c represents the speed of light into free space and n_{eff} is the ERI of the proposed waveguide structure.

Number of guided modes supported by optical fiber is obtained by cutoff condition known as V-parameter. Modeness or V-parameter can be calculated by the following equation [99]

$$V = \frac{2\pi rf}{c}\sqrt{n_1^2 - n_2^2} \tag{7}$$

Here, n_1 and n_2 denote the effective refractive index (ERI) of the core and cladding region respectively, f indicates the operating frequency and c represents the velocity of light in free space.

According to the value of V-parameter, fiber can be classified in two types. If , $V \leq 2.405$, then the fiber will be considered as single mode fiber (SMF) and if $V > 2.405$, then the fiber will act as a multimode fiber (MMF).

For terahertz PCFs, chemical sensitivity totally intensity of light-matter interaction dependent but this is a function of absorption coefficient at a particular frequency. It can be expressed as per Beer-Lambert law [100-102].

$$I(f) = I_0(f)\exp[-r\alpha_m l_c] \tag{8}$$

where *I(f)* and I_0 are the intensities of light with and without the presence of the analyte needed to be detected and *r* is relative sensitivity, α_m represents the absorption coefficient and l_c is the channel length, and *f* is the operating frequency.

The absorbance of the analytes to be detected can be determined as [100].

$$A = \log \frac{I}{I_0} = -r\alpha_m l_c \tag{9}$$

If n_r is the refractive index of the sample needed to be detected, n_{eff} is the modal effective index, *k* represents how much light interact with the matter, then relative sensitivity coefficient *r* can be calculated as

$$r = \frac{n_r}{n_{eff}} \times k \tag{10}$$

$$k = \frac{\int_{sample} R_e(E_x H_y - E_y H_x)dxdy}{\int_{total} R_e(E_x H_y - E_y H_x)dxdy} \times 100 \tag{11}$$

where *Ex* , *Ey* and *Hx* , *Hy* are the electric field and magnetic field components of the guided modes respectively.

For sensing purpose polarization maintaining property is very important to improve the sensitivity. When we will use a PCF for polarization maintaining terahertz application, it is very essential to increase the birefringence as much as possible. Highly asymmetric core and cladding structure will give high birefringence. If we denote *B* is denoted the birefringence and n_x and n_y are considered as the effective refractive indices of the x and y polarization modes respectively, then we can write [103].

$$B = \left| n_x - n_y \right| \tag{12}$$

The light compile ability of a PCF is defined as a numerical aperture (NA). It's actually calculated from critical angle. The value of NA depends on refractive index difference of

core and cladding. For sensing application large value of NA is desirable which can be achieved when the refractive index difference between the core and cladding is large. NA can be expressed as [104].

$$NA = \frac{1}{\sqrt{1 + \frac{\pi A_{eff} f^2}{c^2}}} \tag{13}$$

Where, *Aeff* is the effective area of the proposed THz sensor.

For optical devices nonlinearity is an essential parameter. Power density inside the optical devices defines nonlinearity as a function of effective area. The nonlinearity of a fiber can be expressed by,

$$\gamma(\lambda) = \frac{2\pi}{\lambda} \frac{n_2}{A_{eff}}, W^{-1}m^{-1} \tag{14}$$

where, n_2 is the nonlinear coefficient

The radius of the beam is called Spot size which can be represented by the following formula.

$$w_{eff} = R \times (0.65 + \frac{1.619}{V^{3/2}} + \frac{2.879}{V^6}) \tag{15}$$

where, *R* interpret the radius of the lattice.

Beam divergence is an important parameter which measure how fast the beam spreading. Beam spreading can be calculated as,

$$\theta_{radian} = \tan^{-1}(\frac{\lambda}{\pi w_{eff}}) \tag{16}$$

Where, w_{eff} Spot size

2.5 Conclusion

In this Chapter, different types of THz waveguide, their guiding mechanism and various applications are explained. Moreover different losses and limitation of THz waveguide are discussed elaborately. The theoretical analysis of guiding and sensing properties is also discussed.

Chapter 3

Proposed Terahertz Waveguide

In this Chapter a photonic crystal fiber structure for THz wave propagation is presented. Design methodology of proposed PCF structure using COMSOL software is discussed in this chapter. Different wave guiding properties of presented PCF are analyzed. Numerical outcomes of designed THz waveguide are evaluated here for ensuring the capability of this THz waveguide. Finally fabrication feasibility of presented waveguide is discussed with a brief conclusion.

3.1 Design Methodology of Proposed PCF

A sectored cladding with a square core PC-PCF is designed for THz wave guidance. The 2D cross-sectional view of the proposed PCF structure and the amplified view of the core are shown in Figure 3.1. The cladding of the proposed PCF is constructed by four (4) air fragments which are arranged in a circular manner where TOPAS is used as a bulk material. In our suggested PCF we consider the height of the fragment, h = 1176μm, width of the strut, S = 7.5μm and length of the strut, L = 1114μm as an optimum value. Four (4) square air holes are used to fill the squared core section. Where the side length of the core is fixed at L_s = 300μm after proper analysis. In core region, side length of each air block L_1 = 138.75μm, center to center distance of adjacent air lattices and opposite air lattices are L_2 = 146.25μm and L_3 = 206.80μm respectively. To get the desired output, the above values have been selected as optimum. For optical waveguides, several polymer materials such as PMMA, Teflon, TOPAS, and Zeonex etc. can be used as the background material.

In this reported PCF, Topas is considered as a host material which has some excellent properties that make TOPAS unique from the other materials. For example, refractive index of TOPAS is constant over 0.1–2 THz, as a result dispersion is negligible, bulk material loss is lower at wide range of frequency which is minimum compared to other polymers, it is insensitive to environmental aspects such as humidity and water vapor absorption and it has chemical inertness with special bio-sensing properties etc.

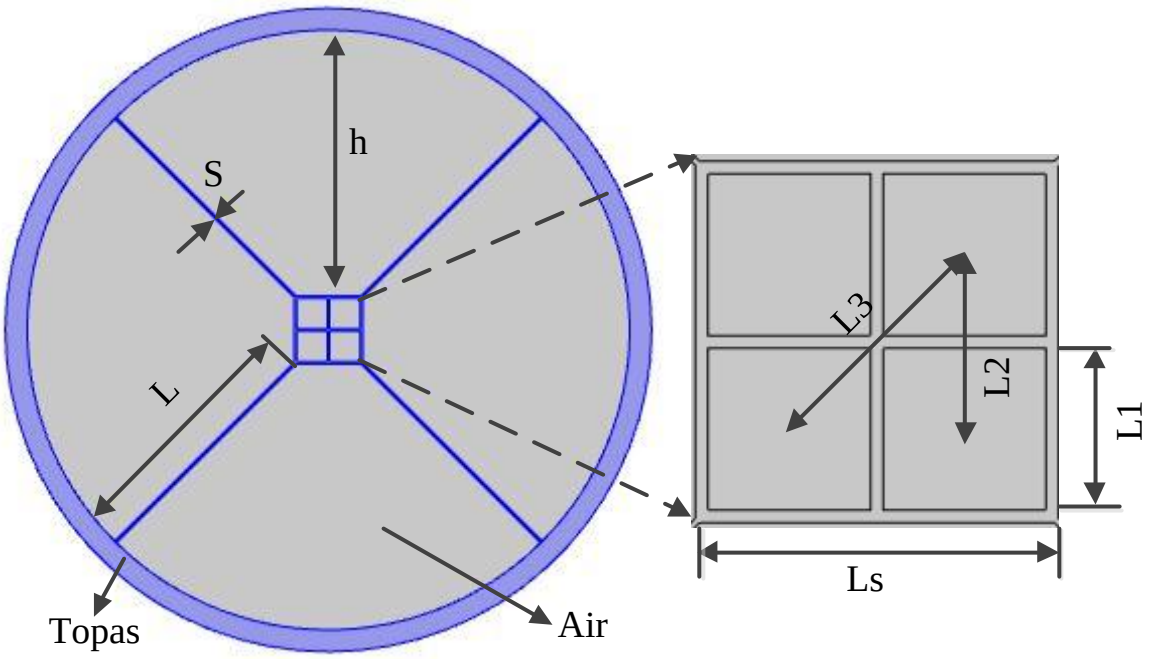

Figure 3.1: Geometry of the proposed PC-PCF design.

3.2 Results and Analysis

The distribution of light at different frequencies is shown in Figure 3.2 and from this figure it is clearly seen that the light is tightly confined inside the core and negligible interaction of light in the cladding section. To design and evaluate the performance of proposed PC-PCF structure a finite element method (FEM) based software COMSOL 5.3a has been used because of the ability of FEM to deal with any photonic waveguide devices. If the design structure is very complex, it is also able to provide full vector analysis. A circular perfectly matched layer (PML) has been considered as a boundary condition to the outer structure to absorb the electromagnetic field propagating towards the surface.

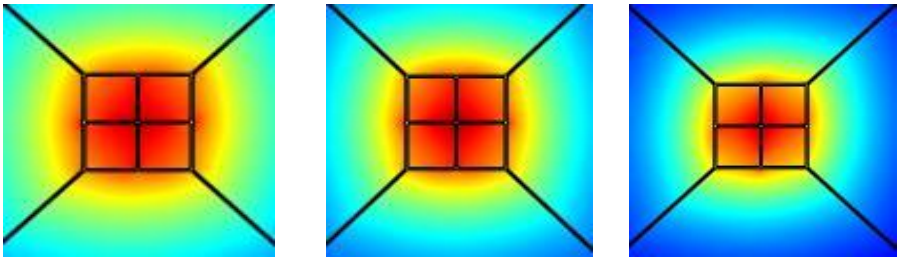

Frquency= 0.8 THz Frquency = 0.9 THz Frquency = 1 THz

Figure 3.2: Distribution of light at different frequencies

The light absorption by the background material is the main defeat in porous core photonic crystal fiber based THz wave guide. This loss is termed as effective material loss (EML). Effective material loss depends on how much light interact with the background materials. Confinement loss is another important parameter that must be considered in PCF design. It depends on the core porosity and the number of air holes used in the cladding. It is calculated by taking the imaginary part of the complex refractive index.

The response of EML and Confinement loss at different parameters are shown in Figures 3.3 – 3.6. From Figure 3.3 it can be observed that EML is enhanced due to the growth of frequency, which fulfill the theoretical postulate of calculating EML as per empirical formula $\alpha(\nu) = \nu^2 + 0.63\nu - 0.13$ [dB/cm] [101]. It is also investigated from Figure 3.3 and 3.4 when increase the core side length or decrease the core porosity as a function of frequency, the EML responses as a upward manner because when increase the core size or decrease the core porosity, the amount of background material in the core region will be increased. This is true, because increasing the volume of background material, the interaction of light with material will be increased, which consequently boost the EML. At optimum design parameters, core side length = 300µm and porosity = 85%, a very negligible EML of 0.009 cm^{-1} is obtained at 1THz operating frequency which is the lowest among the previously reported [10-16] PC-PCF.

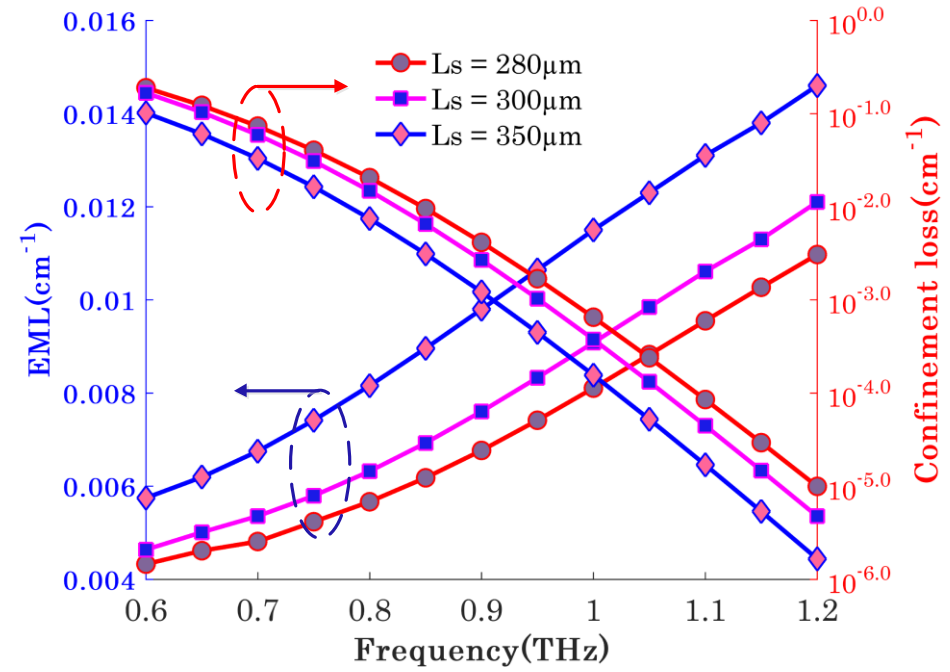

Figure 3.3: EML and Confinement loss as a function of frequency for different core size (Ls).

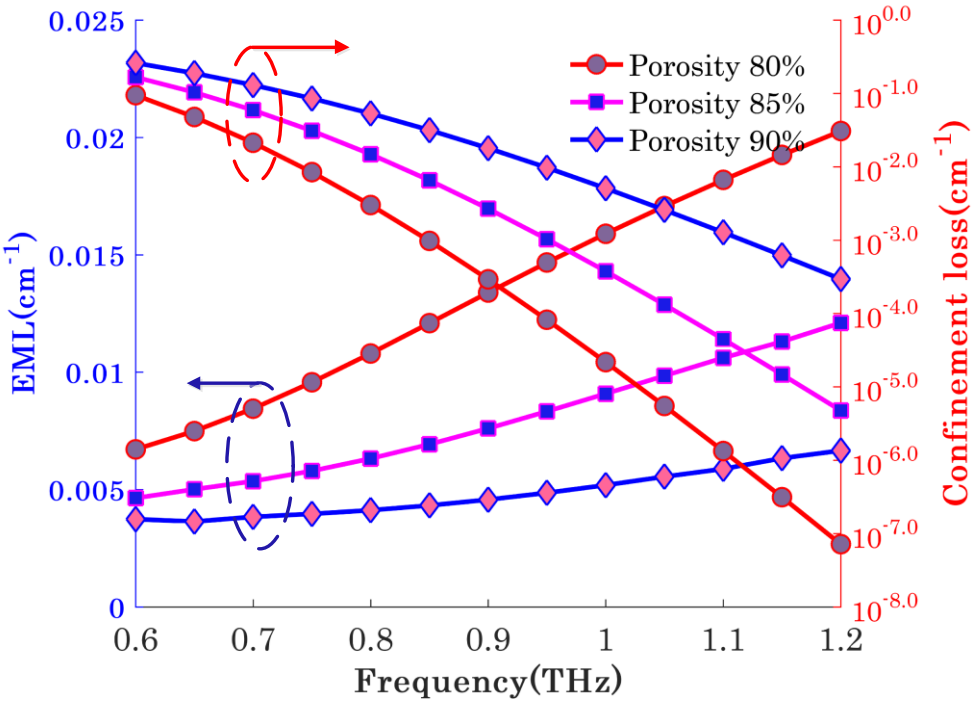

Figure 3.4: EML and Confinement loss as a function of frequency for different porosity.

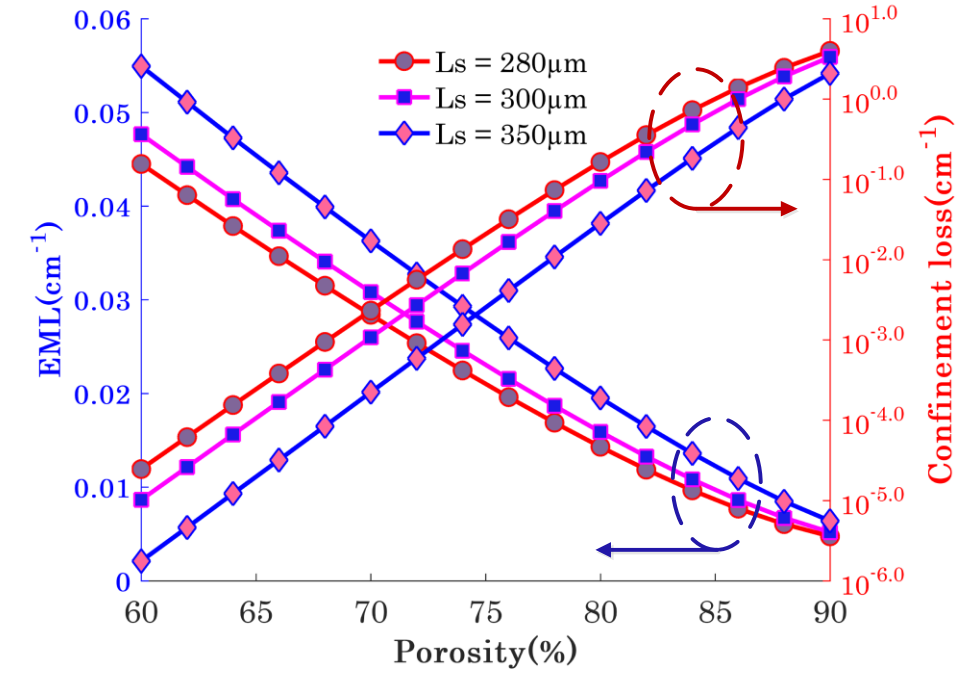

Figure 3.5: EML and Confinement loss as a function of porosity for different core size (Ls).

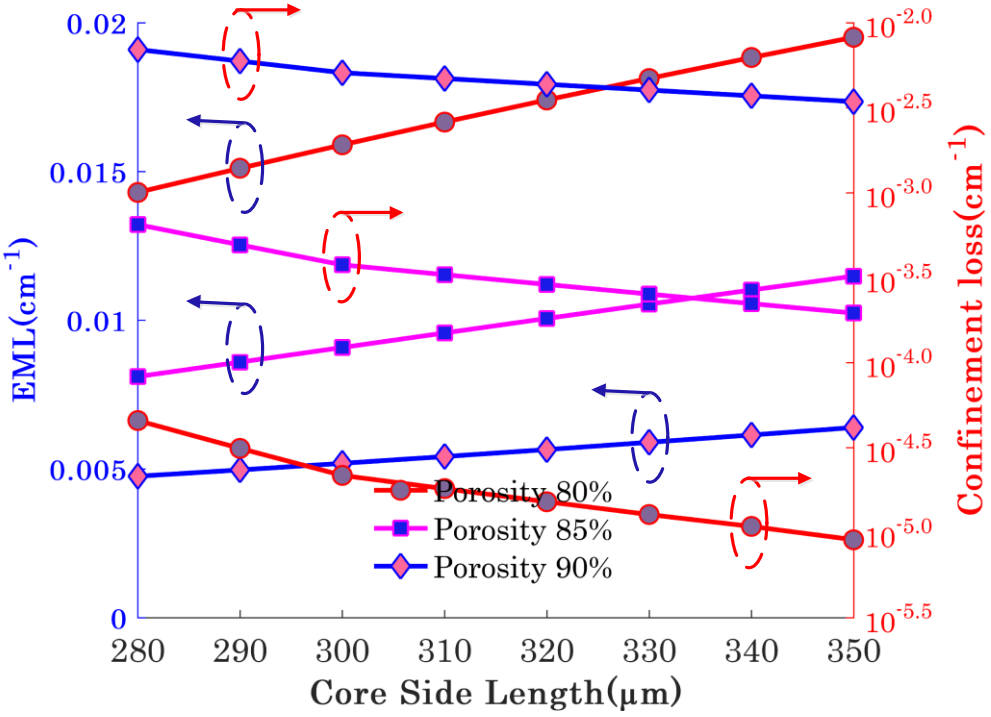

Figure 3.6: EML and Confinement loss as a function of core side length for different porosity.

The behavior of confinement loss is also depicted in Figure 3.3 and 3.4 varying the frequency for different core sizes and different porosities. From these figures it is described that the confinement loss swiftly drops with the increase of frequency, the reason is that the refractive index difference between the core and cladding is increased when frequency is increased, as results the imaginary part of the complex refractive index is increased which consequently reduces the confinement loss. The value of confinement loss of 10^{-4} cm^{-1} is found at optimum parameters which is also very negligible. The behavior of EML and confinement loss for different porosities and variations of core size at optimum frequency 1THz are also elaborately depicted in Figure 3.5 and 3.6.

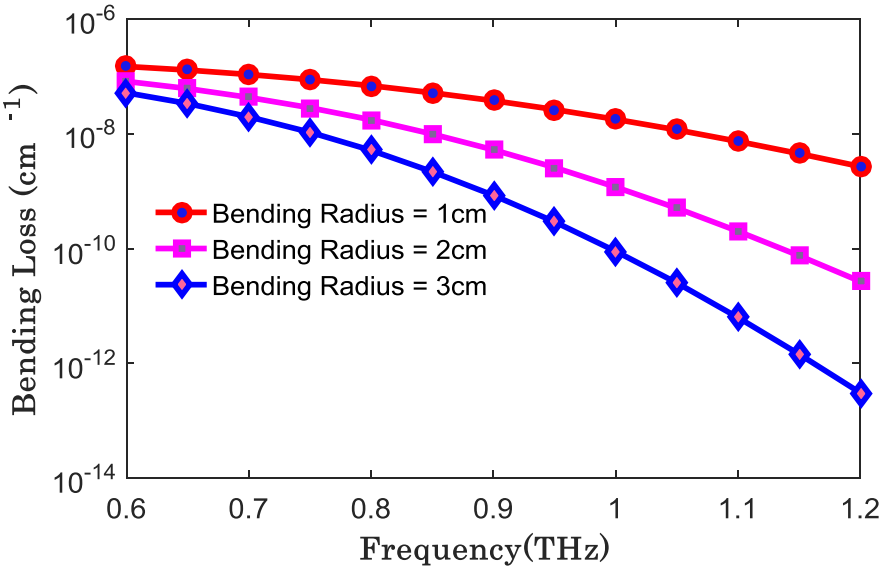

Figure 3.7: Bending loss with respect to frequency for different bending radius.

In practical implementation the THz waveguide faces another loss which is called bending loss. When the bending radius exceeds some critical value of highly porous PCF it creates a large impact on total transmission loss. The behavior of bending loss with the increment of frequency is presented in Figure 3.7. This figure reveals that the bending loss is a decrement function with the increment of frequency and the numerical value of bending loss of proposed PCF is very negligible. At optimum design parameters this proposed PCF design exhibits bending loss are 0.0179×10^{-6} cm^{-1} at bending radius Rb =

1cm, 0.0118×10^{-7} cm-1 at Rb = 2cm, and 0.0009×10^{-7} cm^{-1} at Rb = 3cm, which is very low compared to EML and confinement loss.

Another vital parameter for PCF is effective mode area. It concern us the quantitative measurement of core area when the mode field is tightly confined inside the core region. A_{eff} as a function of frequency for different core lengths and various porosities which are shown in figure 3.8 and figure 3.9. It is explained that the effective area is a decreasing function with increasing frequency. Increasing the frequency helps less light is being confined in the core region and as a result the effective area is decreased. At optimum parameters of core side length = 300μm and porosity = 85%, the proposed design achieved effective area of 5.48×10^{-7} m^2. It can be also observed that from figure 3.8 and figure 3.9, the increment of core porosity enhances the effective area. The reason is that the mode power is confined by the porous core at lower value of core porosity, consequently the effective area reduces readily.

Power fraction is the quantity that describes the amount of total power propagates in various regions of the PC-PCF. Core power fraction versus Frequency is reported in figure 3.8 and figure 3.9 in the right y axis for various core sizes and porosities. Illustrated from figures, the mode power fraction in the core section increases consequently with the increase in frequency because increase in frequency assists the PCF for tighter confinement, hence the power fraction inside the core increases. Figure 3.8 and figure 3.9 also shows that the core power fraction is flourishing with the increment of core length. The reason is that, when core length increases, more power travel through the core area and in turn the mode power within the core area increases. If we consider different porosities in the case of core power fraction versus frequency then the core power fraction behaves in the opposite way of core length variation. Due to the increment of porosity, some effective powers start to penetrate into the cladding. As a consequence, core power fraction becomes downward but more light passes through the air hole of the core with augmentation of porosity. From our proposed design we attained almost maximum 53% of mode power transmitted through the core region for porosity equal to 80%.

In figure 3.10 and figure 3.11 the nature of effective area and core power fraction for different porosities and core sizes are delineated in detail. It is observed that at optimum parameters, the calculated effective area and core power fraction is very much comparable to previously reported PCF structure [10-16].

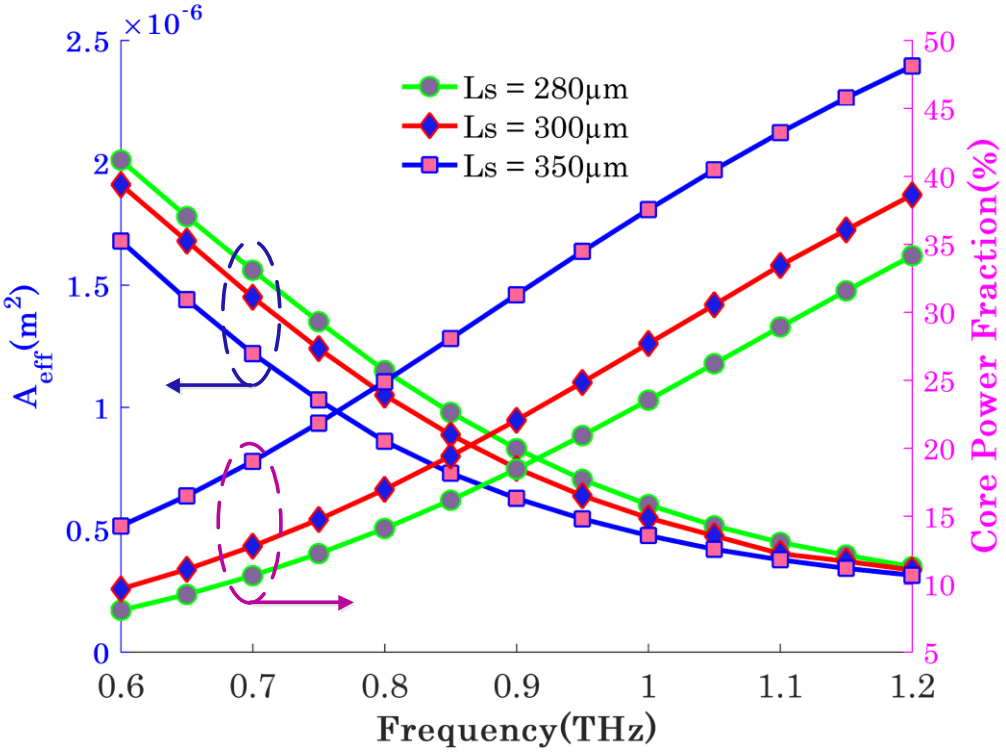

Figure 3.8: Effective area and Core Power Fraction as a function of frequency for different core size (Ls).

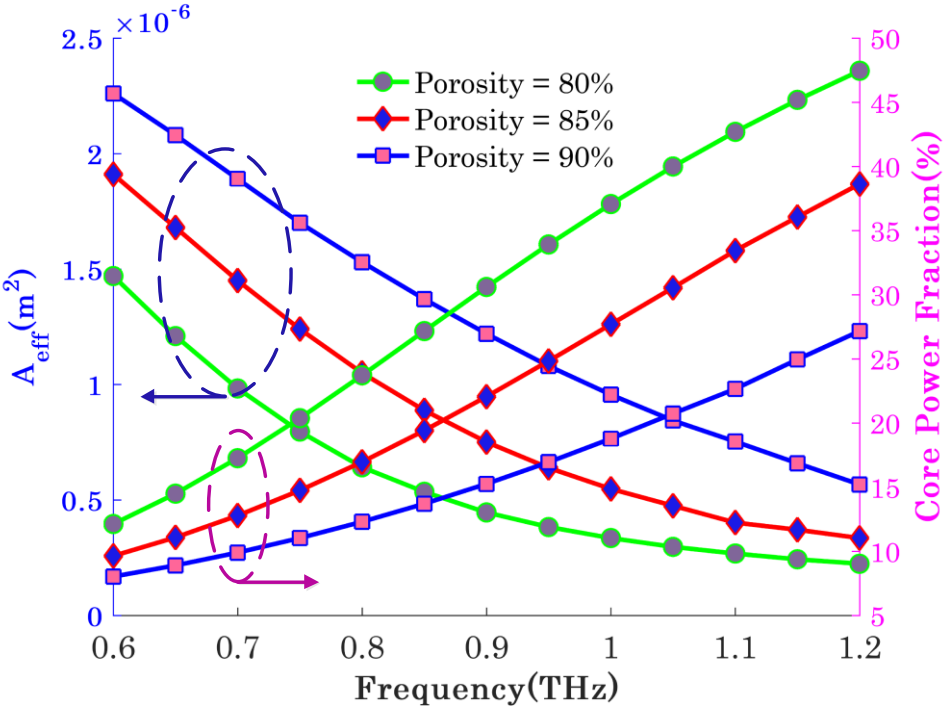

Figure 3.9: Effective area and Core Power Fraction as a function of frequency for different core porosity.

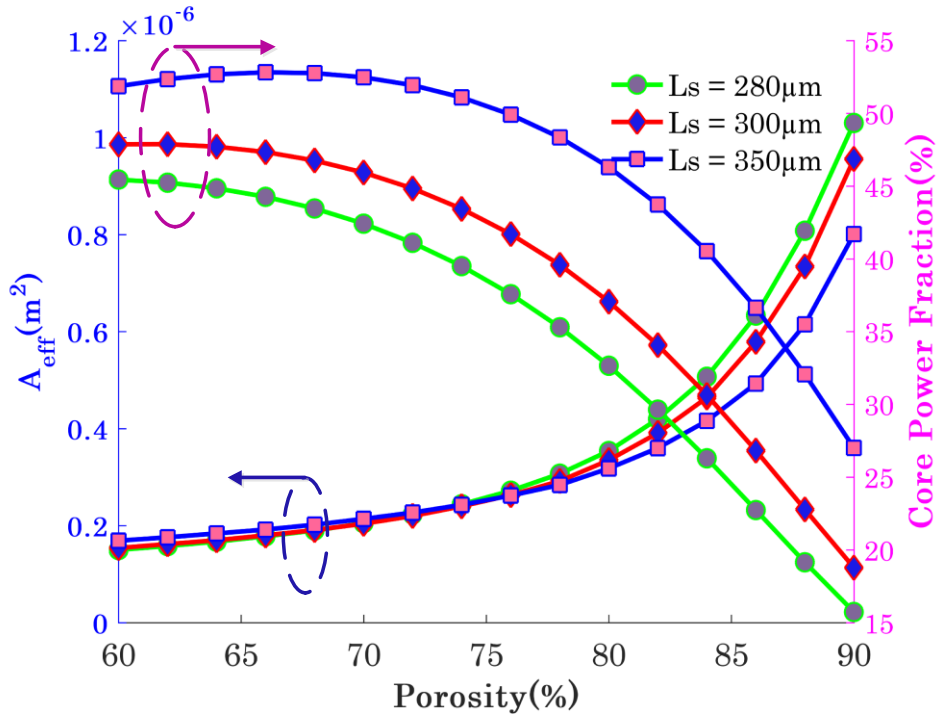

Figure 3.10: Effective area and Core Power Fraction as a function of porosity for different core size (Ls).

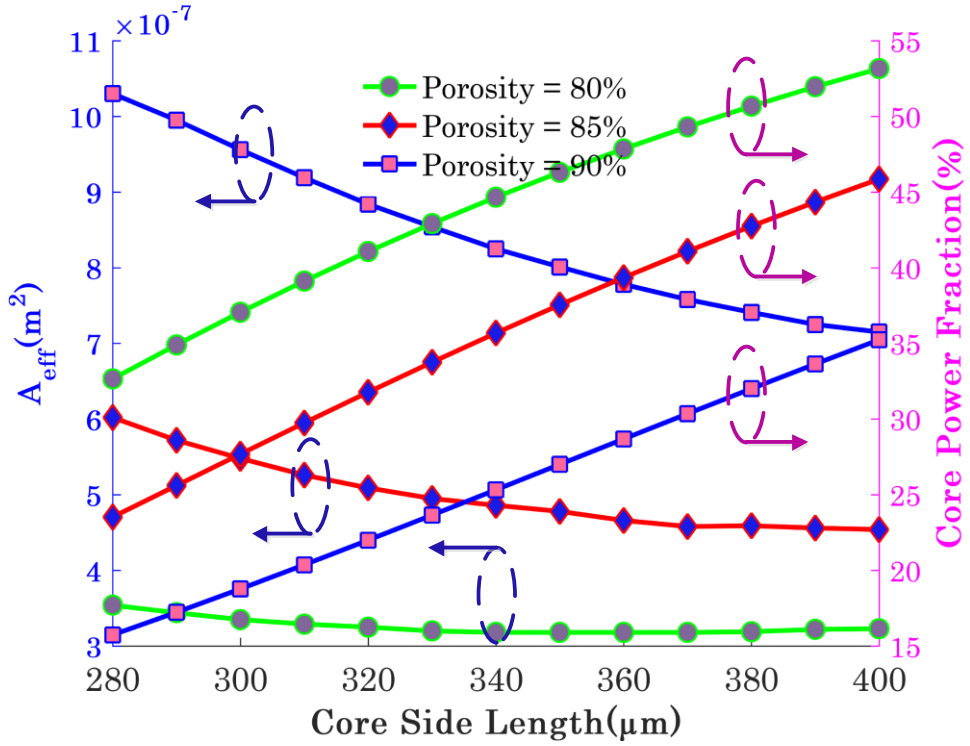

Figure 3.11: Effective area and Core Power Fraction as a function of core side length for different porosity.

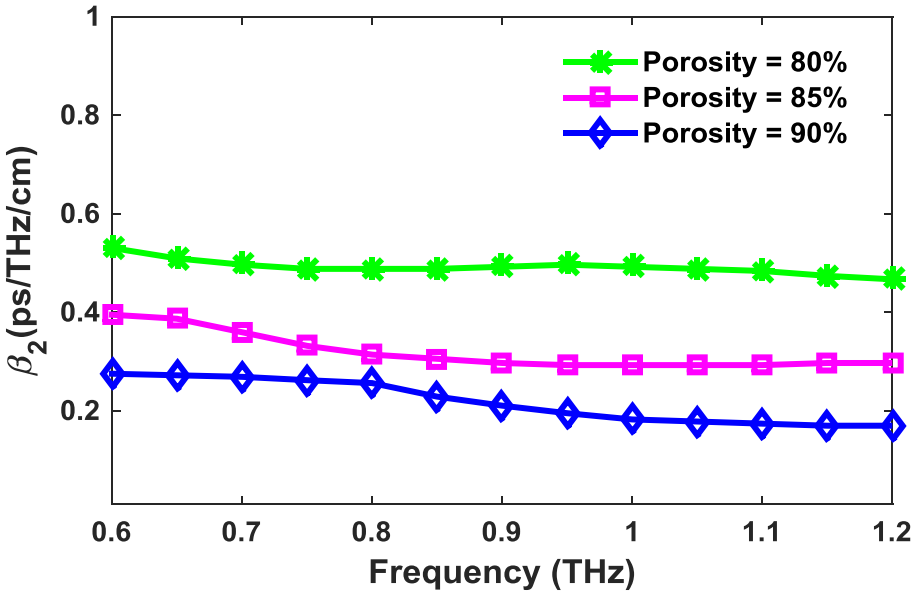

Figure 3.12: Dispersion with respect to Frequency for different Porosities.

Dispersion is an important wave guiding property that measures the amount of pulse spreading of a fiber. The waveguide dispersion as a function of frequency for different porosities is shown in figure 3.12, which nicely visualized that the proposed PCF design has a flattened dispersion and very close to zero over a wide frequency range from 0.6 THz to 1.2 THz. At optimum design parameters of core side length = 300µm and porosity = 85%, the achieved dispersion is 0.3 ps/THz/cm which is less than previously reported THz waveguide designs [10, 14, 16],

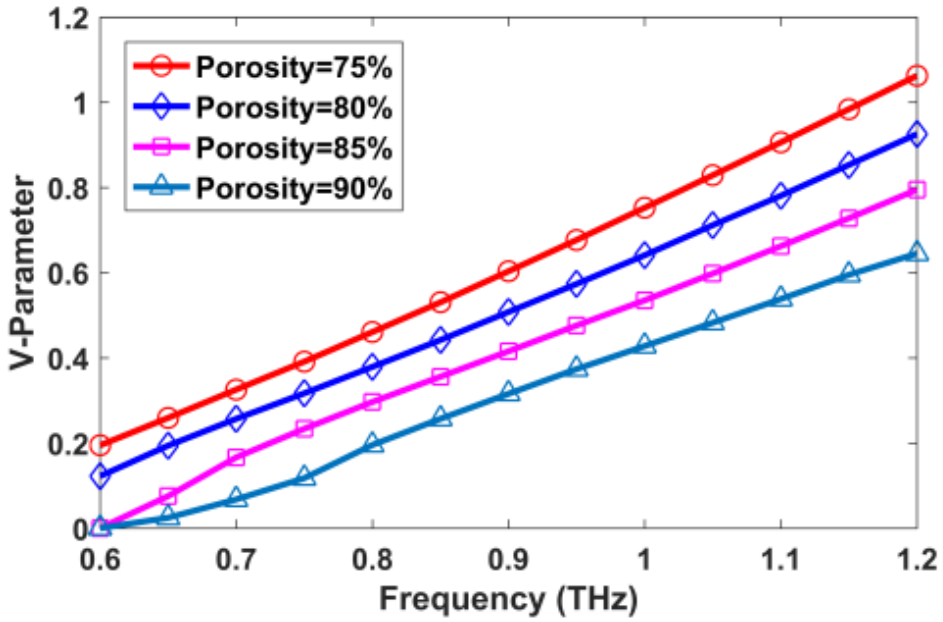

Figure 3.13: V-parameter with respect to Frequency for different Porosities.

Depending on the value of V-parameter, fiber can be classified in two types. If , $V \leq 2.405$, then the fiber will be act as single mode fiber (SMF) and if $V > 2.405$, then the fiber will considered as a multimode fiber (MMF). The behavior of V-parameter within the wide THz frequency range for the proposed fiber is revealed in Figure 3.13. It can be noticed that, the value of V-parameter changes from 0-1. For different porosities, the response of V- parameters are also exhibited in this figure and the value of modeness is less than 2.405 in the range of frequency of 0.6 to 1.2 THz. So our proposed PCF is capable to perform as a single mode fiber which is very demandable for long-haul communication.

Table 3.1: Performance comparison existing porous core PCFs and proposed PC-PCF.

Standard article and Published year	Operating Frequency	EML (cm^{-1})	Geometry	
			Cladding	Core
[10] 2017	1 THz	0.049	Octagonal	Circular
[11] 2017	1 THz	0.035	Hexagonal	Rectangular
[12] 2018	0.85 THz	0.086	Hexagonal	Rectangular
[13] 2018	1 THz	0.06	Rectangular	Elliptical
[14] 2018	1 THz	0.05	Circular	Elliptical
[15] 2018	1 THz	0.030	Hexagonal	Hexagonal
[16] 2018	1.3 THz	0.029	Kagome	Hexagonal
Proposed PC-PCF	**1 THz**	**0.009**	**Sectored (Circular Manner)**	**Square**

Table 3.1 shows the Comparison among previously proposed different shaped porous core PCFs and proposed PC-PCF. From this table it is clearly seen that our proposed design achieved an incredible change in EML reduction and the obtained EML is lowest than ever proposed by any terahertz waveguide at 1THz. Compared to recent published remarkable PCF structures, our proposed geometry is very simple. So, we can audibly say that the geometry and lowest EML of the proposed PCF will play a great role in THz communication and optical communication system.

3.3 Fabrication Possibilities

The proposed PC-PCF contains only four air fragments in the cladding section which are arranged in a circular manner with a square core structure which carry four symmetrical square air hole. The proposed PCF structure is shown in Figure 3.1. Different fabrication techniques are available now to fabricate different shape of air core PCF. Capillary stacking, stack and draw and sol-gel techniques are usually used for circular shaped air holes PCF fabrication but the extrusion and 3D printing fabrication technology are capable to fabricate any types of symmetrical and asymmetrical PCF structures [106-110]. Recently Max Plank Institute fabricated different complex structures PCF using the extrusion technology [109]. So, the proposed simple sectored cladding with square air core structure PCF is easily fabricable using existing PCF fabrication techniques.

3.4 Conclusion

A simple structured photonic crystal fiber has been proposed for ultra-low EML and flattened dispersion THz wave propagation. Numerical value of suggested PCF presents extremely low effective material loss of 0.009 cm^{-1} and flat dispersion of ±0.05 ps/THz/cm at optimum design parameters of core side length = 300 μm, porosity = 85% and 1THz operating frequency. In addition, it exhibits very large effective area of 9.56×10^{-7} m^2 and a high core power fraction of 53.159% at 1THz frequency. Moreover, the simple geometry indicates that the proposed PCF structure will open a new window for PCF applications, as well as for further research in THz propagation.

Chapter 4

Proposed Polarization Maintaining THz Waveguide

In this Chapter a polarization maintaining photonic crystal fiber geometry is presented for THz wave propagation in both polarization modes. Design methodology of proposed PCF structure using COMSOL software is discussed in this chapter. Different wave guiding properties and polarization maintaining characteristics of presented PCF are analyzed. Numerical outcomes of designed THz waveguide are evaluated here for ensuring the capability of this THz waveguide. Finally fabrication feasibility of presented waveguide is discussed with a brief conclusion.

4.1 Design Methodology of Proposed PCF

The end faces view with the enlargement of the core section of designed PCF is shown in figure 4.1. The proposed THz wave guide constructed with hexagonal core structure which filed by a hexagonal sectored four air fragments, where three rectangular sectored the hexagonal structure. The width of the rectangular is W_1 = 5μm and the length of the rectangular depend on the porosity of the core. Porosity is defined as the ratio of air lattices area in the core and total core area. The radius of the core is selected as, r = 150μm and diameter of core D_{core} = 2r = 300μm. In the cladding section eight (08) rectangles are used to sector the whole cladding section, where three types of air fragments are introduced. The rectangular width of the cladding region is also selected, W_2 = 5 μm. More lower value of rectangular width may can causes overlapping between the two adjacent air lattice during fabrication. A perfectly matched layer (PML) is used to protect the unwanted effects by the environment. The geometry and all above mentioned parameters value are selected as optimum for efficient THz wave propagation in both polarization mode with lower EML, less confinement loss, higher core power fraction, large effective area and near zero flattened dispersion.

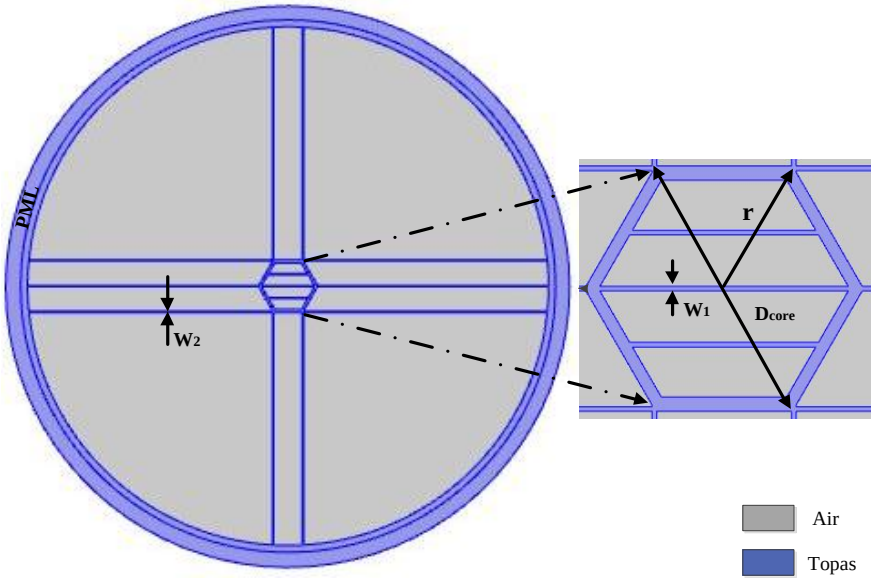

Figure 4.1: End face view of proposed PCF with enlargement of core.

4.2 Results and Analysis

The electromagnetic mode distribution of proposed polarization maintaining PCF is shown in figure 4.2. From figure 4.2 it is very clear the light is tightly confined in the core section in both polarization modes.

Because of asymmetric structure of PCF there is a difference in effective refractive index (ERI) of x-polarization and y-polarization, as a result birefringence is exist in this PCF. A significant ERI difference between x & y mode is required to maintain the polarization maintaining fiber characteristics. The ERI difference between x & y mode with respect to frequency is shown in figure 4.3, which represents a significant ERI difference in x & y mode. The birefringence with respect frequency and core diameter are shown in figure 4.4 and figure 4.5 respectively. At optimum design parameter core diameter = 300µm, porosity = 85% and operating frequency 1 THz the birefringence is 9.2×10^{-3}.

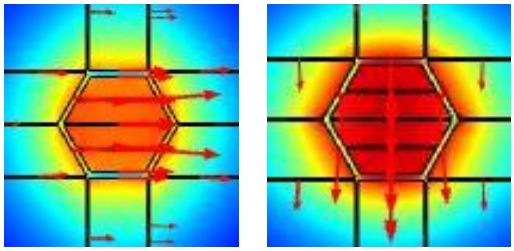

Figure 4.2: Electromagnetic field distribution of proposed PCF, x-mode (left), y-mode (right).

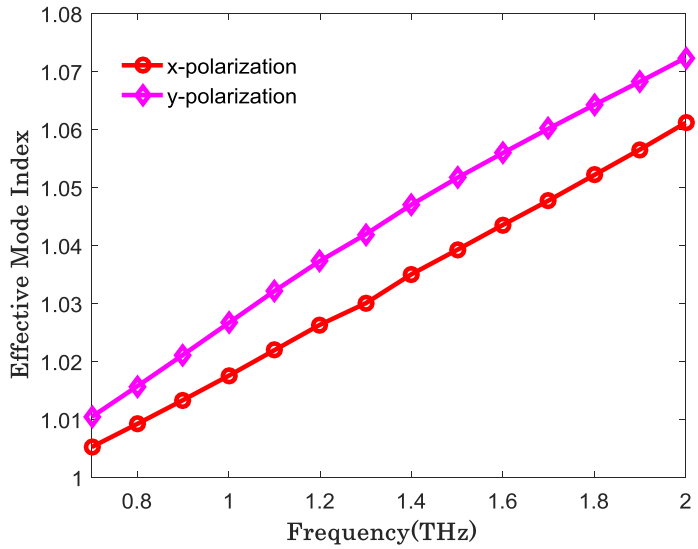

Figure 4.3: Response of EMI with respect to frequency.

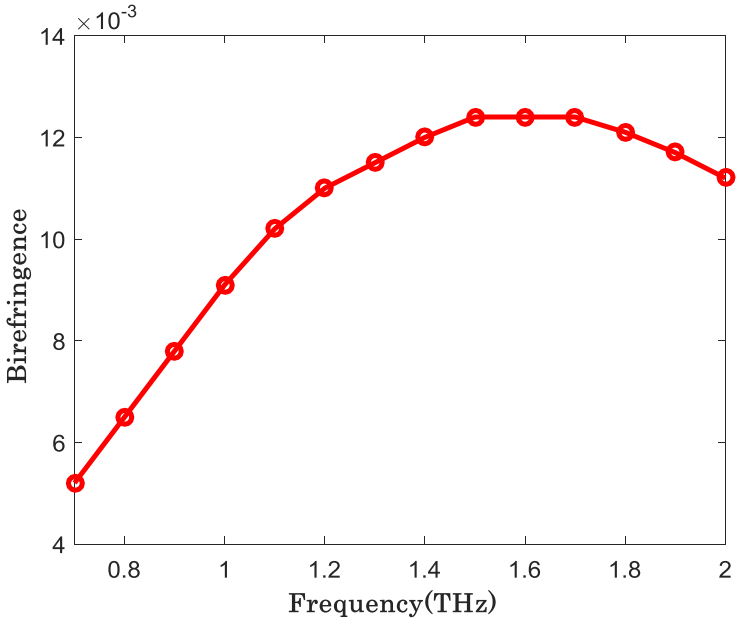

Figure 4.4: Birefringence with respect to frequency.

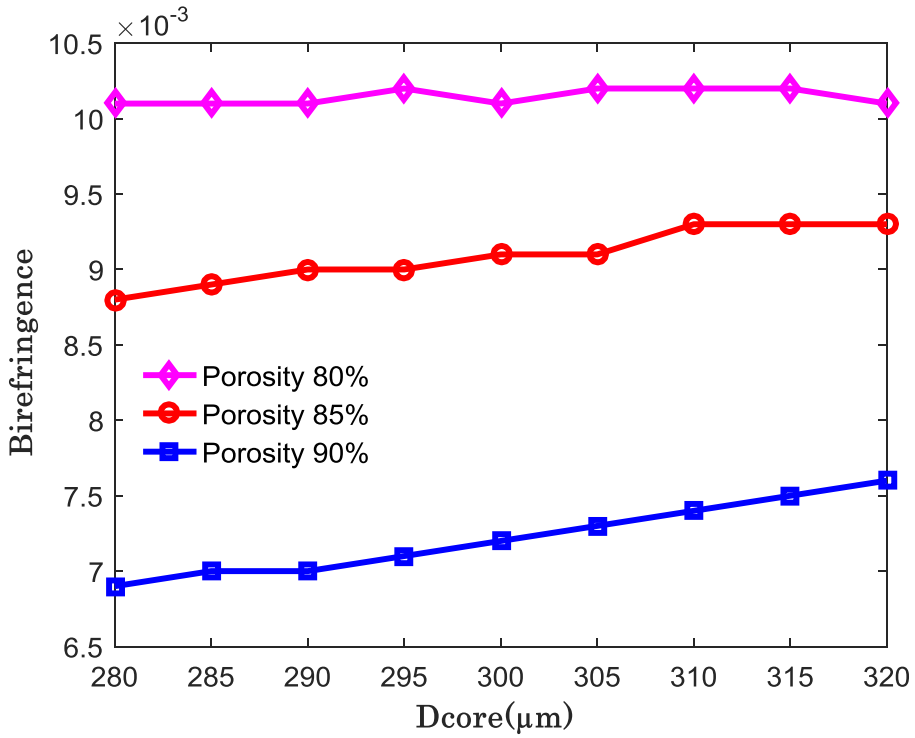

Figure 4.5: Birefringence with respect to core diameter at different porosity.

Figure 4.6 (a) and (b) shows the scenario of EML and confinement loss with the incremental value of frequency for both x and y polarization mode. From these figures it is noticed that the relation between EML and frequency is proportional. This satisfies the theoretical consequence of EML calculation by the empirical equation. This is because the electromagnetic frequency is proportional to EML. At lower frequency, EML is very low but for achieving an optimal structure EML is considered at 1 THz frequency. At 1 THz optimal frequency, values of EML are 0.015 cm^{-1} and 0.025 cm^{-1} for x and y polarization respectively which is lower than previously proposed renowned articles [13,17-20].

Figure 4.6 (a) and (b) also exhibits of confinement loss as a function of frequency for x and y polarization respectively. If frequency is increased then mode power will start to compress in the inner portion of the core, decreasing the confinement loss. At optimal design parameter (f = 1THz, D_{core} = 300μm) , value of confinement losses are 0.00014 cm^{-1} and 0.004cm^{-1} for x and y polarization respectively, which is very low.

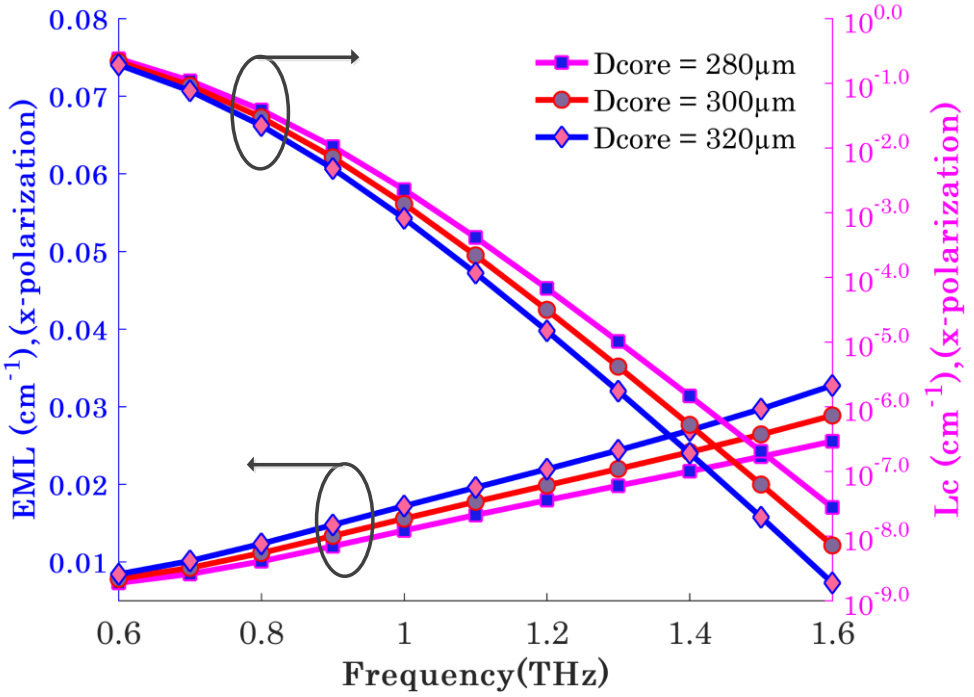

(a)

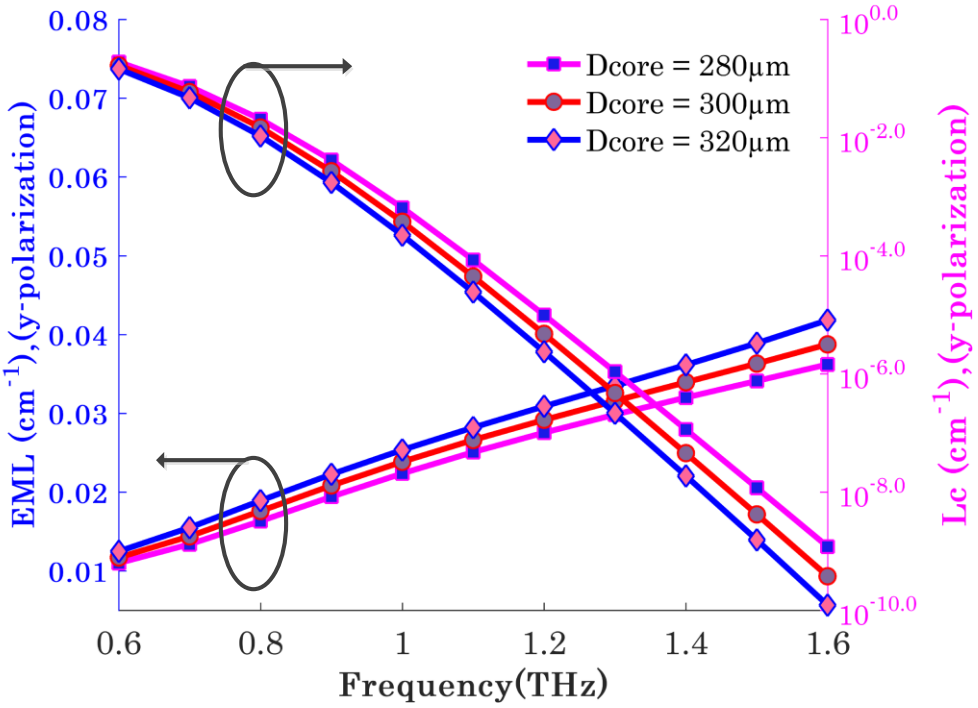

(b)

Figure 4.6: EML and confinement loss with respect to frequency at different core diameter (a) x-polarization, (b) y-polarization

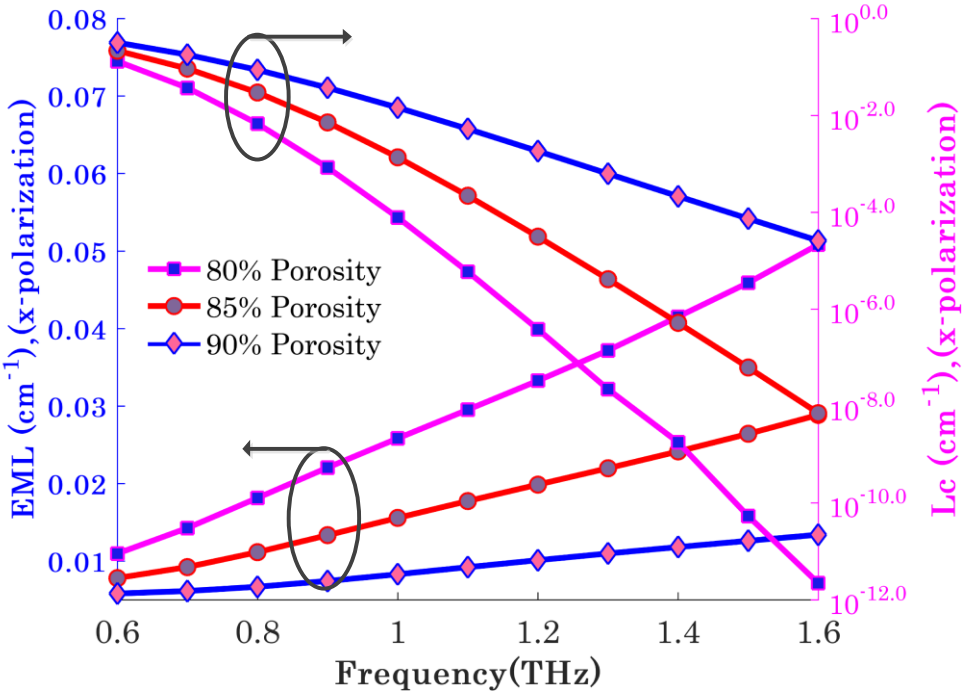

(a)

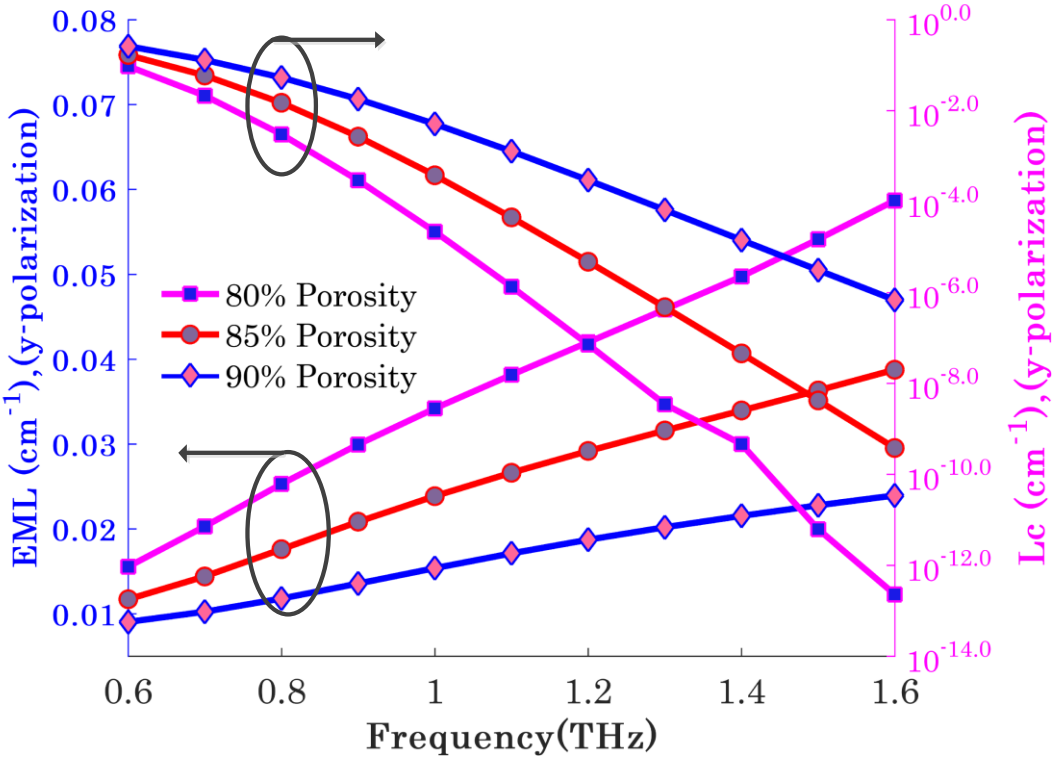

(b)

Figure 4.7: EML and confinement loss with respect to frequency at different porosity (a) x-polarization, (b) y-polarization

It is also observed that when the value of core diameter is scaled up then EML will also increase. This is because if core diameter is increased then background material will obviously increase in the core area, as a result EML will be increased. Besides it is noticed that when the value of core diameter is scaled up then confinement loss is decreased. Because if core diameter is increased then light pulse will more closely propagate through the core region. As a result confinement of light will be tighter with the incremental value of core diameter and confinement losses become downward. Same behaviors in EML and confinement loss will happen when we reduced the core porosity, which is presented in figure 4.7.

Figure 4.8 is depicts effective area and core power fraction as a function frequency for both x and y polarization. From above figures it is observed that when the value of frequency is increased then the value of effective area is decreased sharply. This is because if the range of frequency is increase then light will be confined shortly in the area of core, as consequence of effective area also decreases.

It is also observed that when the value of frequency is scaled up then the value of core power fraction is increased for both x and y polarization mode. The reason behind that if frequency is increased then light absorption by air lattice will obviously increase, because of tightened confinement at higher frequency. As a result core power fraction will be increased. Besides this, it is also depicted in the above figure when core diameter is increased then the value of effective area is decreased rapidly and core power fraction is increased. This is because if the diameter of core is increased then light will be confined closely. So obviously effective area will be decreased. Moreover when the value of core diameter is scaled up then the size of air lattice will obviously increase. Then maximum power will flow through the core region. If major portion of power flows through the internal sector of core then absorption of light by air holes in the core also increased, as a result the value of core power fraction will increase. At optimum design values, this suggested PCF achieved effective area are 3.4×10^{-7} m^2 in x-mode and 2.8×10^{-7} m^2 in y polarization mode. This proposed PCF also shows maximum core power fraction of 47%, which indicates, this PCF able to propagate 47% light through the air holes in the core only.

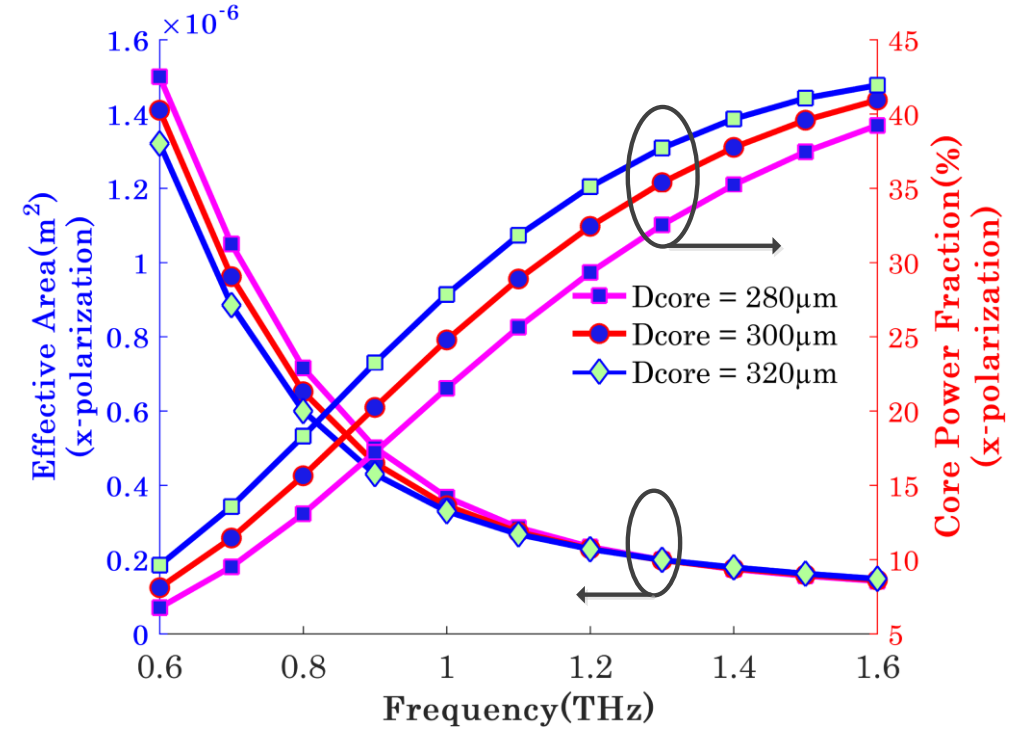

(a)

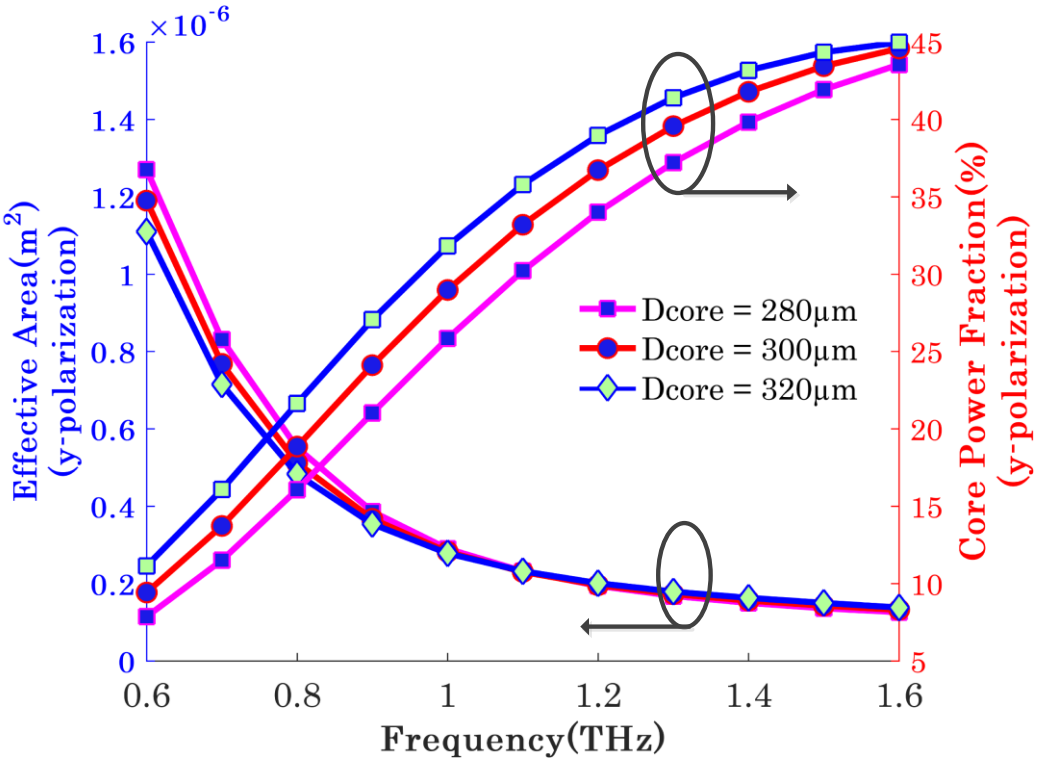

(b)

Figure 4.8: Effective area and core power fraction with respect to frequency at different core diameter (a) x-polarization, (b) y-polarization

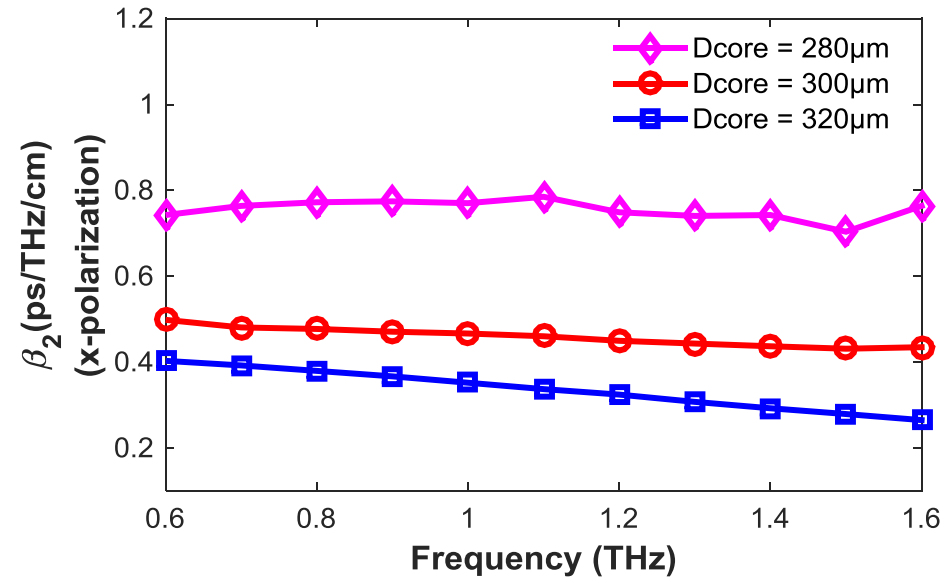

(a)

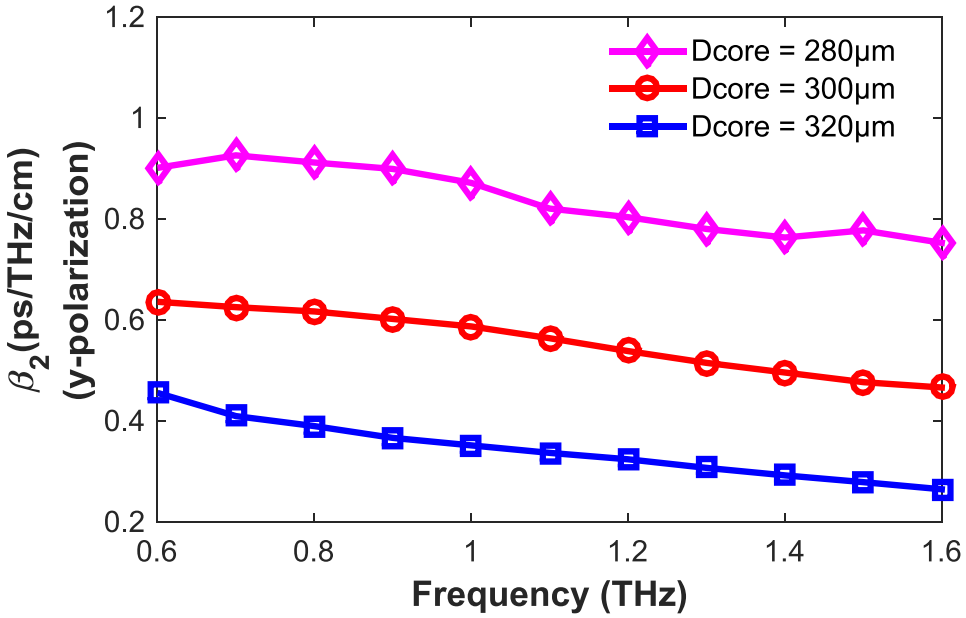

(b)

Figure 4.9: Waveguide dispersion with respect to frequency at different core diameter (a) x-polarization, (b) y-polarization.

Figure 4.9 (a) & (b) shows a flattened dispersion in the frequency range of 0.6 to 1.6 THz for both x and y polarization respectively. In our design, dispersion of 0.46 ± 0.03 (ps/THz/cm) is achieved in x polarization and 0.58 ± 0.08 (ps/THz/cm) y polarization. This is comparable with some other published articles [18-20]. The above mentioned value in this paper satisfies the requirements of lower dispersion in our proposed design. It can be clearly stated that our designed fiber is applicable for long range distance communication. The change of dispersion variation for different core size also depicted in this figures.

Besides performance of different properties as a THz waveguide, practical implementation is a challenge for PCF. Different fabrication techniques are available now for PCF fabrication. Extrusion process is very much efficient for hexagonal core structure PCF fabrication, moreover 3D printing fabrication technique is also applicable for proposed PCF fabrication

4.3 Conclusion

A polarization maintaining PCF is designed and characterizes the different properties for THz wave propagation. The findings of this proposed PCF is that proposed design shows significant birefringence and ultra-low EML in both polarization mode, as well as its display very low confinement loss at optimum design parameters. Additionally its exhibits very flattened dispersion in large range of frequency. Because of considerable high birefringence, large effective area, high core power fraction and design simplicity this PCF is very much feasible for practical implementation as THz wave guide.

Chapter 5

Proposed Terahertz Analytes Sensor

In this Chapter a zeonex based hollow core photonic crystal fiber (PCF) has been proposed for chemicals sensing application. Design methodology of proposed sensor using COMSOL software is discussed in this chapter. Different sensing properties including relative sensitivity, different losses, numerical aperture, beam divergence, spot size, and non-linearity and V-parameter are analyzed here. Numerical outcomes of designed chemical sensor are evaluated for ensuring the capability of this sensor. Finally fabrication feasibility of presented sensor is discussed with a brief conclusion.

5.1 Design Methodology of Proposed PCF

The geometrical cross section view of the proposed HC-PCF sensor is shown in Fig. 5.1 which is constructed by finite numbers of hexagonal lattices in cladding section with a hexagonal shaped hollow core. The HC offers a higher bandwidth while lowering power consumption and being immune to EML over porous core. Besides, the hollow core PCF contains a greater analyte volume inside its core area compared to other core types and the core is only filled with the target analyte instead of bulk material. The proposed infrastructure offers 19 number of hexagonal lattice air holes whereas core is formed by omitting one unit cell. Fig. 5.1 depicts that D is the diameter of air lattice core which is selected to 200 µm as optimum, side length and center to vertex distance of each cell is D/2 and center to center distance of two adjacent lattices is 180 µm.

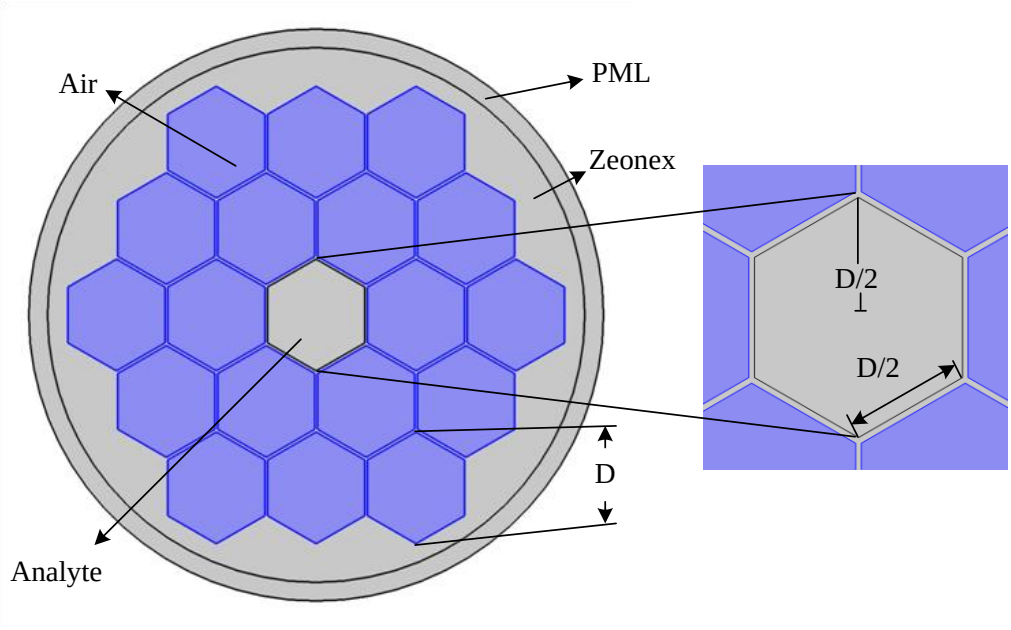

Figure 5.1: Geometry of Proposed PCF.

A perfectly matched layer (PML) absorbing boundary is act as the outer part of the cladding which absorbs outgoing waves of the PCF like an anti-reflecting layer. According to several kinds of analytes, in the core section all supplementary air holes are filled with four different chemicals such as Water (n = 1.33), Benzene (n = 1.366) and Ethanol (n = 1.354), Methanol(n = 1.328) where n is denoted as refractive index [106]. Later, several types of polymer materials are used as a bulk material for optical waveguides such as PMMA (Poly methyl methacrylate), Teflon (Tetrafluroethylyne), Topas (COC), Silica and Zeonex (COP) [111-117].

In our proposed design we selected Zeonex as a background material because of its (i) lower material absorption loss than other polymer materials (0.2 cm^{-1} in terahertz frequency range) (ii) constant index of refraction (n = 1.53) (iii) negligible water absorption (<0.1%) (iv) high glass transition temperature T_g (v) excellent optical stability (vi) high biocompatibility (vii) excellent chemical resistance even at elevated temperatures. [113-114]. If we compare Zeonex and Topas they convey same optical properties but Zeonex has a higher glass transition temperature, high chemical resistivity, higher bio-compatibility, low refractive index and very easy fabrication of the fiber than Topas. Refractive index of the background material is directly related to EML which helps to reduce the effective material loss.

5.2 Results and Analysis

The distribution of light in both polarization mode for different chemicals are shown in Fig. 5.2 and from this figure it is clearly seen that the light is well guided inside the core and interaction of light in the cladding region is very negligible.

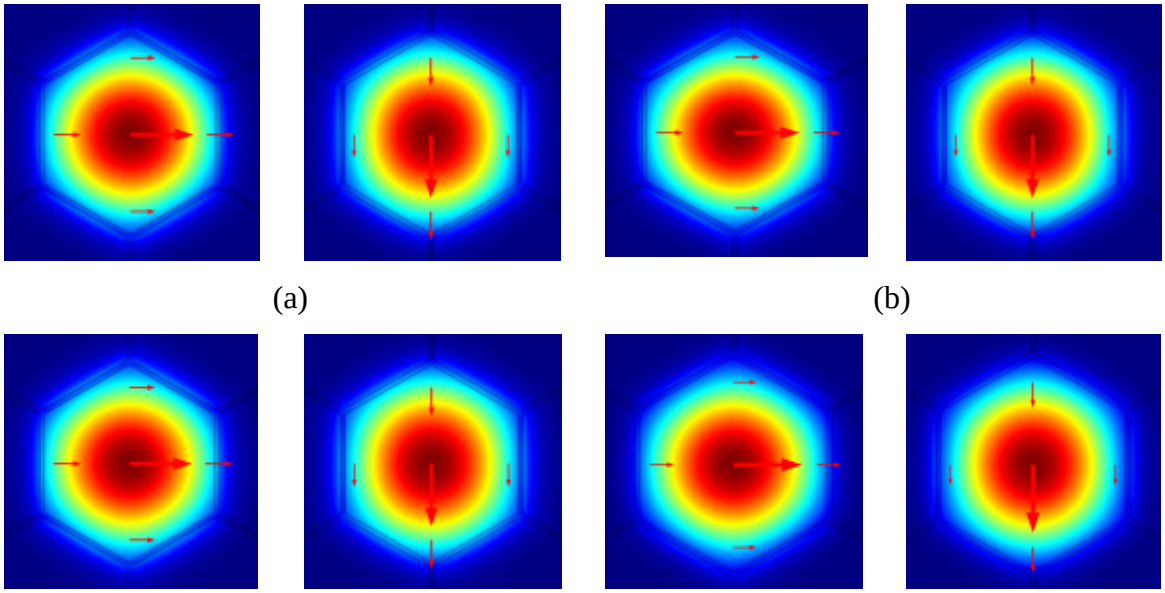

Figure 5.2: Electric field distribution of proposed PCF based sensor for different analytes (a) Water (b)Ethanol (c) Methanol and (d) Benzene in both polarizations mode at 3 THz

The response of relative sensitivity with respect to frequency for different chemicals (ethanol, methanol, water and benzene) are shown in Fig. 5.3. Which delimitates that the relative sensitivity is enhanced due to the growth of frequency because frequency is directly proportional to the effective RI of guided mode and the effective RI of analyte is also balanced with sensitivity according to equation (9). This figure clarifies that the relative sensitivity of benzene is maximum 99% compared to the other three samples which is around (97±1)% at 3THz frequency. After a certain frequency the refractive index of sample is not increased if the frequency changes further. As a result the relative sensitivity became flatter after an indicated frequency. Same scenario happened when sensitivity responded with respect to D_{core}

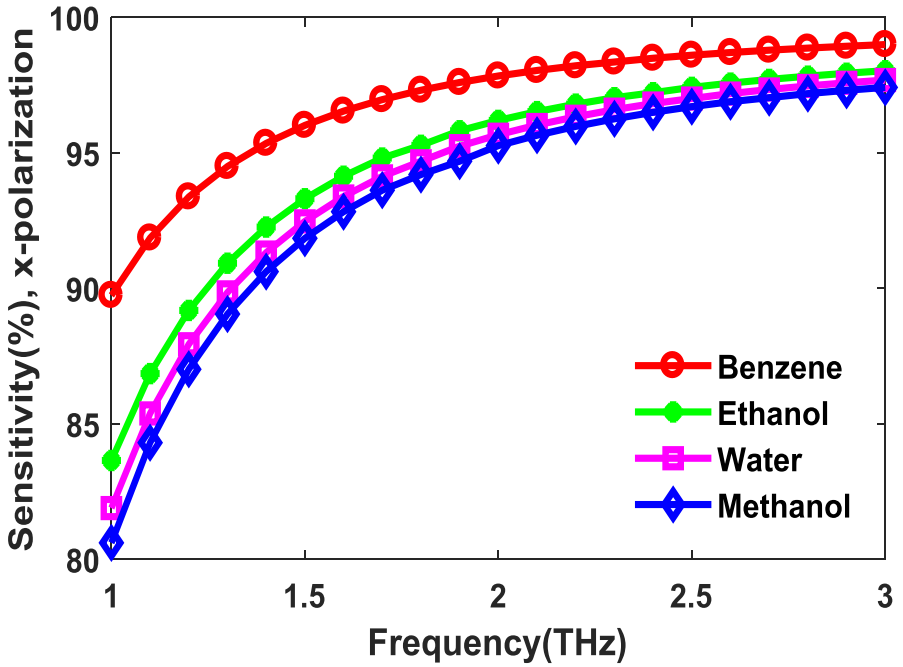

Figure 5.3: Sensitivity Vs frequency with x-polarization mode

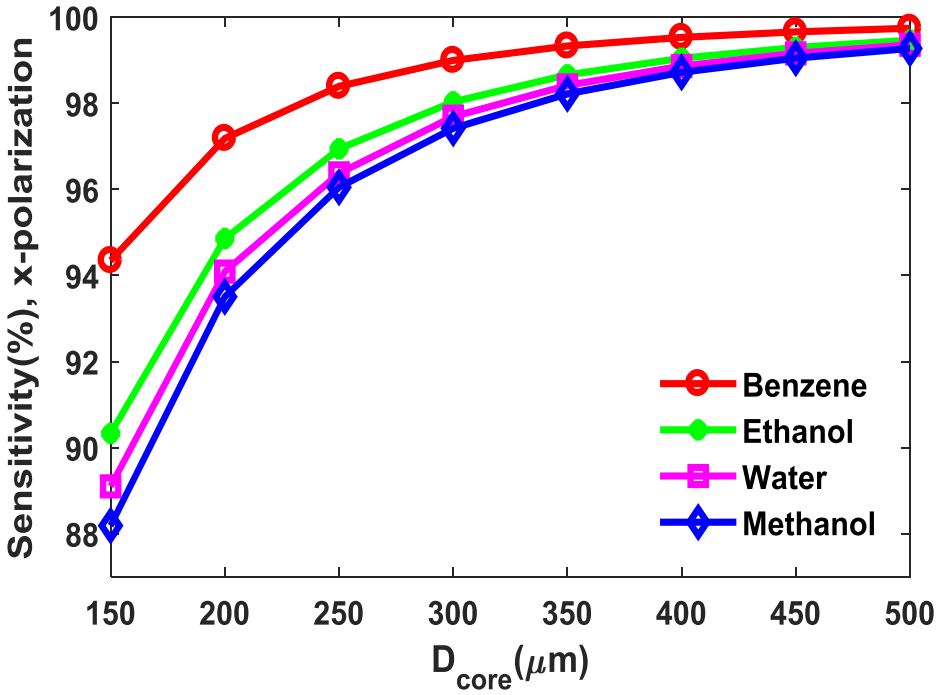

Figure 5.4. Sensitivity Vs D_{core} with x-polarization mode

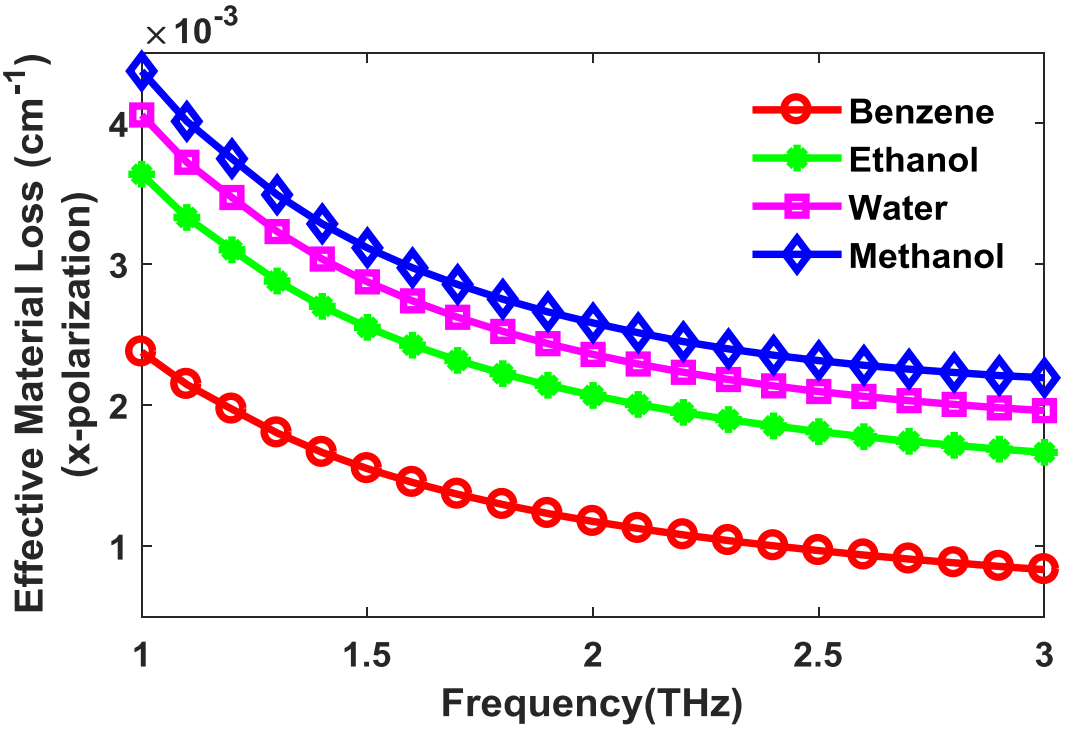

Figure 5.5. EML Vs frequency with X polarization

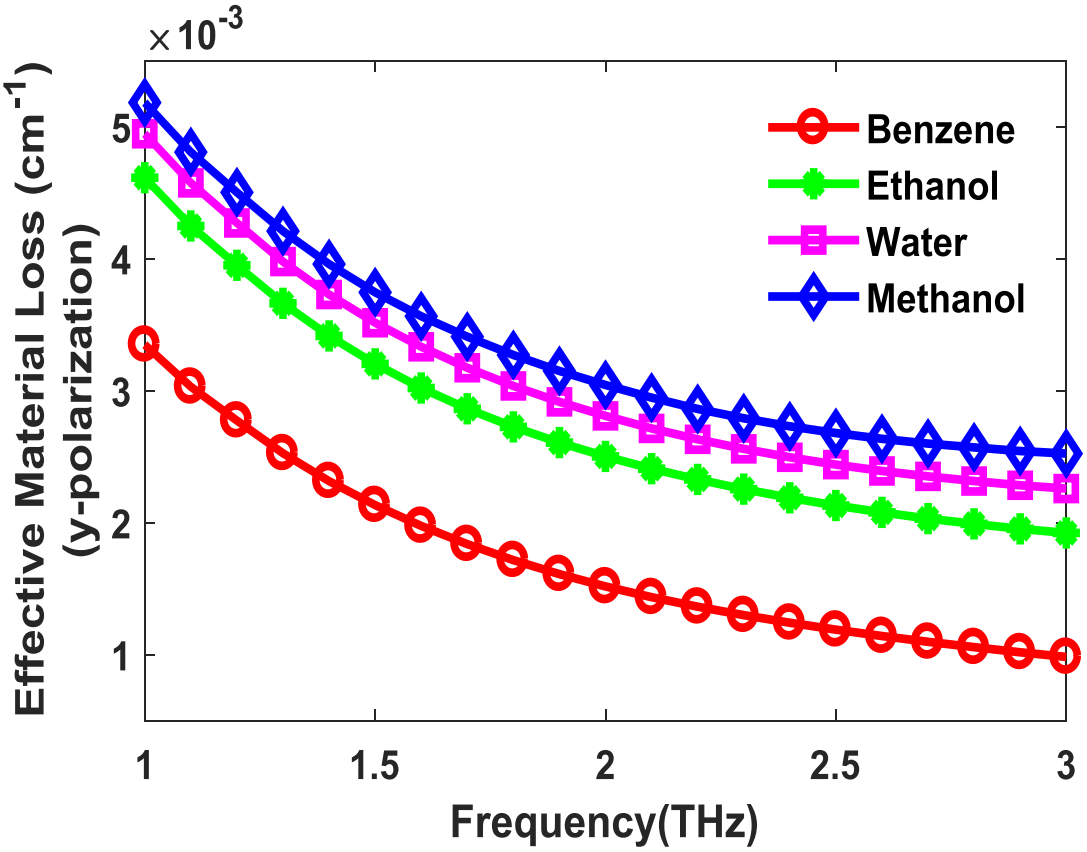

Figure 5.6. EML Vs frequency with Y polarization

which is delineated in Fig. 5.4. At 500 µm core size, the sensitivity is very close to 100% for all the samples.

For different chemicals (Benzene, Ethanol, Water and Methanol) the response of EML as a function of frequency is shown in Fig. 5.5. The downward trend is showed by EML with the incremental change of frequency which fulfills the theoretical postulate of calculating EML as per empirical law. The reason behind that when frequency is increased the light is closely confined through the core section which reduces the interaction of light with the matter, consequently EML is reduced. Among the four chemicals, the EML of methanol is the most and the benzene shows the least material absorption loss. Fig. 5.5 represents the EML of benzene is 0.8×10^{-3} cm^{-1}, for ethanol 1.8×10^{-3} cm^{-1}, for water 2×10^{-3} cm^{-1} and for methanol 2.1×10^{-3} cm^{-1} at 3THz frequency which are extremely low compared to previously proposed PCF sensor design for THz application [21-25]. The numerical results revealed that the EML between x & y polarization are very close.

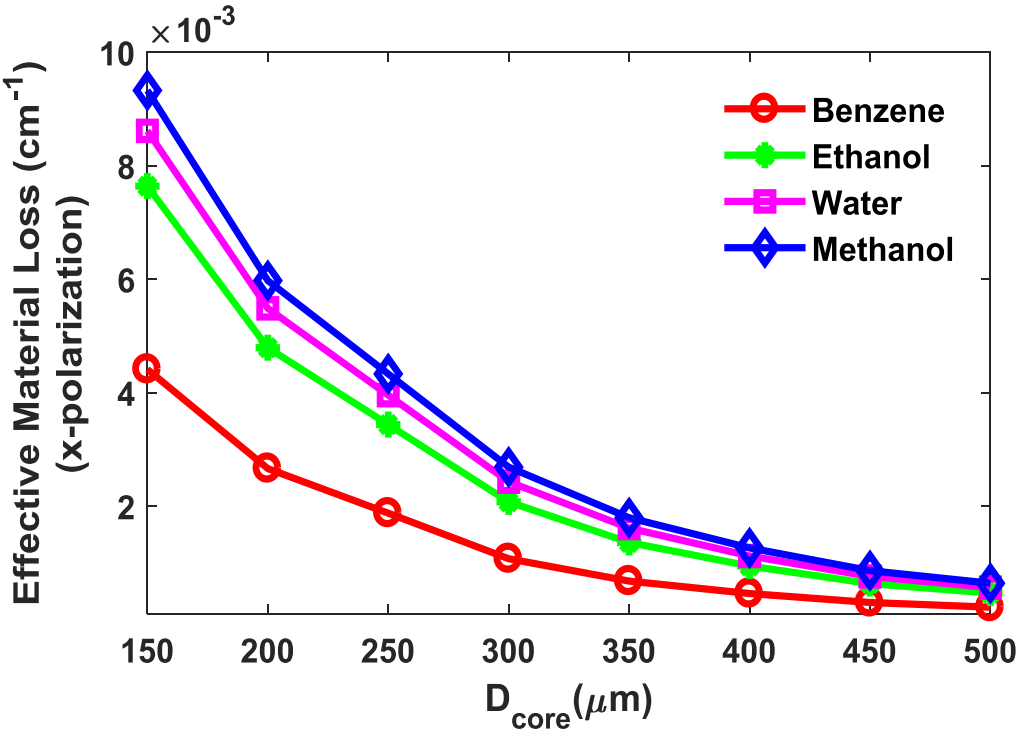

Figure 5.7: EML Vs D_{core} with X polarization.

The behavior of EML with respect to core diameter is shown in Fig. 5.6 for both polarizations. It is explicated from the figure that the EML can be reduced by using a higher value of core size at a fixed operating frequency. The reason of that behavior, when core size is accrescent, the volume of background material decreases accordingly. As a result interaction of light in the core section will be increased that decreases the EML.

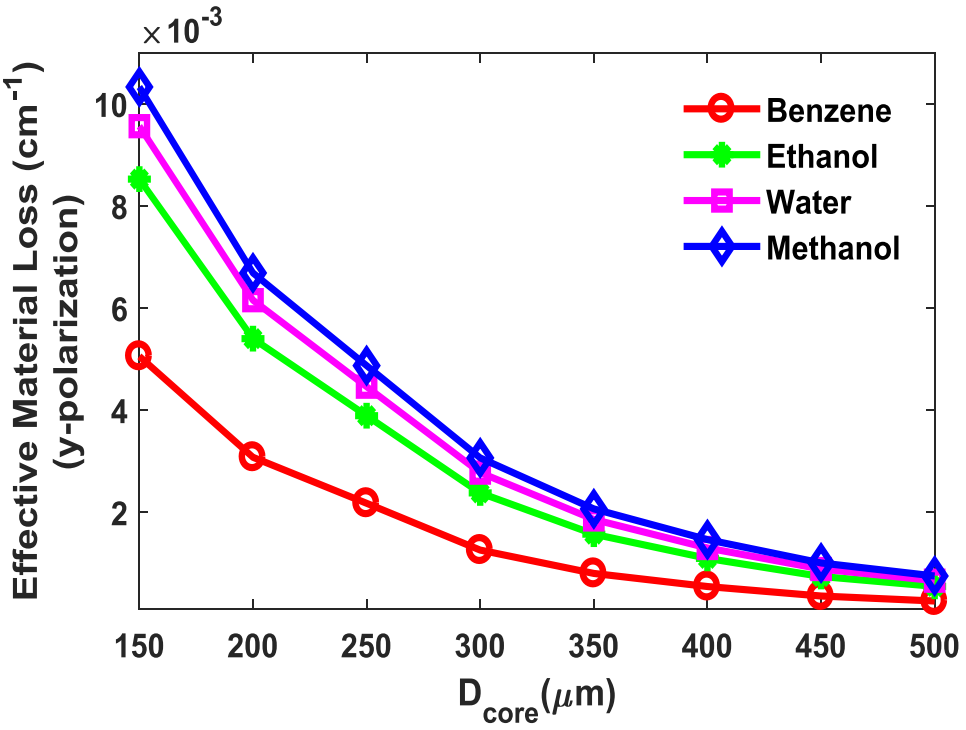

Figure 5.8: EML Vs D_{core} withY polarization

The modal effective area is inversely proportional with respect to frequency and D_{core}, which are shown in Fig. 5.7 & Fig. 5.8 respectively. From Fig. 5.7, it can be observed that the effective area is a decreasing function with increasing frequency because when frequency increases the light is closely confined in the core region , as consequence of effective area decreases with the increment of frequency. The opposite feature can be obtained if the value of the core is increased. The physical reason can be expressed as follows. At a lower value of core size, mode power is restricted by the core; therefore, the effective area decreases. At 200µm core size the proposed design shows effective area is $2\pm0.5 \times 10^{-8}$ m^2 for all the analytes, that are comparable with previously proposed sensor design [113, 117-119].

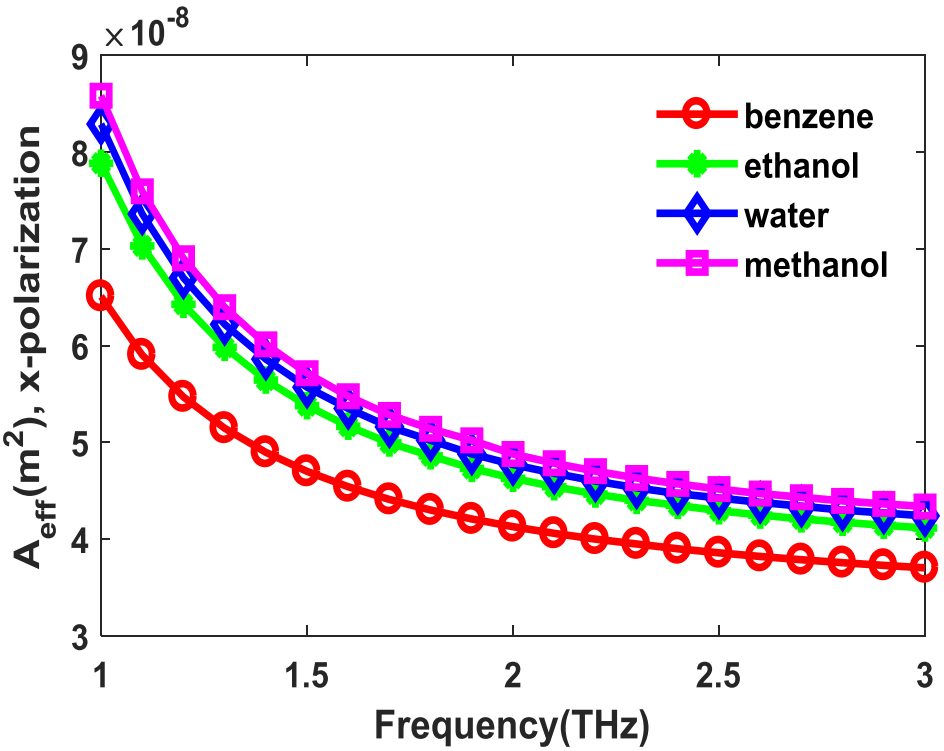

Figure 5.9: Effective Area Vs frequency (x-polarization)

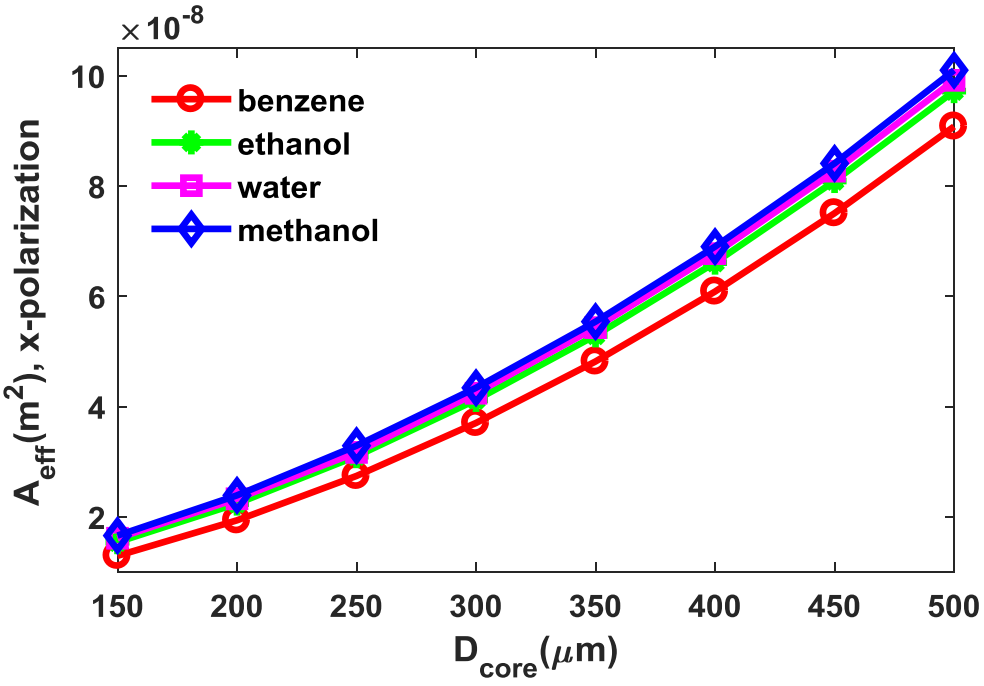

Figure 5.10: Effective Area Vs D_{core} (x-polarization)

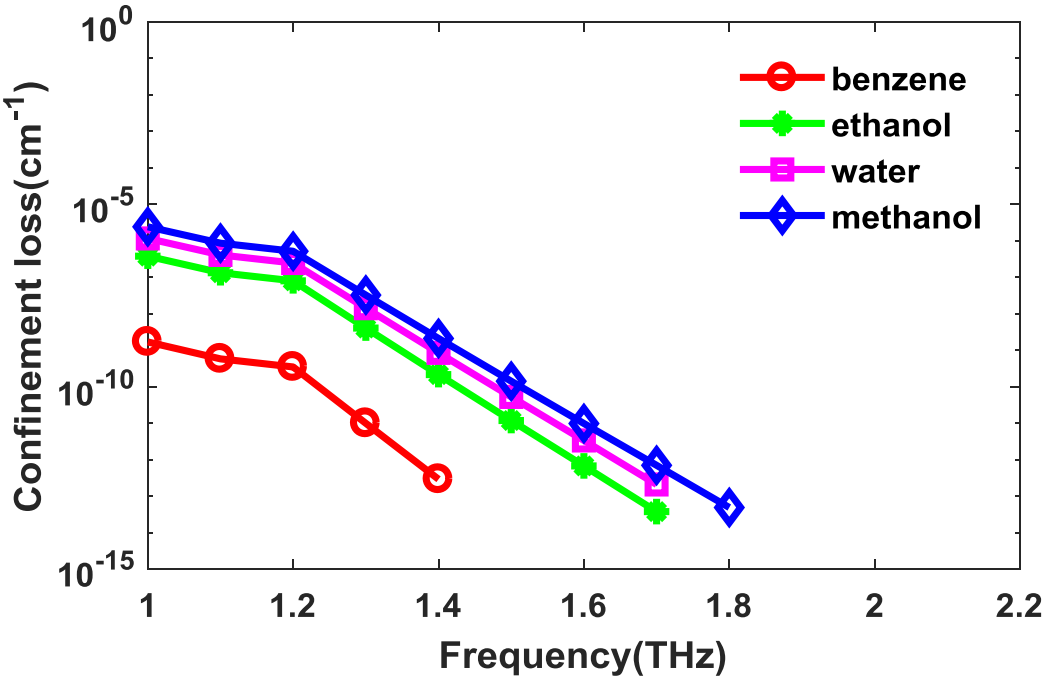

Figure 5.11: Confinement Loss Vs Frequency

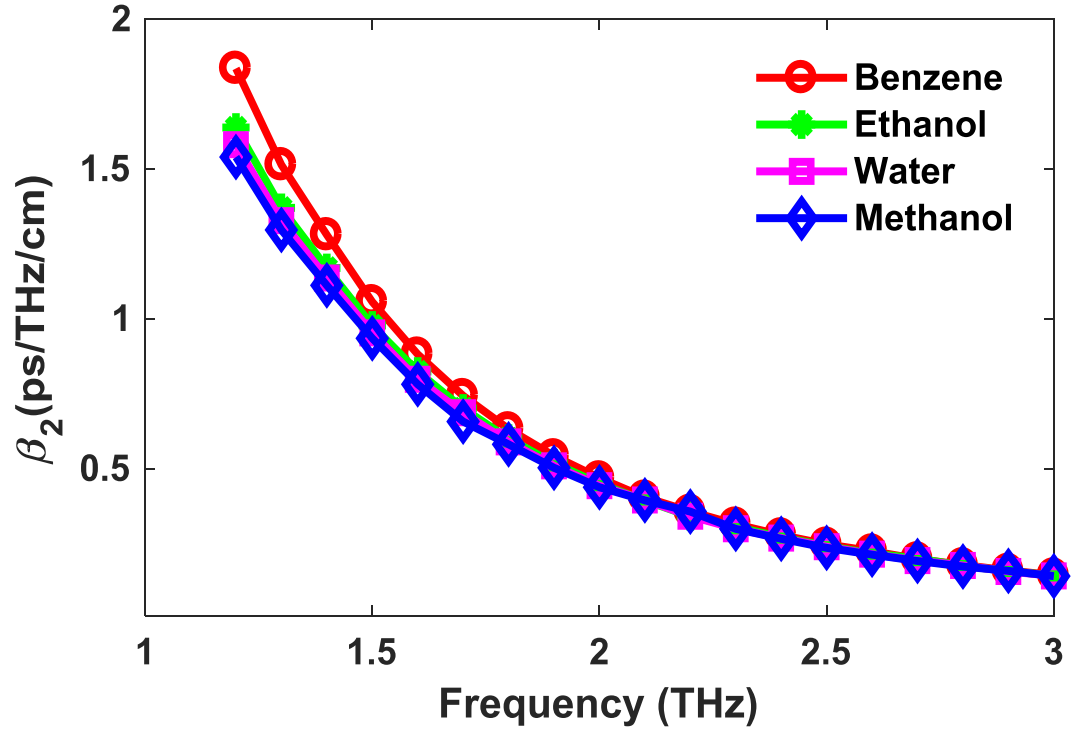

Figure 5.12: Waveguide dispersion Vs frequency.

Confinement loss of our proposed PCF based sensor for incremental change of frequency is shown in Fig. 5.9. From this figure it can be described that the confinement loss is negligible for all these analytes. The range of numerical value is from (10^{-5} to 10^{-14}) cm^{-1} in the frequency range (1-1.8) THz. By increasing the number of air holes in cladding section we can be minimized loss more, although we used few number of air holes in cladding region.

The response of dispersion with respect to frequency of our proposed terahertz sensor is shown in Fig.10 for different analytes. From Fig. 5.10 it can be observed that for different analytes the dispersion is going to be level out with respect to frequency because the refractive index changes with frequency are very low. It attains dispersion fluctuation of 0.5 ps⁄THz⁄cm at a frequency range of 2-3 THz bandwidth, which is better than the previously proposed optical waveguides [113, 117-119].

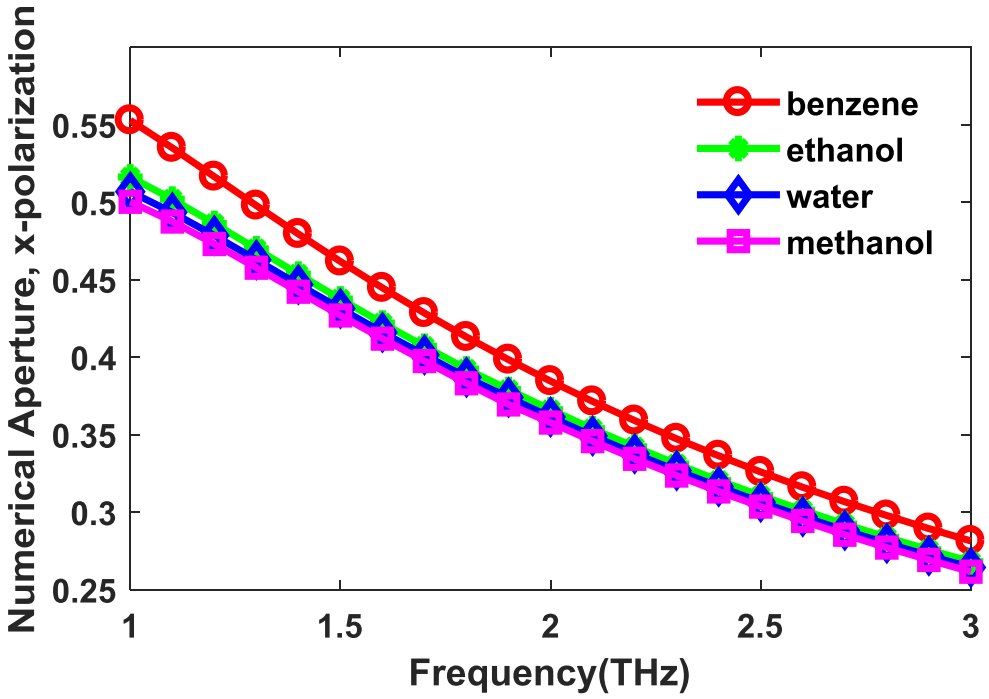

Figure 5.13: Numerical Aperture Vs Frequency.

The behavior of NA as a function of frequency is shown in Fig. 5.11 for different samples. From this figure, it is seen that the NA decreases when frequency is increased. The large value of NA is desirable for different optical applications but most of the previously proposed sensor ignored this property evaluation of PCF [21 -23]. At optimum design parameters we achieved NA(0.5 – 0.55) for different analytes.

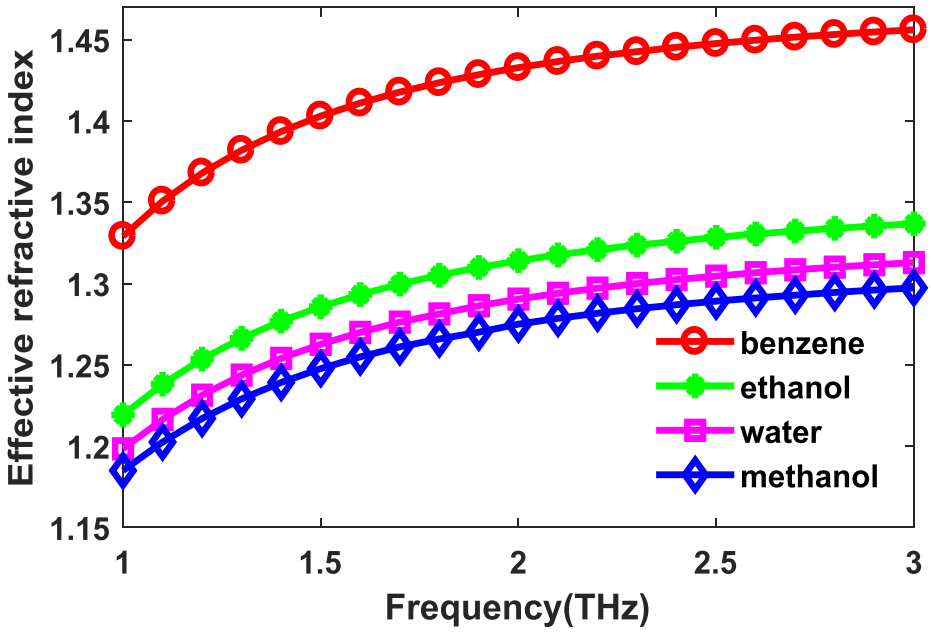

Figure 5.14: Effective refractive index versus Frequency.

Higher value of RI is desirable for higher sensitivity and lower EML. Figure 5.14 represents the response of ERI for different frequencies. We know that the effective refractive index is directly proportional to frequency, which is clarified by Figure 5.14.

The attitude of nonlinearity and V-parameter of proposed PCF for different types of chemicals at different wavelength are shown in Fig. 5.13 and Fig.5.14 respectively. The nonlinearity of the proposed PCF structure for all analytes is decreased with increasing operating wavelength. At optimum wavelength 300μm it is observed, the nonlinearity is almost 5×10^{-5} $Km^{-1}W^{-1}$ for benzene. The V-parameter of our proposed sensor is more than 2.405 for all types of analytes at a wavelength range 100-230 μm. So this PCF supports for multimode applications within this wavelength and it also may offer single mode operation for higher value of wavelength from this range.

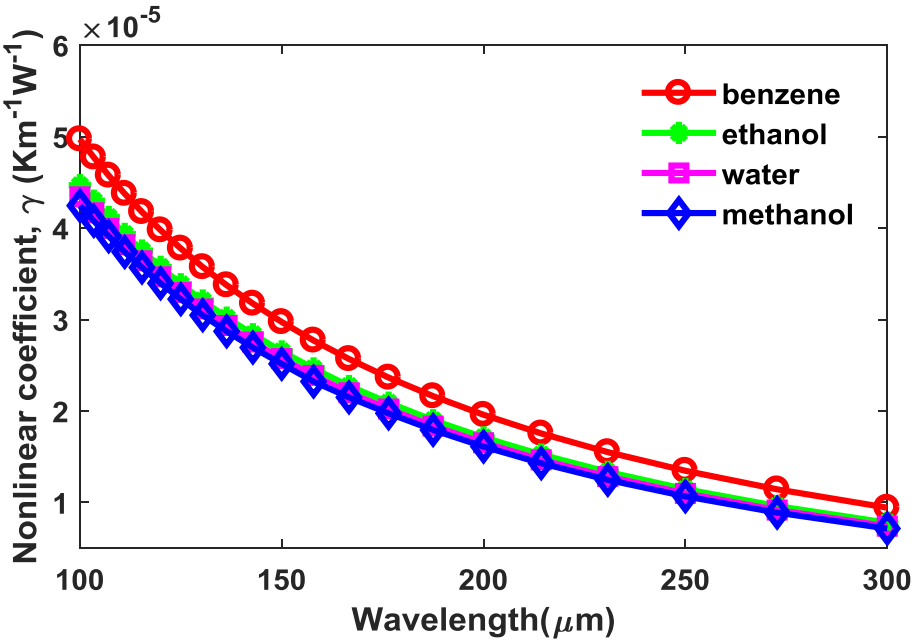

Figure 5.15: Nonlinear coefficient Vs wavelength

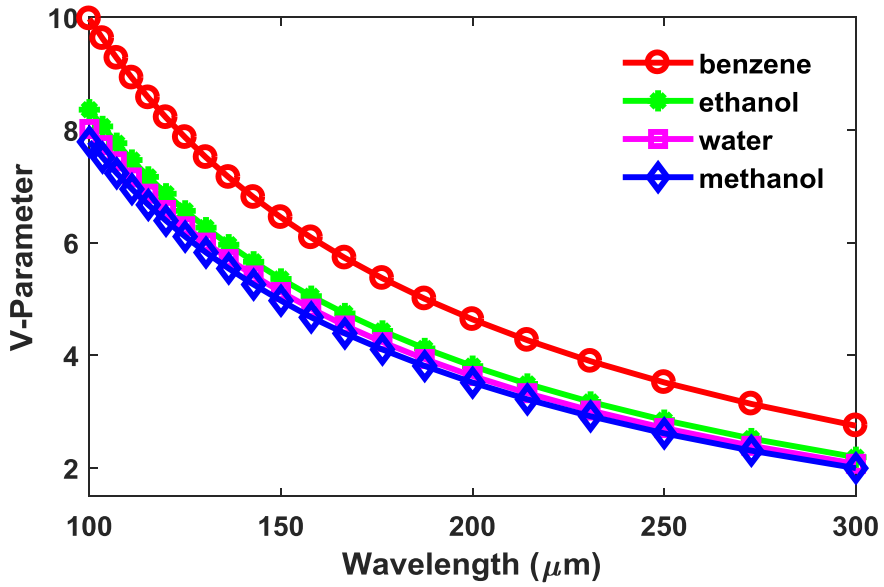

Figure 5.16: V-parameter Vs wavelength

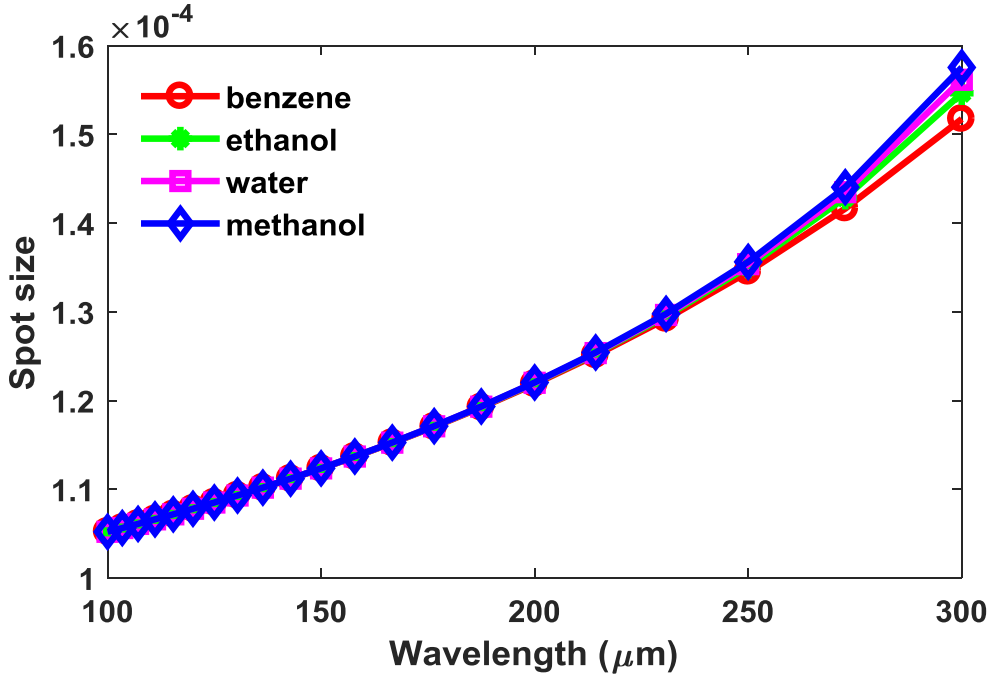

Figure 5.17: Spot size Vs wavelength

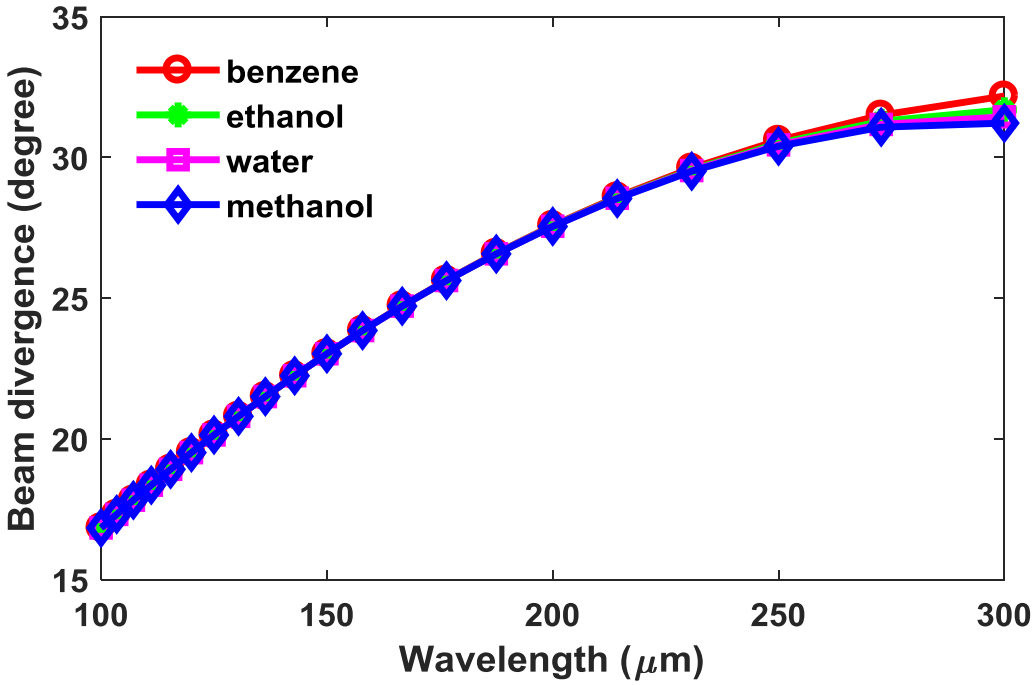

Figure 5.18: Beam divergence Vs wavelength

According to the investigation of Figure 5.17, it can be demonstrated that the spot size is increasing with the increasing of wavelength. The comparison among different analytes with varying wavelength range from 100 µm to 300 µm is also shown. At 100 µm, the spot size is 1.05×10^{-4} and at 300 µm, a higher value of spot size is attained which is close to 1.55×10^{-4}.

Higher value of Beam divergence indicates lower the beam quality. The beam divergence as a function of frequency is shown in Figure 5.18 which exhibits beam divergence increases when frequency increases. At 100 µm wavelength, our simulated results show the beam divergence of 16.5 degree which is very low compared to other proposed design [120].

Table 5.1: Comparison among previously proposed porous core PCFs for analytes sensing and proposed THz analytes sensor.

Ref.	Analytes	Sensitivity (%)	Geometry
[21]	Ethanol Water	49.29	Circular
[22]	Water Ethanol Benzene	59	Hexagonal
[23]	Ethanol	68.87	Hexagonal
[24]	-	64.19	Circular
[25]	Water Ethanol Benzene	26	Hexagonal
[26]	Water Ethanol Benzene	90	Rectangular
This PCF	Water Ethanol Methanol Benzene	99%	Hexagonal

From table 5.1 it is clear that our proposed design is very much comparable with previously suggested different analytes sensor. Our proposed geometry is not complex one, it is similar as most of the previously reported structure but proper pitch size, air hole position, core cladding diameter selection makes it better than the previously proposed analytes sensor.

5.3 Comparison among proposed designs for sensing applications

In this research we proposed three PCF geometry, one of which is hollow core and remaining two are porous core. These three designs, we have applied for chemical (methanol, ethanol, water, benzene) sensing applications whose numerical outcomes are depicted in figure 5.19. From this figure we can explain that the relative sensitivity of hollow core fiber is higher compare to others proposed porous core PCF. The reason behind this, hollow core fiber has greater analyte volume inside the core area and it's facilitating for tight confinement in the core region, which increases the relative sensitivity.

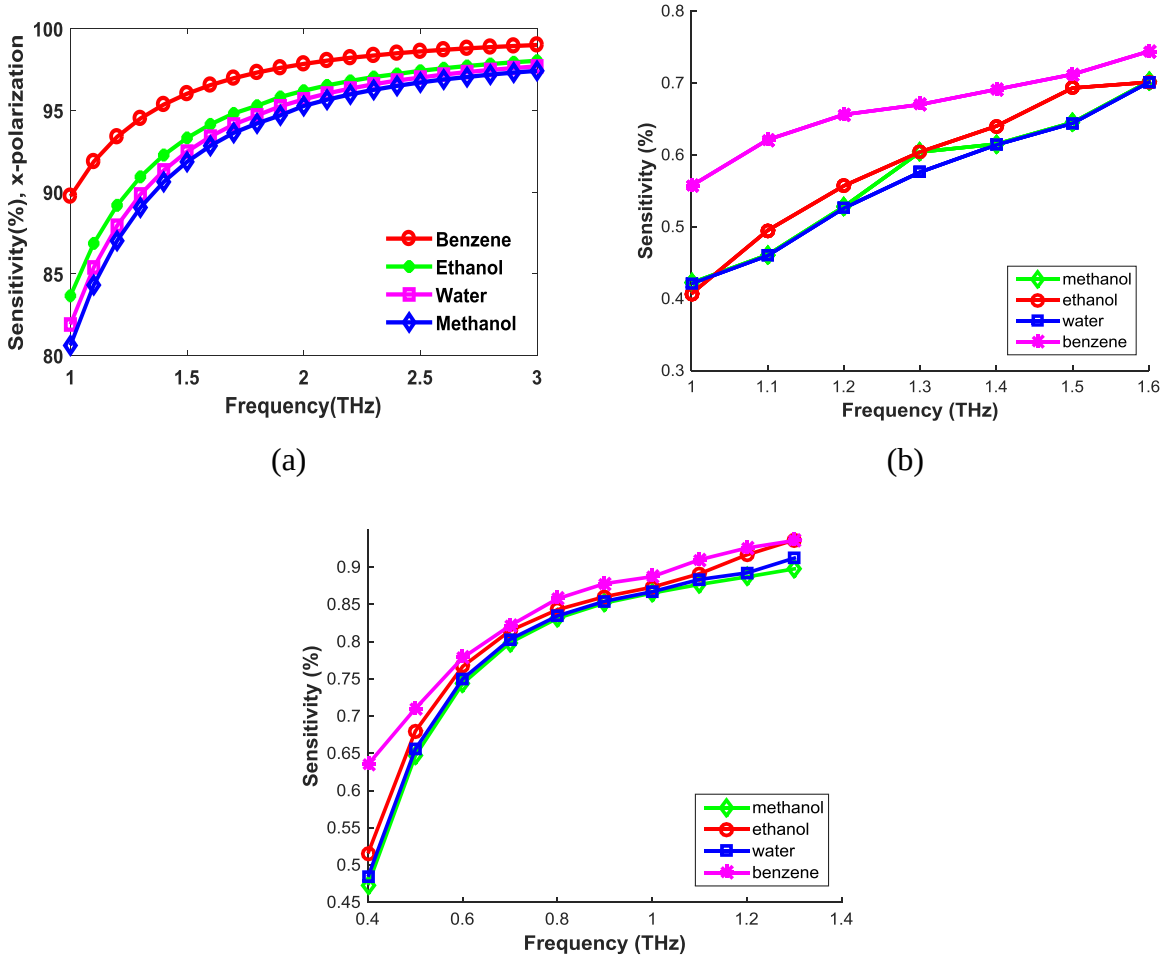

Figure 5.19: Sensitivity Vs Fresquency of different proposed PCFs (a) hexagonal hollow core (b) hexagonal porous core (c) square porous core

Table 5.2: Comparison among our proposed PCFs for different chemical sensing

Proposed PCF	Sensitivity (%)			
	Methanol	Ethanol	Benzene	Water
Hexagonal hollow core	96	97	99	96.5
Hexagonal Porous Core	70.2	70.1	68	70.1
Square Porous Core	89.78	93.66	91.22	93.58

Table 5.2 shows that the comparison of our proposed three PCF structure for different liquid chemical sensing.

5.4 Fabrication Possibilities

The proposed PCF based sensor contains few numbers of hexagonal air core lattices with a symmetrical cladding and hollow core structure. The structure of proposed sensor is shown in Figure 5.1. For circular shaped air holes, PCF fabrication with capillary stacking, stack and draw and sol-gel techniques are frequently used but the extrusion and 3D printing fabrication technology are likely used to fabricate any types of symmetrical and asymmetrical PCF structures [106-108]. Using the extrusion technology, the Max Plank Institute fabricated different complex structured PCF based sensors including a rectangular shaped air hole structure [109]. Therefore, it is feasible to fabricate using existing PCF fabrication process.

5.5 Conclusion

A zeonex based hollow core PCF is designed for different chemicals detection in THz regime. At optimum design parameters, the proposed THz analyte sensor shows relative sensitivity of very close to 100% at 3 THz frequency. This proposed design also revealed very low EML in both polarization mode and negligible confinement loss. Moreover, high effective RI and low dispersion are achieved in this design. In addition, using an existing fabrication process it is feasible for fabrication. Considering all the parameters which we evaluated here, it is noted that this proposed sensor will open a new horizon for PCF sensing application, as well as for further research in THz regime.

Chapter 6

Conclusion and Future Work

The efficient transmission of THz signals using waveguide has been a major challenge since early days of THz science. Loss and dispersion are the primary parameters in THz waveguides that one aims to minimize in order to obtain undistorted propagation of THz pulses. Metallic waveguides suffer from Ohmic losses while dielectric waveguides suffer from material absorption losses. Dry air is the best transparent medium for THz pulses. Therefore, intelligent design of waveguides are required to overcome Ohmic and material loss limitations. Porous fibers are proposed in this thesis for THz wave guidance as well as analytes sensing application.

6.1 Contributions

For THz wave propagation a circular sectored cladding and square core PCF are introduced here. The proposed PCF shows an extremely low EML of 0.009cm^{-1} at 1THz frequency, which also offers very low flattened dispersion of 0.3 ± 0.05 ps/THz/cm, low confinement loss of $10^{-4}cm^{-1}$, large effective area of 5.48 $\times 10^{-7}$ m^2, as well as high core power fraction of 53% at 1 THz operating frequency which is very much comparable with recently published renowned articles. In addition this suggested simple sectored structured PC-PCF is feasible to fabricate by using already developed fabrication process.

An Asymmetrical slotted hexagonal structured porous core photonic crystal fiber is designed for developing polarization maintaining characteristics in THz regime. This presented PCF is performed with a significant differences of refractive index between in x and y polarization mode. It also exhibits very low effective material loss and confinement loss in both polarization modes. Besides, design simplicity, large effective area and high core power indicates that this PCF geometry is suitable for efficient THz wave propagation in both polarization modes.

Here we also introduce another symmetrical hexagonal lattices cladding and hollow core PCF for sensing purpose of Benzene, Methanol, Ethanol and Water. Perfectly detection of these chemicals are so much important because Benzene, Methanol and Ethanol are very harmful

for health which may causes cancer and water detection is also important in data center, HVAC and many other important fields where the existence of water can cause huge injury. The relative sensitivity near about 99% at 3 THz frequency is achieved in our proposed design. To evaluate the performances of our design we also exhibit low effective material loss and confinement loss in both polarizations. Moreover the numerical outcomes of effective area, numerical aperture, effective refractive index, dispersion, v-parameters and spot size show a tremendous performance which ensures the proposed analytes sensor open new window in THz sensing as well as THz applications.

6.2 Future Directions

In summary, this thesis has laid the design of porous core photonic crystal fiber for THz waveguide and a hollow PCF is designed for analytes sensing. Almost all the necessary wave guiding and sensing properties are evaluated. But bending loss and some less important parameters evaluation are not included in this research. So there is a scope to improve the performance by including other parameters characterization like bending loss. Additionally there are now strong opportunities for using it for practical applications, most particularly for bio-sensing.

References

[1]. W. W. chumnankul, G.M. Png, X. Yin, S. Atakaramians, I. Jones, H. Lin, B.S.Y. Ung, J. Balakrishnan, B.W.H. Ng, B. Ferguson, S.P. Mickan, B.M. Fischer and D. Abbott, "T-ray sensing and imaging," Proc. IEEE 95 (8) 1528–1558, (2007).

[2]. M. R. Hasan, M. S. Anower, M. A. Islam, and S. M. A. Razzak, "Polarization-maintaining low-loss porous-core spiral photonic crystal fiber for terahertz wave guidance," Appl. Opt. 55, 4145-4152, (2016).

[3]. J. Balakrishnan, B.M. Fischer and D. Abbott, "Sensing the hygroscopicity of polymer and copolymer materials using terahertz time-domain spectroscopy," Appl. Opt. 48 (12) 2262–2266, (2009).

[4]. A. Lee, W.M., Q. Qin and S. Kumar, "Real-time terahertz imaging over a standoff distance (>25 meters)," Appl. Phys. Lett. 89, (14), p.141125(1–3), (2006).

[5]. S. Fathololoumi, E. Dupont and C. W. I. Chan, "Terahertz quantum cascade lasers operating up to ∼200 K with optimized oscillator strength and improved injection tunneling," Opt. Exp. 20, (4), p. 3866, (2012).

[6]. F. Sizov and A. Rogalski, "THz detectors," Prog. Quantum Electron. 34, (5), pp. 278–347, (2010).

[7]. M. R. Hasan, S. Akter, T. Khatun, A. A. Rifat and M. S. Anower, "Dual-hole unit-based kagome lattice microstructure fiber for low-loss and highly birefringent terahertz guidance," Optical Engineering, 56(4), 043108 (2017).

[8]. M. Skorobogatiy and A. upuis, "Ferroelectric all-polymer hollow Bragg fibers for terahertz guidance," Appl. Phys. Lett. 90 (11) (2007) 113514.

[9]. G. Zhao, M.T. Mors and T. Wenckebach, "Terahertz dielectric properties of polystyrene foam," J. Opt. Soc. Amer. B 19 (6), 1476–1479, (2007).

[10]. A. Kawsar, B. K. Paul, S. Chowdhury, S. Sen, M. I. Islam, M. S. Islam, M. R. Hasan and S. Asaduzzaman, "Design of a single-mode photonic crystal fibre with ultra-low material loss and large effective mode area in THz regime," IET Optoelectron., Vol. 11 Iss. 6, pp. 265-271, (2017).

[11]. M. A. Habib, M. S. Anower, and M. R. Hasan, "Ultrahigh Birefringence and Extremely Low Loss Slotted-core Microstructure Fiber in Terahertz Regime," Current Optics and Photonics, Vol. 1, No. 6, pp. 567-572, (2017).

[12]. M. A. Habib and M. S. Anower, "Low Loss Highly Birefringent Porous Core Fiber for Single Mode Terahertz Wave Guidance," Current Optics and Photonics, Vol. 2, No. 3 pp. 215-220, (2018).

[13]. M. S. Islam, J. Sultana, A. Dinovitser, M. Faisal, M. R. Islam, B. W.-H. Ng, and D. Abbott, "Zeonex-based asymmetrical terahertz photonic crystal fiber for multichannel communication and polarization maintaining applications," Applied Optics, Vol. 57, Issue 4, pp. 666-672, (2018).

[14]. J. Sultana, M. S. Islam, M. Faisal, M. R. Islam a, Brian W.-H. Ng, H. Ebendorff-Heidepriem and D. Abbott, "Highly birefringent elliptical core photonic crystal fiber for terahertz application," Optics Communications, Volume 407, Pages 92-96, (2018).

[15]. B. K. Paul, M. S. Islam, S. Sen, K. Ahmed and M. S. Uddin, "Low material loss and dispersion flattened fiber for single mode THz-wave transmission applications," Results in Physics 11 638–642, (2018).

[16]. S. Rana, A. S. Rakin, M. R. Hasan, M. S. Reza, R. Leonhardt, D. Abbott and H. Subbaraman, "Low loss and flat dispersion Kagome photonic crystal fiber in the terahertz regime," Optics Communications, 410 452–456, (2018).

[17]. K. Ahmed, S. Chowdhury, B.K. Paul, M.S. Islam, S. Sen, M. I. Islam, and S. Asaduzzaman, "Ultrahigh birefringence, ultralow material loss porous core single-mode fiber for terahertz wave guidance," Applied optics, Vol. 56, pp.3477-3483, (2017).
[18]. J. Sultana, M. S Islam, J. Atai, M.R. Islam and D. Abbott, "Near-zero dispersion flattened, low-loss porous-core waveguide design for terahertz signal transmission," Optical Engineering, Vol. 56, PP. 076114, (2017).
[19]. M. S. Islam, J. Sultana, A. Dinovitser, B.W.H.Ng, and D. Abbott, "A novel Zeonex based oligoporous-core photonic crystal fiber for polarization preserving terahertz applications," Optics Communications, Vol. 413, pp.242-248, (2018).
[20]. M. Faisal, and M.S Islam, "Extremely high birefringent terahertz fiber using a suspended elliptic core with slotted air holes," Applied optics, Vol. 57, pp.3340-3347, (2018).
[21]. S. Asaduzzaman, K. Ahmed, T. Bhuyan, and T. Farah, Hybrid photonic crystal fiber in chemical sensing, Springer Plus 5, 748 (2016).
[22]. M. F. H. Arif, K. Ahmed, S. Asaduzzaman, and M. A. K. Azad, "Design and optimization of photonic crystal fiber for liquid sensing applications," Photon. Sens. 6, 279–288,(2016).
[23]. J. Sultana, M. Islam, K. Ahmed, A. Dinovitser, Brian W.-H. NG, and . D. Abbott, "Terahertz detection of alcohol using a photonic crystal fiber sensor," Applied Optics, Vol. 57, No. 10 ,1, (2018).
[24]. B. K. Paul, K. Ahmed, S. Asaduzzaman, and M. Islam, "Folded cladding porous shaped photonic crystal fiber with high sensitivity in optical sensing applications: Design and analysis," Sensing and Bio-Sensing Research, Volume 12, (2017).
[25]. H. Ademgil, and S. Haxha, "PCF Based Sensor with High Sensitivity, High Birefringence and Low Confinement Losses for Liquid Analyte Sensing Applications," Sensors, MDPI, 31833–31842, (2015).
[26]. M. Islam, J. Sultana, A. A. Rifat, Dinovitser. A., Brian W-H N., and Abbott. D. , "Terahertz Sensing in a Hollow Core Photonic Crystal Fiber," IEEE SENSORS JOURNAL, VOL. 18, NO. 10, (2018)
[27]. L. Peng, "Absorption and emission properties of photonic crystals and Metamaterials", UMI Number: 1446140, (2007).
[28]. J. D. Joannopoulos, S. G. Johnson, N. Joshua, D. R. Meade, "Photonic Crystals-Molding the flow of light", Second Edition, Princeton University Press, (2008).
[29]. L. Labadie and O. Wallner, "Mid-infrared guided optics: a perspective for astronomical instruments," OPTICS EXPRESS,Vol. 17, No. 3, (2009).
[30]. G. Keiser, Optical Fiber Communications, 2nd ed. (McGraw-Hill, 1991).
[31]. J. M. López-Higuera, L. R. Cobo, A. Q. Incera, and A. Cobo, "Fiber optic sensors in structural health monitoring," J. Lightwave Technol. 29, 587–608, (2011).
[32]. D. R. Walt, "Fibre optic microarrays," Chem. Soc. Rev. 39, 38–50, (2010).
[33]. J. Faist, F. Capasso, D. L. Sivco, C. Sirtori, A. L. Hutchinson, and A. Y. Cho, "Quantum cascade laser," Science 264, 553–556, (1994).
[34]. K. Eshraghian, "SoC emerging technologies," Proc. IEEE 94, 1197–1213, (2006).
[35]. J. S. Melinger, S. S. Harsha, N. Laman, and D. Grischkowsky, "Guided-wave terahertz spectroscopy of molecular solids [Invited]," J. Opt. Soc. Am. B 26, A79–A89, (2009).
[36]. M. Nagel, M. Först, and H. Kurz, "THz biosensing devices: fundamentals and technology," J. Phys. Condens. Matter 18, S601–S618, (2006).
[37]. S. A. Maier, S. R. Andrews, L. Martin-Moreno, and F. J. Garcia-Vidal, "Terahertz surface plasmon-polariton propagation and focusing on periodically corrugated metal

wires," Appl. Phys. Lett. 97, 176805, (2006).
[38]. V. Astley, K. S. Reichel, J. Jones, R. Mendis, and D. M. Mittleman, "Terahertz multichannel microfluidic sensor based on a parallel-plate waveguide resonant cavities," Appl. Phys. Lett. 100, 231108, (2012).
[39]. G. Gallot, S. P. Jamison, R. W. McGowan, and D. Grischkowsky, "Terahertz waveguides," J. Opt. Soc. Am. B 17, 851–863, (2000).
[40]. R. Mendis and D. Grischkowsky, "Undistorted guided-wave propagation of subpicosecond terahertz pulses," Opt. Lett. 26, 846–848, (2001).
[41]. T. I. Jeon and D. Grischkowsky, "Direct optoelectronic generation and detection of sub-ps-electrical pulses on sub-mm-coaxial transmission lines," Appl. Phys. Lett. 85, 6092–6094, (2004).
[42]. T. I. Jeon, J. Zhang, and K. W. Goossen, "THz Sommerfeld wave propagation on a single metal wire," Appl. Phys. Lett. 86, 161904, (2005).
[43]. A. Bingham and D. Grischkowsky, "Terahertz 2-D photonic crystal waveguides," IEEE Microw. Wireless Compon. Lett. 18, 428–430, (2008).
[44]. T. I. Jeon and D. Grischkowsky, "THz Zenneck surface wave (THz surface plasmon) propagation on a metal sheet," Appl. Phys. Lett. 88, 061113, (2006).
[45]. M. Wächter, M. Nagel, and H. Kurz, "Metallic slit waveguide for dispersion-free low-loss terahertz signal transmission," Appl. Phys. Lett. 90, 061111, (2007).
[46]. R. W. McGowan, G. Gallot, and D. Grischkowsky, "Propagation of ultrawideband short pulses of terahertz radiation through submillimeter-diameter circular waveguides," Opt. Lett. 24, 1431–1433, (1999).
[47]. R. Mendis, "First broadband experimental study of planar THz waveguides," Ph.D. thesis (Oklahoma State University, 2001).
[48]. Y. Xu and R. G. Bosisio, "A comprehensive study on the planar type of Goubau line for millimetre and submillimetre wave integrated circuits," IET Microw. Antennas Propag. 1, 681-687 (2007).
[49]. R. Mendis and D. M. Mittleman, "Comparison of the lowest-order transverse-electric (TE1) and transverse-magnetic (TEM) modes of the parallel-plate waveguide for terahertz pulse applications," Opt. Express 17, 14839–14850 (2009).
[50]. R. Mendis and D. M. Mittleman, "An investigation of the lowest-order transverse-electric (TE1) mode of the parallel-plate waveguide for THz pulse propagation," J. Opt. Soc. Am. B 26, A6–A13 (2009).
[51]. M. Wächter, M. Nagel, and H. Kurz, "Frequency-dependent characterization of THz Sommerfeld wave propagation on single-wires," Opt. Express 13, 10815–10822 (2005).
[52]. K. Wang and D. M. Mittleman, "Metal wires for terahertz wave guiding," Nature 432, 376–379 (2004).
[53]. M. Wächter, M. Nagel, and H. Kurz, "Metallic slit waveguide for dispersion-free low-loss terahertz signal transmission," Appl. Phys. Lett. 90, 061111 (2007).
[54]. J. Dai, J. Zhang, W. Zhang, and D. Grischkowsky, "THz time-domain spectroscopy characterization of the far-infrared absorption and index of refraction of high resistivity, float-zone silicon," J. Opt. Soc. Am. B 21, 1379–1386 (2004).
[55]. B. M. Fischer, "Broadband THz time-domain spectroscopy of biomolecules," Ph.D. thesis (University of Freiburg, 2005).
[56]. Y.-S. Jin, G.-J. Kim, and S.-G. Jeon, "Terahertz dielectric properties of polymers," J. Korean Phys. Soc. 49, 513–517 (2006).
[57]. J. Balakrishnan, B. M. Fischer, and D. Abbott, "Sensing the hygroscopicity of polymer and copolymer materials using terahertz time-domain spectroscopy," Appl. Opt. 48, 2262–2266 (2009).

[58]. P. D. Cunningham, N. N. Valdes, F. A. Vallejo, L. M. Hayden, B. Polishak, X.-H. Zhou, J. Luo, A. K.-Y. Jen, J. C. Williams, and R. J. Twieg, "Broadband terahertz characterization of the refractive index and absorption of some important polymeric and organic electro-optic materials," J. Appl. Phys. 109, 043505 (2011).
[59]. F. Brechet, P. Roy, J. Marcou, and D. Pagnoux, "Single-mode propagation into depressed-core-index photonic-bandgap fibre designed for zero dispersion propagation at short wavelengths," Electron. Lett. 36, 514–515 (2000).
[60]. K. Nielsen, H. K. Rasmussen, P. U. Jepsen, and O. Bang, "Porous-core honeycomb bandgap THz fiber," Opt. Lett. 36, 666–668 (2011).
[61]. T. M. Monro and H. Ebendorff-Heidepriem, "Progress in microstructured optical fibers," Annu. Rev. Mater. Sci. 36, 467–495 (2006).
[62]. J.-Y. Lu, C.-P. Yu, H.-C. Chang, H.-W. Chen, Y.-T. Li, C.-L. Pan, and C.-K. Sun, "Terahertz air-core microstructure fiber," Appl. Phys. Lett. 92, 064105 (2008).
[63]. H. Han, H. Park, M. Cho, and J. Kim, "Terahertz pulse propagation in a plastic photonic crystal fiber," Appl. Phys. Lett. 80, 2634–2636 (2002).
[64]. M. Cho, J. Kim, H. Park, Y. Han, K. Moon, E. Jung, and H. Han, "Highly birefringent terahertz polarization maintaining plastic photonic crystal fibers," Opt. Express 16, 7–12 (2008).
[65]. J. A. Harrington, Infrared Fibers and Their Applications (SPIE, 2004).
[66]. F. Benabid, P. J. Roberts, F. Couny, and P. S. Light, "Light and gas confinement in hollow-core photonic crystal fibre based photonic microcells," J. Eur. Opt. Soc. Rapid Pub. 4, 09004 (2009).
[67]. K. J. Rowland, "Guiding light in low-index media via multilayer waveguides," Ph.D. thesis (The University of Adelaide, 2010).
[68]. J. C. Knight, T. A. Birks, P. S. Russell, and D. M. Atkin, "All-silica single-mode optical fiber with photonic crystal cladding," Opt. Lett. 21, 1547–1549 (1996).
[69]. J. C. Knight, J. Broeng, T. A. Birks, and P. S. J. Russell, "Photonic band gap guidance in optical fibers," Science 282, 1476–1478 (1998).
[70]. B. Temelkuran, S. D. Hart, G. Benoit, J. D. Joannopoulos, and Y. Fink, "Wavelength-scalable hollow optical fibres with large photonic bandgaps for CO2 laser transmission," Nature 420, 650–653 (2002).
[71]. T. Katagiri, Y. Matsuura, and M. Miyagi, "Photonic bandgap fiber with a silica core and multilayer dielectric cladding," Opt. Lett. 29, 557–559 (2004).
[72]. F. Couny, F. Benabid, and P. S. Light, "Large-pitch Kagome-structured hollow-core photonic crystal fiber," Opt. Lett. 31, 3574–3576 (2006).
[73]. A. Argyros and J. Pla, "Hollow-core polymer fibers with a Kagome lattice: potential for transmission in the infrared," Opt. Express 15, 7713–7719 (2007).
[74]. F. Couny, P. J. Roberts, T. A. Birks, and F. Benabid, "Square-lattice largepitch hollow-core photonic crystal fiber," Opt. Express 16, 20626–20636 (2008).
[75]. A. Argyros, S. G. Leon-Saval, J. Pla, and A. Docherty, "Anti resonant reflection and inhibited coupling in hollow-core square lattice optical fibers," Opt. Express 16, 5642–5648 (2008).
[76]. K. J. Rowland, S. Afshar V., and T. M. Monro, "Bandgaps and anti resonances in integrated-ARROWs and Bragg fibers; a simple model," Opt. Express 16, 17935–17951 (2008).
[77]. K. J. Rowland, S. Afshar V., A. Stolyarov, Y. Fink, and T. M. Monro, "Bragg waveguides with low-index liquid cores," Opt. Express 20, 48–62 (2012).
[78]. T. Hidaka, H. Minamide, H. Ito, S.-I. Maeta, and T. Akiyama, "Ferroelectric PVDF cladding THz waveguide," Proc. SPIE 5135, 70–77 (2003).
[79]. M. Yan and N. A. Mortensen, "Hollow-core infrared fiber incorporating metal-wire

metamaterial," Opt. Express 17, 14851–14864 (2009).
[80]. J. A. Harrington, R. George, P. Pedersen, and E. Mueller, "Hollow polycarbonate waveguides with inner cu coatings for delivery of terahertz radiation," Opt. Express 12, 5263–5268 (2004).
[81]. T. Ito, Y. Matsuura, M. Miyagi, H. Minarnide, and H. Ito, "Flexible terahertz fiber optics with low bend-induced losses," J. Opt. Soc. Am. B 24, 1230–1235 (2007).
[82]. O. Mitrofanov, R. James, F. A. Fernandez, T. K. Mavrogordatos, and J. A. Harrington, "Reducing transmission losses in hollow THz waveguides," IEEE Trans. Terahertz Sci. Technol. 1, 124–132 (2011).
[83]. S. Atakaramians, S. Afshar, T. M. Monro and Derek Abbott, "Terahertz dielectric waveguides," Advances in Optics and Photonics 5, 169–215 (2013).
[84]. Y. F. Geng, X. L. Tan, K. Zhong, P. Wang, and J. Q. Yao, "Low loss plastic terahertz photonic band-gap fibers," Chin. Phys. Lett. 25, 3961–3963 (2008).
[85]. G. Ren, Y. Gong, P. Shum, X. Yu, J. Hu, G.Wang, M. O. L. Chuen, and V. Paulose, "Low-loss air-core polarization maintaining terahertz fiber," Opt. Express 16, 13593–13598 (2008).
[86]. C.M. Haapamaki, J. Flannery, G. Bappi, R. Al Maruf, S.V. Bhaskara , O. Alshehri T. Yoon and M. Bajcsy, "Mesoscale cavities in hollow-core waveguides for quantum optics with atomic ensembles", Nano photonics, (2016).
[87]. J. Broeng, "Photonic crystal .bers", in APOC (Hangzhou, 2008).
[88]. A. Hassani, A. Dupuis, and M. Skorobogatiy, "Low loss porous terahertz fibers containing multiple subwavelength holes," Appl. Phys. Lett. 92, 071101 (2008).
[89]. A. Hassani, A. Dupuis, and M. Skorobogatiy, "Porous polymer fibers for low-loss terahertz guiding," Opt. Express 16, 6340–6351 (2008).
[90]. S. Atakaramians, S. Afshar Vahid, B. M. Fischer, D. Abbott, and T. M. Monro, "Porous fibers: a novel approach to low loss THz waveguides," Opt. Express 16, 8845–8854 (2008).
[91]. S. Atakaramians, S. Afshar V., B.M. Fischer, D. Abbott, and T. M. Monro, "Low loss, low dispersion and highly birefringent terahertz porous fibers," Opt. Commun. 282, 36–38 (2009).
[92]. S. Atakaramians, S. Afshar Vahid, M. Nagel, H. Ebendorff-Heidepriem, B. M. Fischer, D. Abbott, and T. M. Monro, "Experimental investigation of dispersion properties of THz porous fibers," in 33rd International IEEE Conference on Infrared, Millimeter, and Terahertz Waves (IEEE, 2009).
[93]. S. Atakaramians, K. Cook, H. Ebendorff-Heidepriem, S. Afshar V., J. Canning, D. Abbott, and T. M. Monro, "Cleaving of extremely porous polymer fibers," IEEE Photon. J. 1, 286–292 (2009).
[94]. S.-Y. Wang, "Microstructured optical fiber with improved transmission efficiency and durability," U.S. patent 6,418,258 (July 9, 2002).
[95]. J. Sultana, M. Islam, K. Ahmed, A.Dinovitser, W.-H. NG Brian and D Abbott, "Terahertz detection of alcohol using a photonic crystal fiber sensor," Applied Optics, (2018).
[96]. J. Sultana, M. S. Islam, J. Atai, M. R. Islam, and D. Abbott, "Near zero dispersion flattened, low-loss porous-core waveguide design for terahertz signal transmission," Opt. Eng. 56, 076114, (2017).
[97]. M. R. Hasan, M. S. Anower, M. A. Islam, "Polarization-maintaining low-loss porous-core spiral photonic crystal fiber for terahertz wave guidance," Appl. Opt., 55, (15), pp. 4145–4152, (2016).

[98]. S. Rana, G.K.M. Hasanuzzaman, S. Habib, S.F. Kaijage, R. Islam, "Proposal for a porous core octagonal photonic crystal fiber for T-ray wave guiding," Opt. Eng. 53 (11) 064105, (2014).
[99]. M. R. Hasan, M. A. Islam and A. A. Rifat, "A single mode porous-core square lattice photonic crystal fiber for THz wave propagation," Journal of the European Optical Society-Rapid Publications, (2016).
[100]. H. Ademgil et al, "Highly sensitive octagonal photonic crystal fiber based sensor," Optik-Int. J. Light Electron Opt., vol. 125, no. 20, pp. 6274–6278,(2014).
[101]. H. Ademgil and S. Haxha, "PCF based sensor with high sensitivity, high birefringence and low confinement losses for liquid analyte sensing applications," Sensors, vol. 15, no. 12, pp. 31833–31842, (2015).
[102]. F. H. Arif, K. Ahmed, S. Asaduzzaman, and A. K. Azad, "Design and optimization of photonic crystal fiber for liquid sensing applications," Photon. Sensors, vol. 6, no. 3, pp. 279–288, (2016).
[103]. J. Sultana, M. Islam, M. Faisal, M. R. Islam, Brian W.-H. Ng, H. E-Heidepriem, D. Abbott, "Highly birefringent elliptical core photonic crystal fiber for terahertz application," Optics Communications Volume 407, Pages 92-96, (2018).
[104]. S. Chowdhury, S. Sen, K. Ahmed, and S. Asaduzzaman, "Design of highly sensible porous shaped photonic crystal fiber with strong confinement field for optical sensing," Optik 142, 541–549 (2017).
[105]. M.S. Islam, J. Sultana, J. Atai, D. Abbott, S. Rana, M.R. Islam, "Ultra low loss hybrid core porous fiber for broadband applications," Appl. Opt. 56 (9), 1232–1237, (2017).
[106]. A. Ghazanfari, W. Li, M. C. Leu, and G. E. Hilmas, "A novel freeform extrusion fabrication process for producing solid ceramic components with uniform layered radiation drying," Additive Manuf vol. 15, pp. 102–112, (2017).
[107]. R. T. Bise and D. J. Trevor, "Sol-gel derived microstructured fiber, Fabrication and characterization," in Tech. Dig. Opt. Fiber Commun. Conf. (OFC/NFOEC), p. 3, (2005).
[108]. H. Ebendorff-Heidepriem, J. Schuppich, A. Dowler, L. Lima-Marques, and T. M. Monro, "3D-printed extrusion dies: A versatile approach to optical material processing," Opt. Mater. Expvol. 4, no. 8, pp. 1494–1504,(2014).
[109]. D. Russell, "Fabrication of Photonic Crystal Fiber," Max Planck Institute for the Science of Light, (2018).
[110]. M. S. Islam, "A novel approach for spectroscopic chemical identification using photonic crystal fiber in the terahertz regime," IEEE Sensors J., vol. 18, no. 2, pp. 575–582, Jan. (2018).
[111]. H. Han, H. Park, M. Cho, and J. Kim, "Terahertz pulse propagation in a plastic photonic crystal fiber," Appl. Phys. Lett., vol. 80, no. 15, p. 2634, (2002).
[112]. M. Goto, A. Quema, H. Takahashi, S. Ono, and N. Sarukura, "Teflon photonic crystal fiber as terahertz waveguide," Jpn. J. Appl. Phys., vol. 43, no. 2B, p. L317, (2004).
[113] M. S. Islam, "Extremely low material loss and dispersion flattened TOPAS based circular porous fiber for long distance terahertz wave transmission," Opt. Fiber Technol., vol. 34, pp. 6–11, Mar, (2016).
[114]. J. Anthony, R. Leonhardt, A. Argyros, and M. C. J. Large, "Characterization of a microstructured Zeonex terahertz fiber," J. Opt. Soc. Amer. B, Opt. Phys., vol. 28, no. 5, pp. 1013–1018, May (2011).

[115]. G. Woyessa, A. Fasano, C. Markos, A. Stefani, H. K. Rasmussen, and O. Bang, "Zeonex microstructured polymer optical fiber: Fabrication friendly fibers for high temperature and humidity insensitive Bragg grating sensing," Opt. Mater. Exp., vol. 7, no. 1, pp. 286–295, (2017).

[116]. H. Bao, K. Nielsen, H. K. Rasmussen, P. Uhd Jepsen, and O. Bang, "Design and optimization of mechanically down-doped terahertz fiber directional couplers," Opt. Express 22, 9486–9497 (2014).

[117]. M. S. Islam, J. Sultana, J. Atai, D. Abbott, S. Rana, and M. R. Islam, "Ultra low loss hybrid core porous fiber for broadband applications," Appl. Opt. 56, 1232–1237 (2017).

[118]. R. Islam, M. S. Habib, G. K. M. Hasanuzzaman, S. Rana, M. A. Sadath, and C. Markos, "A novel low-loss diamond-core porous fiber for polarization maintaining terahertz transmission," IEEE Photon. Technol. Lett. 28, 1537–1540 (2016).

[119]. M. S. Islam, B. K. Paul, K. Ahmed, S. Asaduzzamana, M. I. Islam, S. Chowdhury, S. Sen and A. N. Bahara, "Liquid-infiltrated photonic crystal fiber for sensing purpose: Design and analysis," Alexandria Engineering Journal, Volume 57, Issue 3, Pages 1459-146, (2018)